UNITED STATES DEPARTMENT OF THE INTERIOR

GEOLOGICAL SURVEY

Geoelectric structure of the Gila-San Francisco Wilderness area, Graham and Greenlee Counties, Arizona from audio-magnetotelluric data

by

Douglas P. Klein

and

Michael J. Baer

U.S. Geological Survey
Denver, Colorado 80225

Open-file Report 83-815

This report is preliminary and has not been reviewed for conformity with U.S. Geological Survey editorial standards and stratigraphic nomenclature.

1983

STUDIES RELATED TO WILDERNESS

Bureau of Land Management Wilderness Study Areas

The Federal Land Policy and Management Act (Public Law 94-579, October 21, 1976) requires the U.S. Geological Survey and the U.S. Bureau of Mines to conduct mineral surveys on certain areas to determine their mineral resource potential. Results must be made available to the public and be submitted to the President and the Congress. This report presents the results of an audio-magnetotelluric survey of the Gila-San Francisco Wilderness Study Area, Graham and Greenlee Counties, Arizona.

Contents

Contents (continued)

Page

Figures

ABSTRACT

Electromagnetic induction data using distant field sources, mostly of natural origin, in the frequency range of 4.5-27,000 Hz are analyzed to depict the geoelectric structure in an area of volcanic-rock cover located in southeastern Arizona between the Morenci and Safford porphyry copper deposits. The data for each station consist of scalar electromagnetic measurements at descrete frequencies for two-orthogonal magnetic and electric field pairs. Observations spaced about 5-km apart indicate resistivities in the range of 100-700 ohm-m for the unweathered Tertiary volcanic rocks to a depth of 200 to 500 m. Beneath this zone the data indicate resistivities in the range of 10-100 ohm-m that suggest the existence of an older volcanic rock unit. The less resistive unit appears to be displaced upward beneath Turtle Mountain, an area bounded to the northeast and southwest by mapped Basin and Range faults, and bounded to the southeast by an unmapped fault of older origin that trends northeast. Lateral changes in the resistivity of the two main geoelectric layers result in lowered resistivity in an area of known hot-springs near the confluence of the Gila and San Francisco Rivers, as well as along a north-south trending zone located on the east flank of Turtle Mountain, about 5-km (3-mi) west-northwest of the hot springs. This second anomaly is at a probable depth of 400-500 m and is interpreted to indicate a buried fault or fracture zone.

Geoelectric structure of the Gila-San Francisco Wilderness area, Graham and Greenlee Counties, Arizona from audio-magnetotelluric data

by

Douglas P. Klein

and

Michael J. Baer

Introduction

Twenty-one audio-magnetotelluric (AMT) soundings (4.5-27,000 Hz) were made in the northern Peloncillo and Gila Mountains of southeastern Arizona. Nineteen of these stations are located in the Gila-San Francisco wilderness area, which also incorporates the Gillard geothermal area (Figs. 1 and 2). These nineteen soundings are spaced at intervals of about 5 km (3 mi) and provide a reconnaissance picture of the geoelectrical structure to interpretated depths of about 1,000 m (3,280 ft). The majority of the observations were made as part of the wilderness mineral evaluation program of the U.S. Geological Survey (USGS). The data presented also include five stations (50-54) obtained during a study of the Gillard and Clifton geothermal areas (Klein and others, 1980). Stations 53 and 54 are located about 13 km (8 mi) northeast of the Gila-San Francisco area. The data from these last two stations do not contribute to the interpretative discussion of this report but are included in the Appendices because they have been subjected to more complete processing than previously reported.

AMT data consist of recordings of natural magnetic field variations and their corresponding induced electric fields in the Earth at descrete frequencies in the range of a few Hz to tens of kHz. The principles of the AMT method correspond to those of the magnetotelluric (MT) method (Cagniard, 1953, Vozoff, 1972, Vozoff and others, 1963) but the signals employed are at higher frequency and originate mainly from distant atmospheric electric disturbances rather than from ionospheric and magnetospheric phenomena. Strangway and others (1973) have considered the potential and limitations of the AMT method in mineral exploration. Examples of the character of the telluric signals employed in the AMT method, along with a summary of results obtained at 800 stations distributed mainly in geothermal prospects in the northern Basin and Range Province, is provided by Hoover and others (1978). Particular case histories of the AMT method in geothermal and mineral environments have been described by Strangway and Kozier, 1979, Hoover and others, 1976, Hoover and Long, 1976.

This study supplements previous geological and geophysical descriptions of the Gila-San Francisco study area that provide considerable detail on its geological setting and mineral potential (Richter and Lawrence, 1981, Richter and others, 1982, Klein, 1983). The study area straddles the juncture of the Gila River and San Francisco River (fig. 1). Topographic elevations in the area range from a low of 975 m (3,200 ft) where the Gila River flows into the

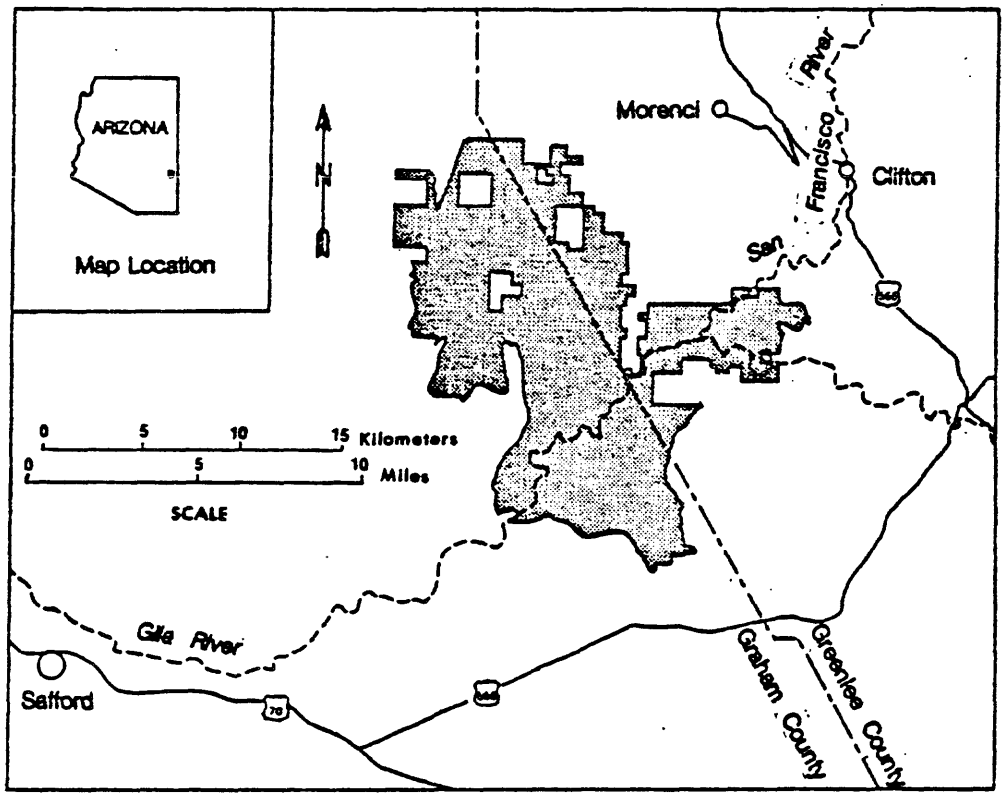

Fig. 1 -- Map showing location of Gila-San Francisco wilderness study area (shaded) in Graham and Greenlee Counties, Arizona (from Richter and others, 1981).

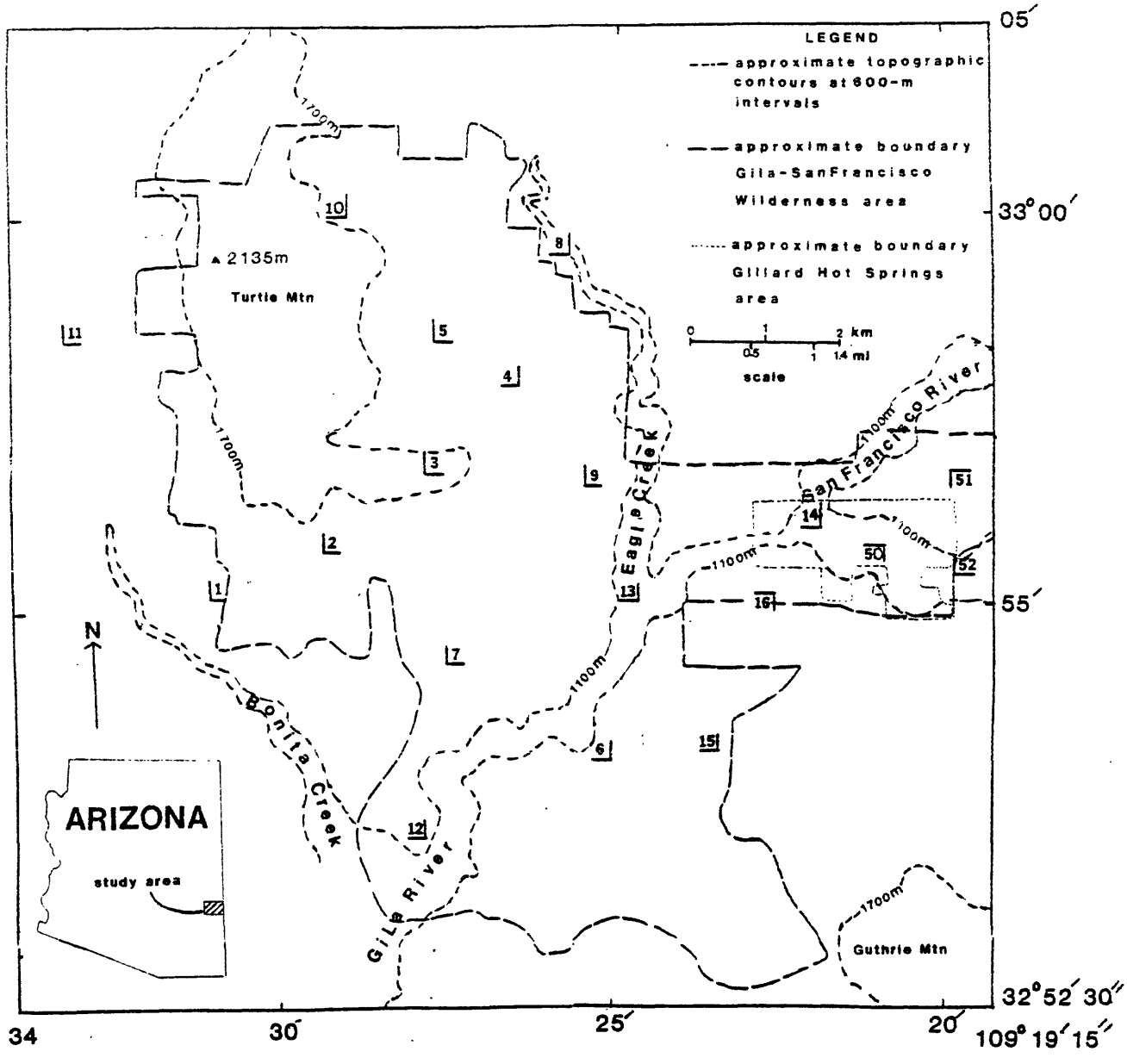

Fig. 2 -- Map showing AMT station locations. Stations 53 and 54 are off the map to the northeast and do not contribute to the interpretive discussion of the present report (see Klein and others, 1980). The lines at each station indicate the orientation of electric field dipoles.

Safford Basin, to a high of 2,135 m (7,004 ft) on top of Turtle Mountain in the north part of the area. Exposed rocks consist mainly of Tertiary andesite and basaltic andesite lava flows and volcaniclastic rocks. A number of eruptive centers are mapped in or adjacent to the study area. Northwest-trending normal faults related to Basin and Range extensional tectonism bound the northeast and southwest sides of the study area. Mining activity in the area consists of small and intermittently operated placer gold deposits along the Gila and San Francisco Rivers and a small manganese deposit. Geothermal springs exist in the eastern part of the area near the confluence of the Gila and San Francisco Rivers. The Morenci porphyry copper deposit lies about 5-km (3-mi) northeast of the study area and the copper deposits of the Safford area lie about the same distance to the southwest.

No references to previous electrical surveys in the study area are known, however, the Safford area to the southwest has traditionally been the test site for numerous electrical methods (Vozoff and others, 1963, Brant, 1966, Robinson and Cook, 1966, Strangway and others, 1973, Wynn and Zonge, 1975). The AMT tests by Strangway and others (1973) are illuminating because some of the Safford ores are deposited in Cretaceous volcanic rocks, intruded by granitic plutons, and buried by Tertiary volcanic rocks, the latter similar to those exposed in the present study area. Mineralization in both the Safford area (Robinson and Cook, 1966) and the Morenci area (Moolick and Durek, 1966) is controlled partly by northeast-trending faults. These faults may extend beneath the Tertiary volcanics of the Gila-San Francisco area. The thickness of the Tertiary volcanic rocks that cover the study area is unknown.

The apparent resistivities obtained with AMT equipment and reported by Strangway and others (1973) range from 10-20 ohm-m for a zone of sulfide mineralization, to 20-200 ohm-m for older pyritized volcanic rocks, to 300-1,400 ohm-m for an inferred buried igneous plug beneath an exposed extrusive center. Strangway and others (1973) also reported apparent resistivity values of 1,000 ohm-m or more obtained on younger volcanic rocks with the dipole-dipole method. None of their AMT data (frequencies up to 5 kHz) detected a surface zone of this high resistivity although the younger volcanics were known to have a thickness of at least 122 m(400 ft) over about 1/3 of one of their traverses.

Data Acquisition and Processing

The USGS AMT system (Hoover and others, 1976, 1978; Hoover and Long, 1976) records in analog form two sets of orthogonal magnetic (H) and electric (E) field amplitudes for each of several frequency bands. Stations 50-54 (fig. 2, corresponding to stations G1-G3 and C1-C2, not shown, respectively of Klein and others, 1980) were observed in April, 1979. Stations 1-16 (fig. 2) where acquired in May, 1980, using an improved AMT receiver that has a wider frequency range, modified band-pass filters and is more compact. Whereas the old system used a constant Q filter (50) for all frequencies, the new system has narrower pass bands (Q=100) for the range from 450 to 4,500 Hz. Figure 3 shows the frequencies observed at each station for each of the two AMT systems. The signals sought were all natural in origin except for the band between 10,000 to 20,000 Hz which partly utilizes navigation and communication signals.

Simultaneous peaks from each pair of orthogonal E-H records were scaled and combined to compute apparent resistivity (ohm-m, proportional to $(E/H)^2$)

for the geographic north-south E-field orientation ($\rho_a$ns) and the east-west E-field orientation ($\rho_a$ew). The computation procedure and the calculator program used is documented in Appendix D. The logarithmic mean of the data samples at each frequency, the number of samples, and the 95-percent confidence interval of the mean (as percentage of a log-cycle) are tabulated in Appendix A. The confidence interval is a measure of the statistical consistency in the data but it does not reveal possible bias due to constant signal distortion. Such bias might be due to errors in system calibration, cultural electromagnetic interference, or signal polarization effects resulting from picking data that does not provide a random sampling of H-field directions. Such a bias can be discovered only if independent data is available or if the bias is restricted to a limited number of frequencies. In the latter case, a bias may be apparent because part of the data does not conform to a consistent or a physically plausible plot of apparent resistivity against frequency. This was the assumption used to reject some of the data as discussed below.

The reduced data were edited to reject data that were considered inconsistent with the trend of the sounding curve (the bi-logarithmic plot of apparent resistivity against frequency). The selection of data for rejection was performed independently on the $\rho_a$ns and $\rho_a$ew curve for each station. Smooth differences between the two curves can have interpretable geologic significance with regard to heterogeneity or anisotropy in the Earth.

Figure 3 show histograms of the percentage of data rejected for each frequency and thus indicates which observed frequencies were less reliable. Figure 4 shows three examples of complete soundings which illustrate the type of data rejected, and indicates the overall data quality. Those data that are not connected by the lines ($\rho_a$ns) or dashes ($\rho_a$ew) were discarded. The heavy solid lines show a cubic polynomial fitted to the logarithmic mean of the edited data.

It can be seen from figure 3 that the frequencies higher than 1,360 Hz were rejected at about the 50-percent level compared to the data in the 45 to 750 Hz range which was rejected at about the 20-percent level. Two of the examples on figure 4, stations 6 and 11 are among the better data sets of this survey, whereas station 4 (fig. 4) illustrates data typical of the poorer soundings. Note in particular the low apparent resistivities in the 1 to 10 kHz range for station 4. These values are attributed to the combination of weak natural signals which have a spectral minimum centered roughly on 2,000 Hz (Strangway and others, 1973, Hoover and others 1978) and an inadequate signal-to-noise ratio in the measurements for these signals. The loss of data in the 7.5- to 450-Hz frequency range, about 25- to 40-percent rejection (fig. 3), is unusual, but probably the result of the surveys being performed before the onset of the summer period when signal strength peaks because of increased thunderstorm activity.

Table 1 summarizes in a qualitative sense the parameters that indicate the quality of the present AMT data. Comparison of this table to the examples (fig. 4), or the data in Appendices A and B illustrate the type of data indicated by the descriptors under each column. These descriptors could be quantified, but the gain in insight on the data by such quantification would probably be minimal unless there were independent data sets to be compared.

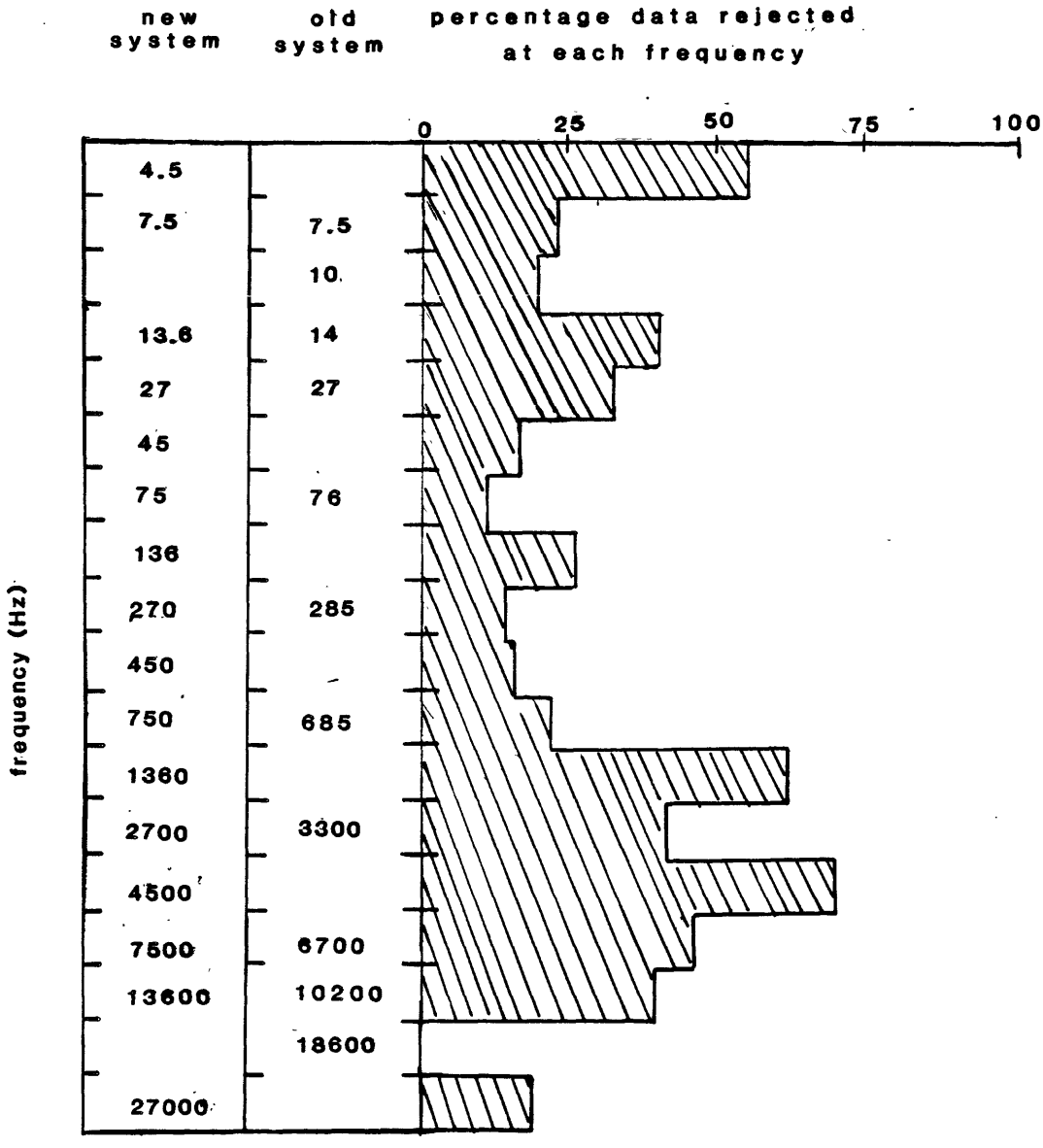

Fig. 3 -- Histogram showing the percentage of AMT data rejected for each observed frequency. The two frequency scales refer to frequencies observed for stations 50-54 (old system) stations 1-16 (new system). Note that data for frequencies within about 10-percent of each other are combined.

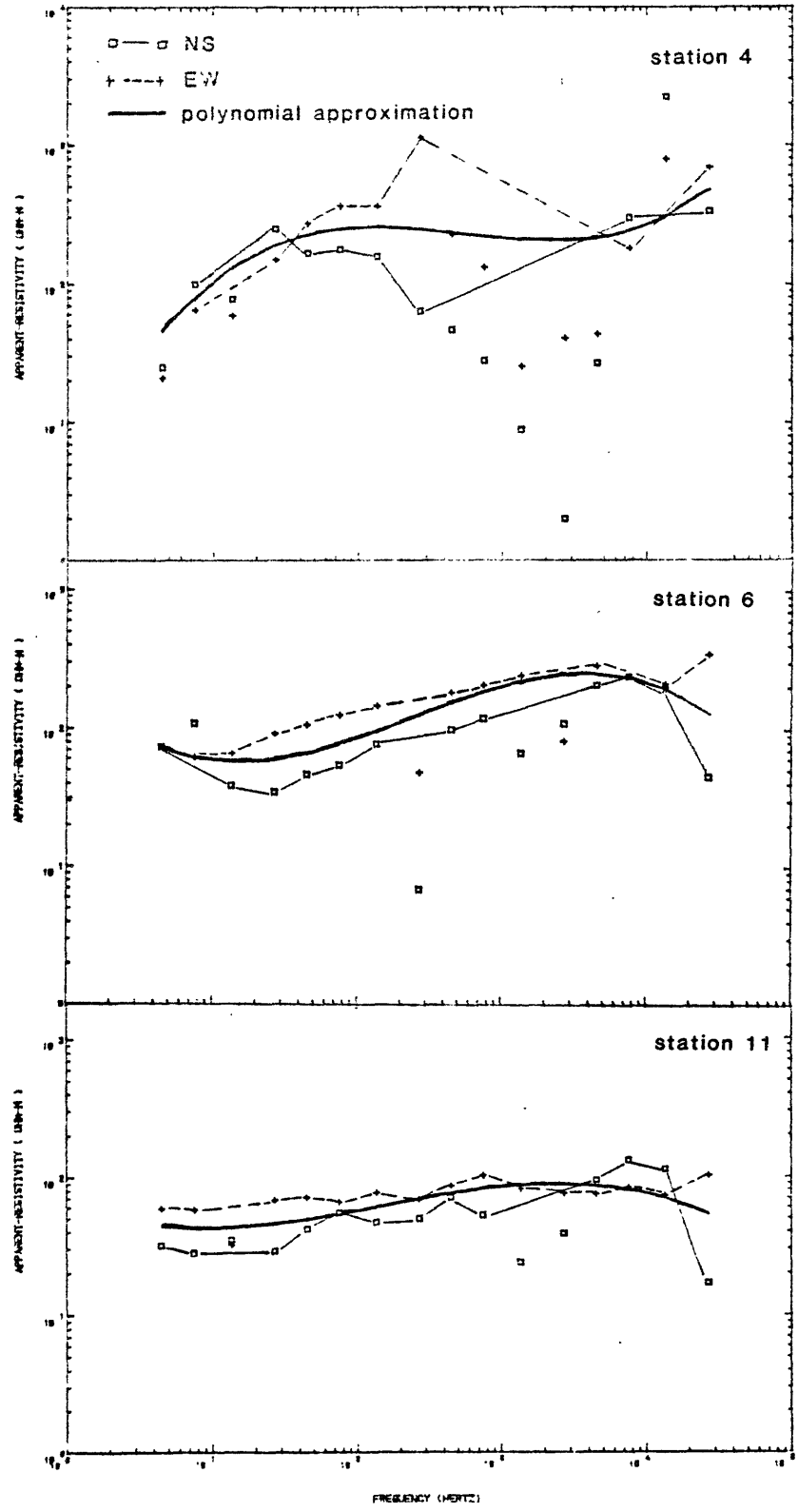

Fig. 4 -- Examples of apparent resistivity - frequency curves prior to rejecting data. The cubic polynomial shown is based on the logarithmic mean of edited data where those points not connected have been rejected. Station 4 illustrates one of the poorer data sets in the present survey, whereas stations 6 and 11 illustrate two of the better data sets obtained. See also Table 2 and Appendices A and B.

TABLE 1 -- Summary of data quality parameters. Relative data consistency (smoothness) qualitatively describes the signal/noise relationships among the data; this is based on examination of the scatter of data from a smooth curve. Apparent anisotropy qualitatively describes the separation of the $\rho_a$ns and $\rho_a$ew sounding curves; the relative magnitudes shown as weak, moderate and strong refer to the ratio log ($\rho_a$ew/$\rho_a$ns) as roughly in the ranges of 0.1-0.25, 0.25-0.7 and 0.7-1.0 respectively. Consistent anisotropy refers to the apparent anisotropy having the same directional sense over about 80-percent of the frequency range. The direction of lower apparent resistivity is given in the last column. See also the sounding curves in Appendix B, and the examples of figure 4.

Station	Relative Data Consistency (smoothness)	Apparent Anisotropy	Direction of Lower Apparent Resistivity
1	fair	moderate, consistent	N-S
2	fair	weak, inconsistent	N-S
3	poor	strong, consistent	N-S
4	poor	weak, inconsistent	N-S
5	fair	weak, consistent	N-S
6	good	weak, consistent	N-S
7	fair	weak, inconsistent	?
8	fair	weak, consistent	N-S
9	fair	weak, consistent	N-S
10	fair	strong, consistent	N-S
11	good	weak, consistent	N-S
12	fair	moderate, inconsistent	E-W
13	fair	moderate, consistent	E-W
14	good	weak, consistent	E-W
15	fair	unknown ($\rho_a$ns discarded)	?
16	good	strong, consistent	N-S
50	poor	weak, consistent	E-W
51	poor	moderate, inconsistent	N-S
52	fair	inconsistent	?
53	good	weak, consistent	N-S
54	fair	strong, consistent	N-S

The apparent anisotropy (defined as the log ($\rho_a$ns/$\rho_a$ew)) is basically a parameter determined by geological structure rather than by the quality of the data. However, inasmuch as the present analysis uses the logarithmic average of orthogonal apparent resistivities, the apparent anisotropy indicates those stations where this analysis is open to criticism. It may be noted that to make quantitative use of apparent anisotropy, the measured data should be mathematically rotated so as to maximize ρ_a on one axis and minimize ρ_a on the other (Word and others, 1971, Vozoff, 1972). This rotation requires phase as well as amplitude information whereas the present AMT data includes only amplitude information. It is emphasized that apparent anisotropy for scalar data is dependent on the orientation of the field sensors with respect to the geoelectric structure. A pervasive polarization of the source field may affect this parameter as may a relative error in system calibration. The latter is not considered a serious source of misinformation in the present survey.

In order to estimate an average sounding curve at each station, a cubic polynomial was fitted to the logarithmic mean of the $\rho_a$ns and $\rho_a$ew data. The polynomial serves the purpose of finding a smooth approximation to the data as required by the electromagnetic response of the Earth (Weidelt, 1972). It also provides an objective means of filtering out random noise in the data and interpolating between gaps in the data. The value of polynomial fitting has been previously recognized (Larsen, 1975, Strangway and Kozier, 1979). Other types of smoothing functions that fit through the whole data set may be equally appropriate in averaging out noise and in interpolation, but piecewise splining may be singled out as inappropriate in the present case because, without constraints, it retains noise in the data. The resulting polynomial sounding curves, along with the edited data, are plotted in Appendix B (see also fig. 4).

An estimate of the resistivity distribution with depth was obtained by transforming the smoothed data to a resistivity-depth function using Bostick's method (Bostick, 1977, Bockick and others, 1977, Goldberg and Rotstein, 1982). The results of this transformation were refined to better fit the smoothed data by one-dimensional forward modelling using the computational method for a horizontally layered earth, described by Schmucker (1971). The misfit between the apparent resistivity calculated for the layered Earth model (ρ_m) and the smoothed apparent resistivity sounding curve (ρ_a) was measured by the relative rms error given by

$$\left(\frac{1}{N}\sum_{i=1}^{N}(\rho_{m_i}-\rho_{a_i})^2/\rho_{a_i}^2\right)^{1/2}$$

The summation is with respect to the i=1,...,N frequencies corresponding to those of the observed data. The models were refined to bring the relative rms error to a value less than 0.15. Except for stations 3, 4, 50, 51 and 53 the final rms errors ranged from 0.03 to 0.10.

The resulting models of depth-resistivity are shown in Appendix C, along with the smoothed apparent resistivities versus skin-depth. The models are are the basis for the cross-sections in figures 8 and 9. The models are thought to display the main features of the resistivity distribution but the solutions obtained are not the only solutions that might fit the data. Inaccuracies and poor resolution may arise in one-dimensional modelling because of scatter and bias in the measurements, and because of the limited

range and number of frequencies observed (Oldenburg, 1979). More important in the present data however, is the fact that nearly all data show a response to lateral resistivity variations as indicated by the apparent anisotropy. Those data which show moderate to strong apparent anisotropy (Table 1) are particularly suspect to sensing lateral resistivity changes at a horizontal distance equivalent to the vertical depth of resistivity change shown in the models.

Resistivity Patterns

The results of the AMT data analysis, based on one-dimensional modelling of the smoothed logarithmic mean of $\rho_a$ns and $\rho_a$ew (Appendix C) are summarized on Table 2 and in figures 5-9. Figures 5-7 display the resistivity-depth (or thickness) parameters interpreted for three horizontal layers of distinct geoelectric properties. These parameters are shown with contour maps of the smoothed mean apparent resistivities for frequencies that are thought to reflect lateral contrasts in resistivities associated with each layer. Figures 8-9 show contoured cross-sections of the modelled resistivity-depth relationships.

The data indicate a surface layer, generally 2-10 m (6-32 ft) in thickness, of variable resistivity, overlaying a layer of relatively high resistivity, greater than 100 ohm-m, followed by a deeper layer of lowered resistivity in the range of 40 ohm-m or less. The depth to the layer of lower resistivity varies between soundings from about 200 to 400 m (660 to 1220 ft). Departures from these norms are indicated on Table 2.

Figure 5 illustrates the distribution of the surface layer resistivities and thicknesses. The interpreted resistivity and thickness of the layer is shown by each AMT station; the accompanying contours show the general pattern of lateral change in the smoothed apparent resistivities for the frequency of 7,500 Hz. On this map, as well as on figs. 6 and 7, the discrepancies between the interpreted resistivities and the apparent resistivities are due to the fact that the sounding curves (apparent resistivity-frequency curves) do not track modelled resistivities. The apparent resistivity at a particular frequency is a weighted mean function of the total geoelectric section, where the weighting function peaks at a depth less than the skin-depth of that frequency and apparent resistivity (Weidelt, 1972, note also the curves of Appendix C).

The total range of the modelled surface resistivities lies from 7 to 900 ohm-m but the majority of data fall in the 30 to 100 ohm-m range. Abnormally low surface resistivities (12-23 ohm-m: stations 13, 14, and 52) are generally located in the drainage beds and may be related to high pore-water content in fairly saline alluvium. The pattern is not consistent, however, because stations 50 and 8 both of which are within drainage beds shows resistivities of 50-60 ohm-m. A major exception to this pattern is at station 10 (7-ohm-m) on the northeast flank of Turtle Mountain and well off of the drainage beds. The 7 ohm-m resistivity is modelled for the upper 2-m (6-ft) of the Earth at station 10, but the data would be consistent with a thicker layer of low resistivities. This station is located on an area mapped as an extrusive complex (Richter and Lawrence, 1981) and hydrothermal alteration of the near surface rocks may be responsible for the low resistivity. Station 10, as well as stations 13 and 16, show moderate to

TABLE 2 -- Interpretive summary of modelled layers. The three main horizons of contrasting resistivity parameters (modelled resistivity and depth or thickness, see Appendix C) as tabulated are also shown on figures 5, 6 and 7. The tabulated resistivities shown are rough logarithmic means over the intervals shown as thickness or depth. Resistivities annotated by ± show significant variability across their depth range. Major transition zones, or layers that do not follow the general 3-layer pattern are noted in the last column.

	Surface Layer		Intermediate Layer		Deep Layer		Notes
Station	Resistivity (ohm-m)	Thickness (m)	Resistivity (ohm-m)	Depth Range (m)	Resistivity (ohm-m)	Depth Range (m)	
1	80	9	300	9-150	100	150-900	resistivity increases below 900 m.
2	65	9	150	9-190	50	190-?	
3	100	(75)	150	(75)-180	3 or less	250-?	the surface zone and intermediate zone cannot be readily distinguished
4	900	12	200±	12-800	10 or less	800-?	
5	300	9	80	9-250	3 or less	500-?	
6	75	9	450	9-150	40	150-900	resistivity increases below 900 m.
7	35	8	150	8-200	3 or less	500-?	there is a zone of resistivity 20± 200 to 500 m.
8	60 or more	20	40	20-420	20 or less	420-?	
9	700	10	280	10-80	40	150-?	there is a zone of resistivity 80± from 80 to 150 m.
10	7	2	100±	2-200	12	600-?	there is a zone of resistivity 40 from 200 to 600 m.
11	40	8	90±	8-120	40	120-500	slight indication of resistivity increase at 400 to 600 m.
12	40	15	25±	15-400	12	400-?	
13	12	5	750	5-110	25	300-?	there is a zone of resistivity 100± from 110 to 300 m.
14	23	7	250	7-150	20 or less	150-?	
15	85	9	500	9-150	40 or less	350-?	there is a zone of resistivity 100± from 150 to 350 m.
16	35	10	50	10-200	10 or less	200-?	
50	50	2	10±	2-250	3 or less	250-?	
51	250	6	not indicated		15±	6-?	resistivity increases below 100 m.
52	20	5	50±	5-60	3 or less	150-?	

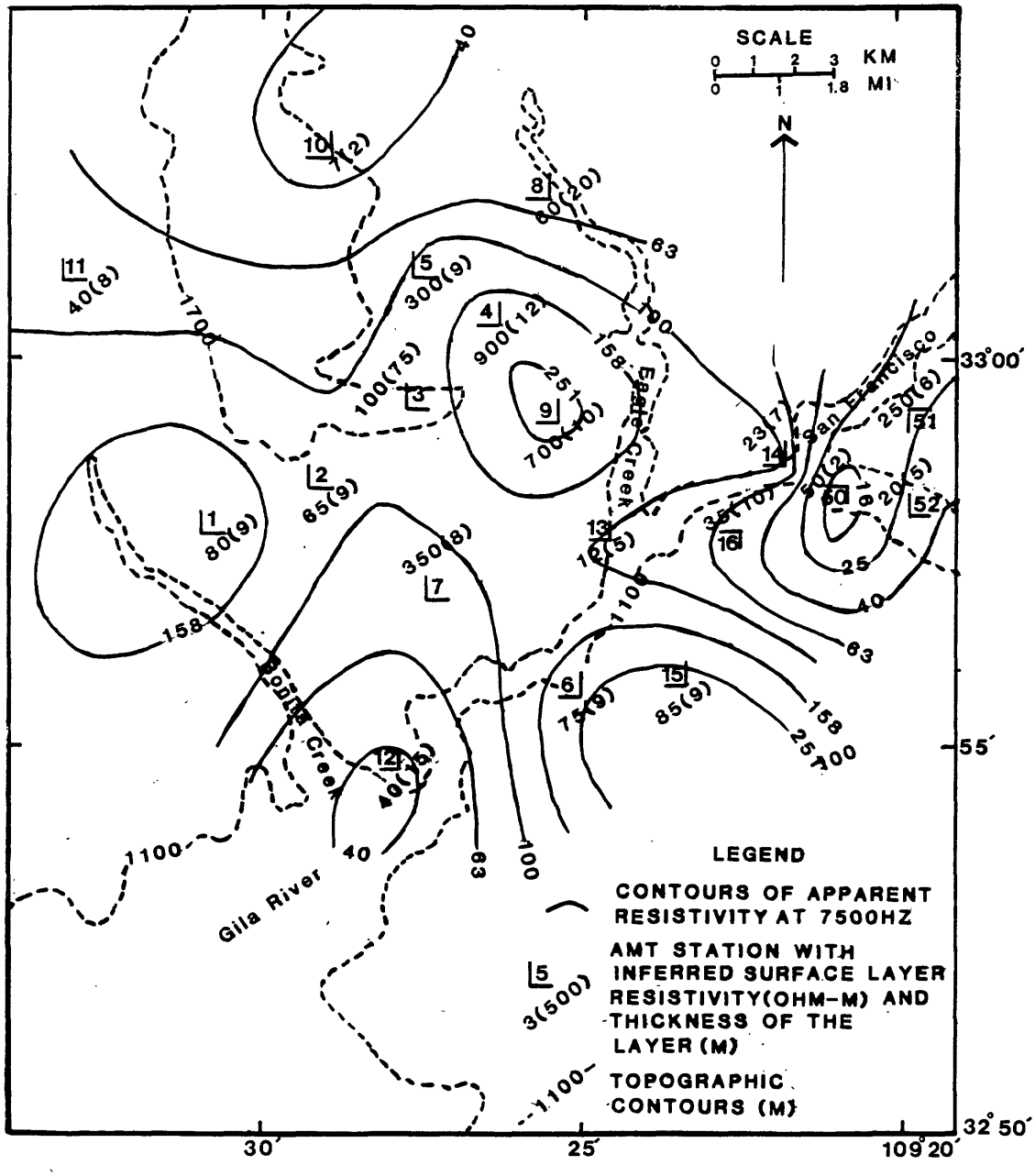

Fig. 5 -- Map showing modelled surface-layer resistivity parameters and contoured apparent resistivity at the frequency 7,500 Hz. The contours are computer plotted, spaced at equal intervals of 5 divisions per decade on a logarithmic scale, and are based on a 1-km grid interval contoured by a USGS contour program (R. G. Godson, USGS, Denver, unpublished).

strong and consistent apparent anisotropy (Table 1). This indicates significant lateral resistivity contrasts within the distance of detection.

Abnormally high surface resistivities in the surface layer (300-900 ohm-m: stations 4, 5, 9) are modeled at the mid-elevations of the east slope of Turtle Mountain and at station 51 (250 ohm-m) which is located on a topographic high on the east side of the study area.

The higher-frequency AMT data (7,500 Hz and up) are probably detecting variations in lithology, weathering and alteration, within a near-surface zone which could be explored by geological observations, or shallow drilling. Presumably, the near surface rocks with higher resistivity relate to dryer and/or less clay-rich material. The importance of the higher frequency data is that it allows a more complete definition of the sounding curve and thus more reliable modelling of the lower frequency data. It is worth noting that the data from 7.5 kHz upward required modelling in the upper tens of meters in order to fit the smoothed sounding curves whereas Strangway and others (1973) inferred that the surface material in the Safford area was essentially transparent to their data (frequencies up to 5 kHz). The presently modelled resistivities for the higher-frequency spectrum may represent minimum values inasmuch as AMT data are relatively insensitive to high resistivities.

Figure 6 shows the interpreted resistivities and thickness of the intermediate-depth resistive (100-300 ohm-m) layer. These data are shown beside each station along with contours of the smoothed apparent resistivity for the frequency of 270 Hz. This layer is typically 100 to 200 m (330 to 660 ft) in thickness and generally shows a significant contrast with the deeper and lower resistivities. The contrast is apparent in the majority of the models in Appendix C. Lateral variations are depicted in a general sense on the profiles of figs. 8 and 9.

The resistivities of this layer are probably typical of the uppermost basaltic-andesite and andesite volcanic rocks of the study area at a depth where they are relatively free of the effects of surface weathering. The resistivity in this layer is lowered considerably (10-50 ohm-m) in Gillard geothermal area, east of stations 13 and 15; this layer is possibly absent at station 51, northeast of the Gillard geothermal area. Station 51 is the only station whose data indicate a strong concave-upward appearance (high-low-high resistivity-frequency function, see Appendix B) which suggests a different lithological sequence with depth.

There is also an area of relatively low resistivity (40-100 ohm-m) in the intermediate depth layer across the north-central part of Turtle Mountain (stations 8, 5, 10, 11). The data south of these stations, with the exception of station 12, and those of Gillard area, show modelled resistivities greater than 150 ohm-m. There is no known explanation for the low anomaly at station 12. However, the apparent anisotropy at this station is quite large at frequencies at and above 270 Hz suggesting that part of the apparent anomaly may be a lateral change in resistivity relating to the Gila River Basin located south of the station.

Figure 7 shows the interpreted depth and low resistivities of the deeper layer, along with contours of smoothed apparent resistivity at a frequency

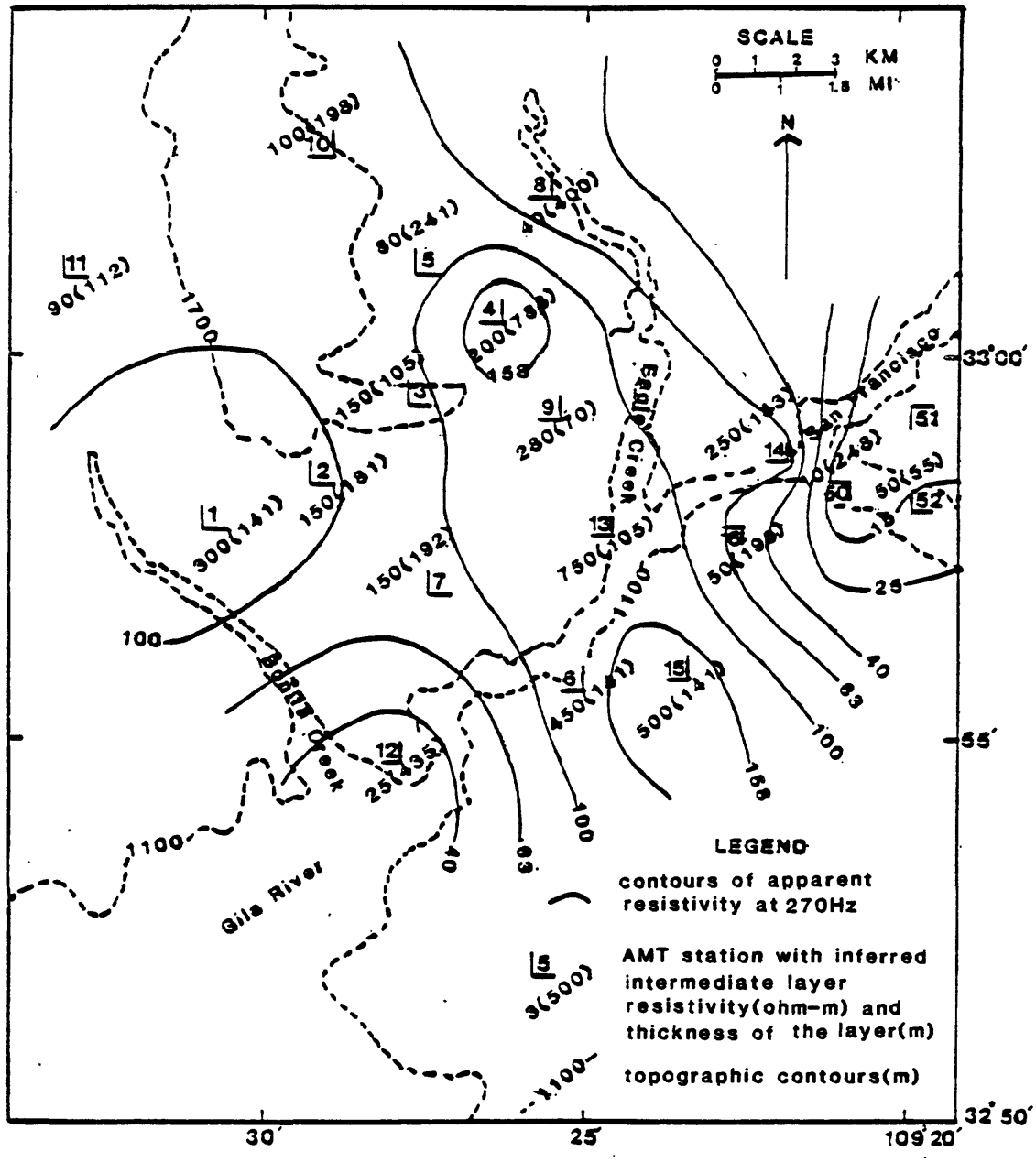

Fig. 6 -- Map showing modelled intermediate resistive layer parameters and contoured apparent resistivity at the frequency 270 Hz. The contours are computer plotted, spaced at equal intervals of 5 divisions per decade on a logarithmic scale, and are based on a 1-km grid interval contoured by a USGS contour program (R. G. Godson, USGS, Denver, unpublished).

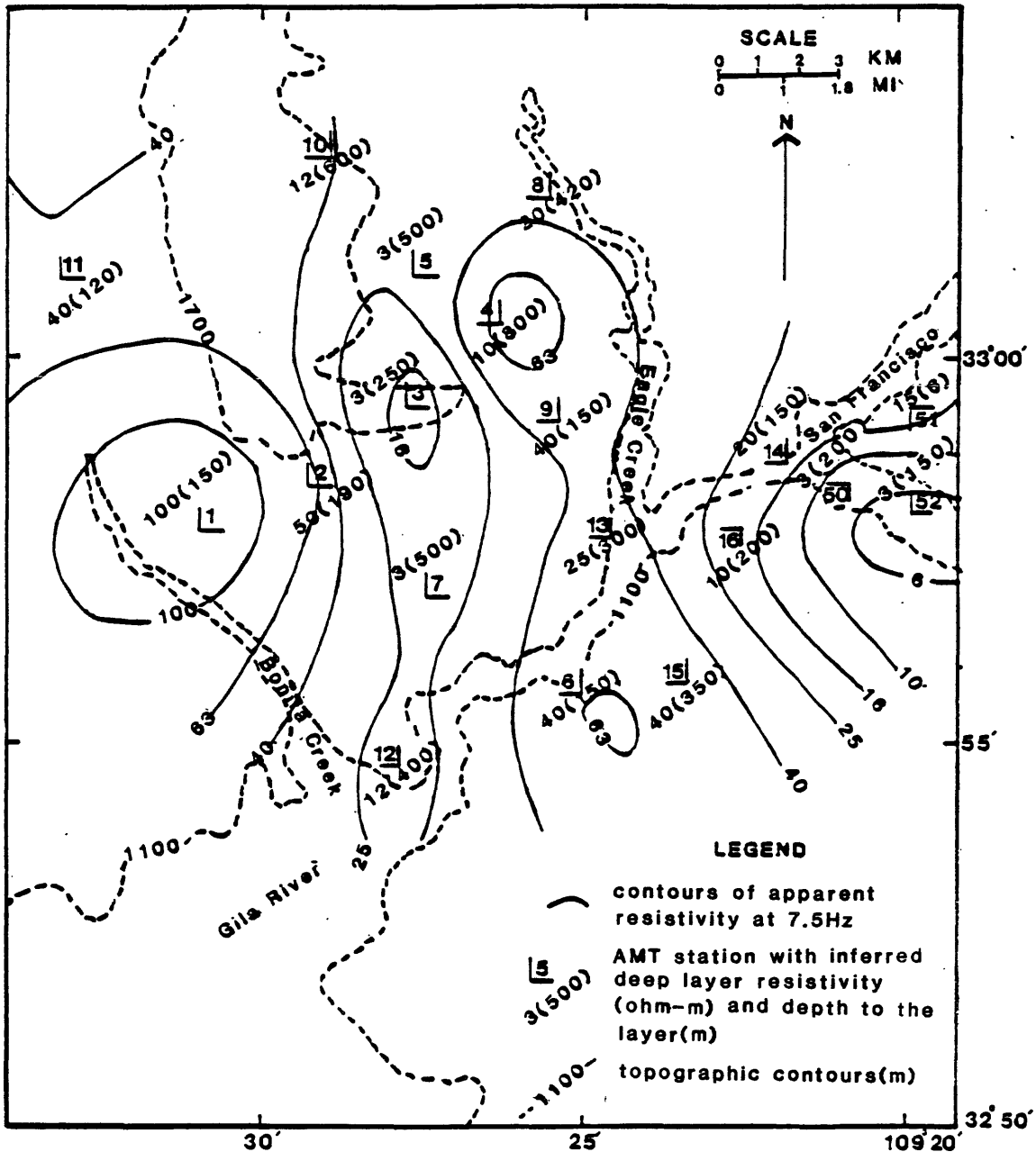

Fig. 7 -- Map showing modelled deep conductive layer parameters and contoured apparent resistivity at the frequency 7.5 Hz. The contours are computer plotted, spaced at equal intervals of 5 divisions per decade on a logarithmic scale, and are based on a 1-km grid interval contoured by a USGS contour program (R. G. Godson, USGS, Denver, unpublished).

of 7.5 Hz. This deeper layer typically with modeled resistivities of 10 to 50 ohm-m was detected at all stations. The highest modelled resistivity of this layer is found at station 1, roughly 100 ohm-m; this value still contrasts significantly with the shallower resistivities. The contrast of this layer with the overlying layer, a factor of 10 or more, indicates a fundamental change in lithology and/or pore-water content starting from 150-500 m (490-1,640 ft). Stations in the east part of the study area generally show lower resistivities at shallower depth (60-250 m, 197-820 ft) than those in the west. Here the effect of geothermal alteration or the presence of warm fluids is suspected to be superimposed on the layer. Stations 10, 5, 3, 7, 12, roughly aligned north-south on the east flank of Turtle Mountain, also show anomalously low resistivities (3-12 ohm-m) although at greater depths of about 400 m (1,310 ft). It may be noted again that the apparent resistivity contours suggest the pattern of contrasts pointed out above, but the apparent resistivity values differ from the modelled values.

Data from three stations (1, 6, 11) suggest that the lower freqencies may be detecting the base of the low-resistivity layer. The more definite indications are at stations 1 and 6 on the southwest and south edges of the study area. The modelling for these two stations defines a higher resistivity beginning at about 900-m (2,950-ft) depth (see profiles A and C, figs. 8-9). The data for these two stations show definite increases in apparent resistivity at the lowest frequencies (Appendix 2) and the data are comparatively noise-free although they show moderate apparent anisotropy (Table 1). Station 11, in the northwest corner of the study area shows a weaker suggestion of an increase in resistivity, probably in the depth range of 400-600 m (1,310-1,970 ft). This increase in resistivity does not appear in the modelling, but again the data is relatively clean and moderately anisotropic. The fact that anisotropy are present in all three of these data sets leaves open the possibility that lateral contrasts of resistivity are being sensed rather than vertical contrasts.

Discussion

The relatively low resistivity layer interpreted typically at depths beginning at 200-400 m (660-1,310 ft) throughout the survey area is the fundamental feature discovered from this data. Horizontal resistivity variations in this layer indicate anomalously low resistivity (3-12 ohm-m) along a roughly north-trending zone on the upper east flank of Turtle Mountain (stations 10, 5, 3, 7, 12) and in the area of the confluence of the Gila and San Francisco Rivers (Fig. 7). There are no known drill-hole data within the survey area to correlate with the AMT data, thus the interpretations presented below remain speculative until further information is available.

Known hot springs exist along the Gila River near its juncture with the San Francisco River. It is presumed that the anomalous low resistivities (3 to 12 ohm-m) modelled for the data northeast of station 16 are caused by the presence and alteration effects (Keller, 1970) of geothermal pore waters concentrated along a northeast-trending fault zone. Numerous faults are mapped in this area (Richter and Lawrence, 1981) which extend northwest in lesser concentration. The available AMT data to the northwest (stations 4, 8, 9, 14) does not suggest a similar northwest extension of the geothermal area.

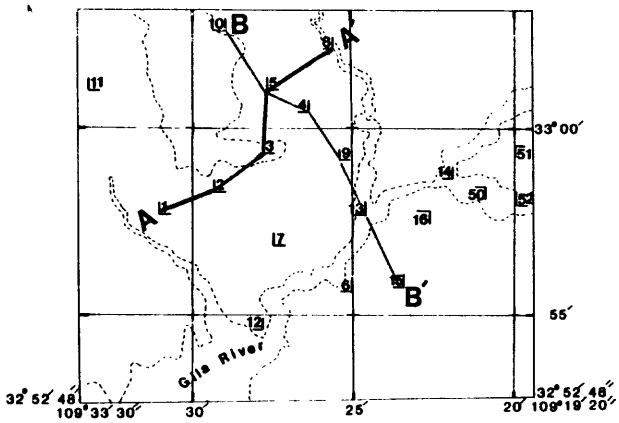

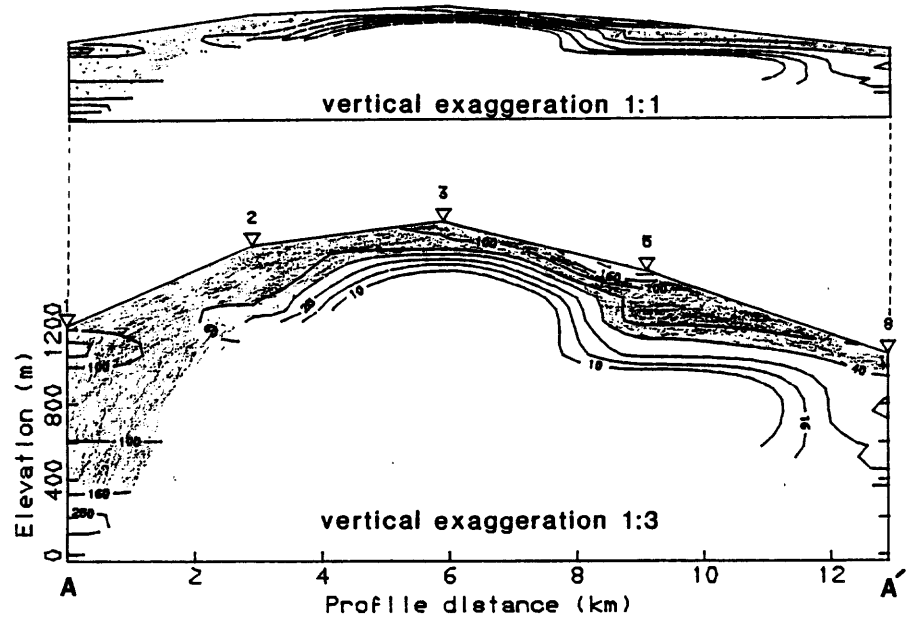

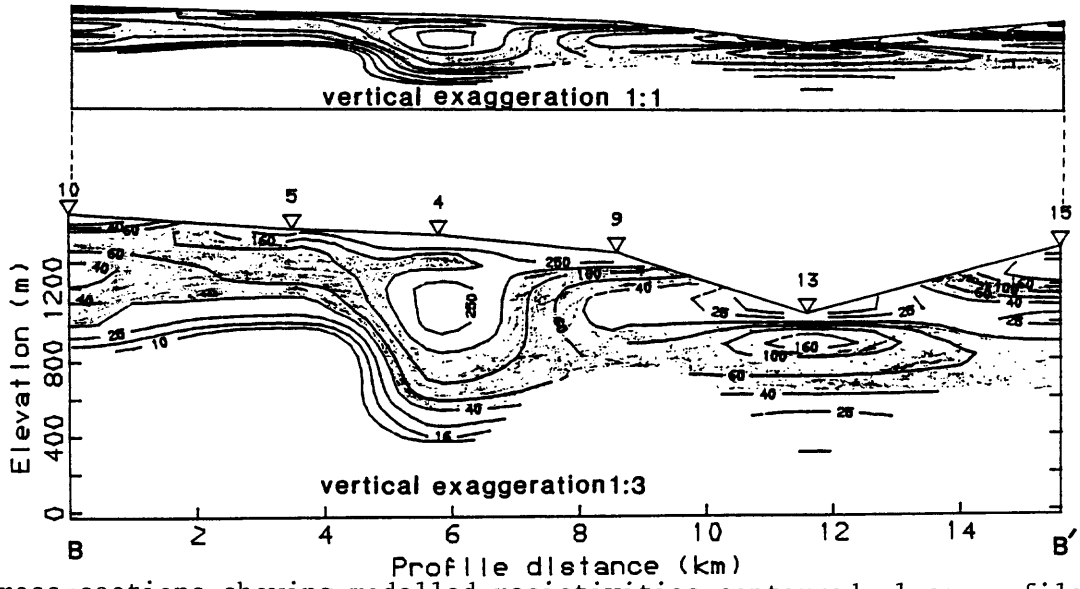

Fig. 8 -- Cross-sections showing modelled resistivities contoured along profiles A-A' and B-B'. The contours are computer plotted, spaced at equal intervals of 5 divisions per decade on a logarithmic scale, and are based on grid intervals of 400 ft vertical and 800 ft. horizontal. The contour interval from 40 to 100 ohm-m is shaded. The contours are created using a USGS contour program (Ray Watts, USGS, Denver, Colorado, unpublished).

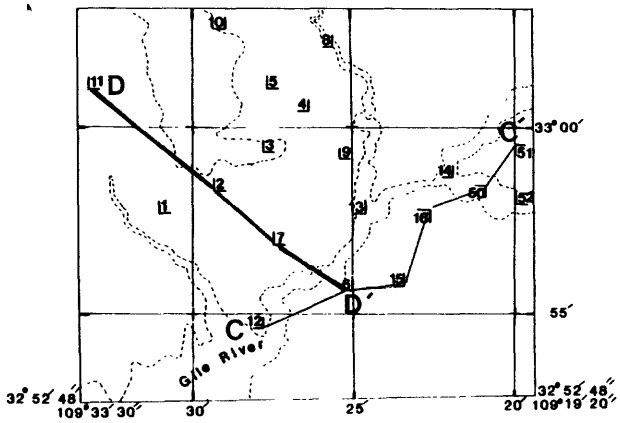

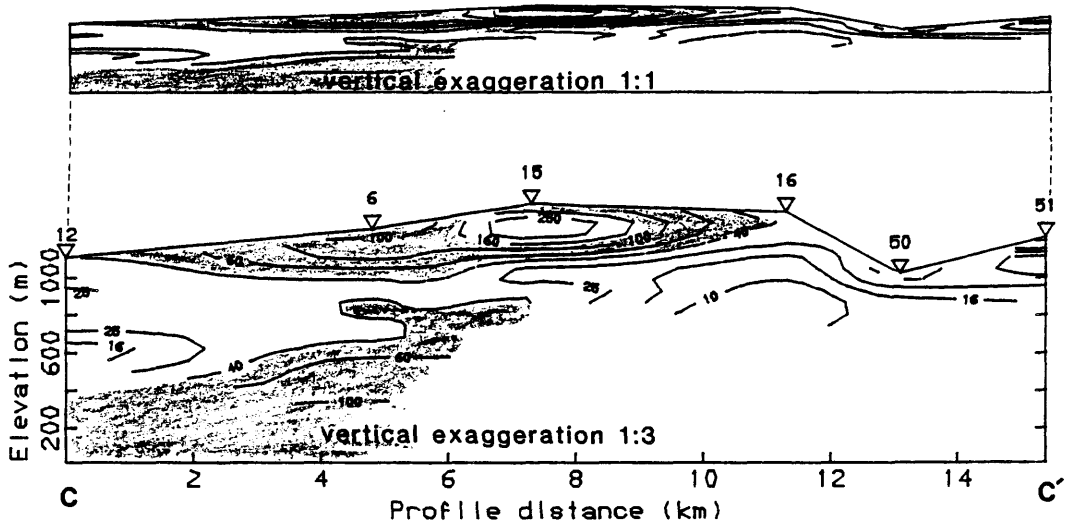

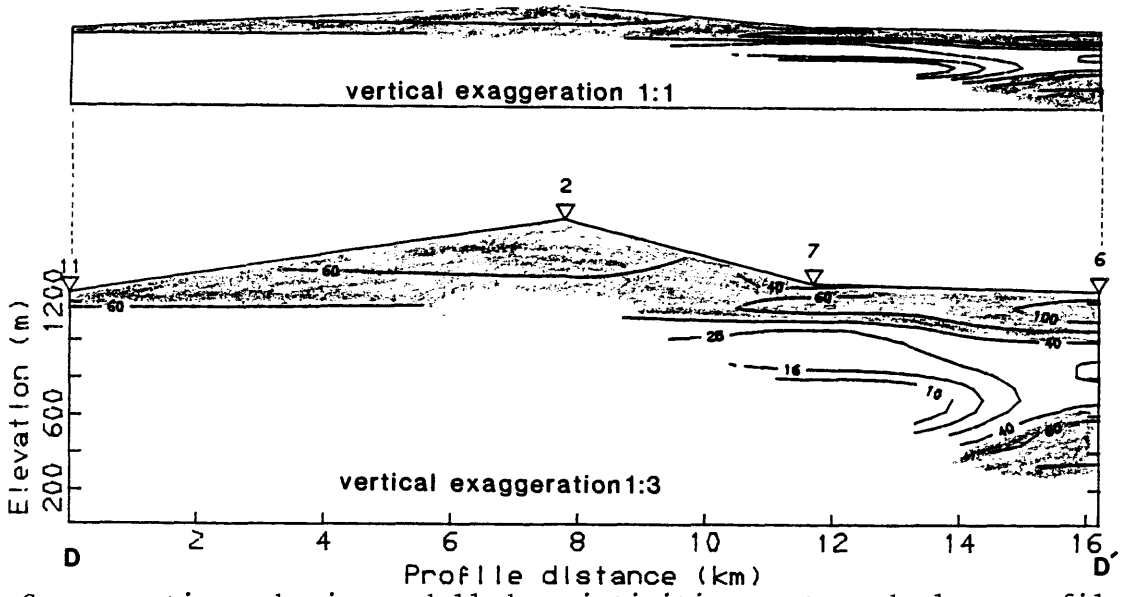

Fig. 9 -- Cross-sections showing modelled resistivities contoured along profiles C-C' and D-D'. The contours are computer plotted, spaced at equal intervals of 5 divisions per decade on a logarithmic scale, and are based on grid intervals of 400 ft vertical and 800 ft horizontal. The contour interval from 40 to 100 ohm-m is shaded. The contours are created using a USGS contour program (Ray Watts, USGS, Denver, CO, unpublished).

The areal extent of the geothermal area appears to be limited to a zone at most 2-km (1.2 mi) wide and extending from the San Francisco River southeast to the vicinity of station 52. Low resistivities determined by modeling of data from stations 51 and 16 are associated with significant apparent anisotropy ($\rho_a$ew greater than $\rho_a$ns) and thus are considered to reveal lateral changes of resistivity, with the low resistivities along the Gila River rather than below the stations. Quaternary alluvium of unknown thickness characterizes the terrane around station 51 and may also contribute to the low resistivities detected at this station. Such material commonly shows low resistivity in the southwestern United States because of its salt content (Strangway, 1970, Hoover and others, 1976).

The resistivities modelled in the geothermal area at depths exceeding 150 m are 1-3 ohm-m (stations 50, 52). The implications of these values for geothermal temperatures are of interest. Relationships governing rock resistivity as a function of temperature, porosity and pore fluid characteristics have been discussed by Dahknov (1962), Keller and Frischknecht (1966), Keller (1970) and Meidav (1970). When one has a reference area to compare to the anomalous resistivity, these relationships can be considered in terms of fractional changes in the appropriate parameters as:

$$\Delta\rho = \Delta\rho_e(\Delta\psi)^{-m}\,[1 + a\Delta t]^{-1}$$

where $\Delta\rho = \rho_a/\rho$, the ratio of the observed rock resistivity in the anomalous area (ρ_a) to that in the reference area (ρ); $\Delta\rho = \rho ea(t)/\rho e(t)$, the ratio of the resistivity of the saturating electrolyte in the anomalous area to that in the reference area, both at the reference temperature (t); $\Delta\psi = \psi_a/\psi$, the ratio of the porosity in the anomalous area to that in the reference area; and $\Delta t = t_a - t$, the temperature difference between the anomalous area and the reference area. The variable "m" is dependent on the pore geometry and the pore interconnections and typically has a value between 1.8-2.2 (Keller and Frischknecht, 1966, p. 21). The variable "a" is the temperature coefficient of the conductivity of the electrolyte that typically has a value of 0.025 (Dahknov, 1962, p. 104). Both "m" and "a" are assumed to be constant in the equation above, as is the pre-exponential term of Archie's law (Keller and Frischknecht, 1966, p. 21) which thus cancels out in the ratio. The fractional term $\Delta\rho_e$ would be expected to be less than 1.0 for a positive Δt because of increased solubility of available ions in the rock, increased availability of ions due to hydrothermal alteration and increased ionic mobility both within the electrolyte and on the surface of the pores.

Stations 13 and 14 provide a reference to compare to stations 50 and 51 inasmuch as these stations are at comparable elevations and in a similar geological setting. The modelled resistivities at depths exceeding 200 m below station 13 and 14 are 20-25 ohm-m, compared to the anomalous resistivities of 1-3 ohm-m in the geothermal area. Using $\Delta\rho = 0.1$, $m=2$, $a = 0.025$, the calculated temperature increases in the anomalous area as a function of $\Delta\rho_e$ and $\Delta\psi$ are shown in Table 3. The tabulated values illustrate temperature differences that may indicate a geothermal resource if the subsurface porosity remains constant or decreases. It is thought, however, that greater fault-induced porosity would contribute to the observed resistivity decrease; a value of $\Delta\psi$ amounting to 1.2 to 1.5 is thought to be

TABLE 3 -- Calculated lateral temperature increases from stations 13 and 14 to stations 50 and 52. Temperature increases are shown in degrees Centigrade as a function of fractional porosity increases, $\Delta\psi$, and fractional decreases of saturating electrolyte resistivity, $\Delta\rho_e$, due to equivalent salinity changes. The observed resistivity at depths exceeding 150 m decreases by a factor of 0.1 from stations 13-14 to stations 50,52.

		$\Delta\psi$			
		1.0	1.2	1.5	2.0
	1.0	360°C	237°	137°	60°
$\Delta\rho_e$	0.5	160°	99°	49°	10°
	0.2	40°	16°		

reasonable. A fractional decrease of electrolyte resistivity of 0.5 corresponds to a twofold increase in equivalent salinity (Keller and Frischknecht, p. 18-19) and is also thought to be reasonable. If the above assumptions are valid, the calculated temperature increase is substantially lowered, roughly in the range of 50° to 100°C which although significant, is insufficient to provide a substantial geothermal resource.

The deeper low resistivities associated with stations 10, 5, 3, 7 and 12 are also in the range of geothermal origin (3-12 ohm-m). Such resistivities are also encountered in sulfide-mineralized rocks and in hydrothermally altered rocks. There appears to be no reason to discount either possibility. Resistivities approaching 3 ohm-m at 250- to 500-m (820-1,640 ft) depth are modelled at stations 5, 3, 7. Higher resistivity, 12 ohm-m, is found at stations 10 and 12. The data at station 12 differs from the other three stations in its anisotropy. Stations 3 and 10 show strong apparent anisotropy with lower apparent resistivity in the north-south direction. Station 5 shows weak apparent anisotropy but with similar north-south low-resistivity orientation. Station 7 shows slight if any apparent anisotropy. Station 12 shows fairly strong apparent anisotropy oriented with lower resistivity in the east-west direction.

It is likely that the low resistivities of the east flank of Turtle Mountain are associated with a buried fault or fracture zone trending north-south along the trend of stations 5, 3, 7. This would provide openings to entrap pore fluids, or control geothermal fluid passage with the possibility of mineralization and the probability of alteration. No surface faults are mapped to support this contention (Richter and Lawrence, 1981), thus any such structure must be buried and must predate the exposed volcanic rocks. Consideration of the depths to the low resistivity zone, and the increasing elevation to the north of stations 12 or 7 (see cross-sections A-A′, stations 3, 5, and D-D′, station 7) requires that the host rock for this presumed fracture system be uplifted beneath Turtle Mountain relative to similar host rock to the northeast, southwest, and southeast.

Evidence for a possible east- or northeast-trending fault paralleling the Gila and San Francisco Rivers is suggested from gravity and aeromagnetic trends (Klein, 1983). The possibility was also suggested as an explanation for the localization of the geothermal area in the area of juncture of the San Francisco and Gila Rivers (Klein and others, 1980). Pre-or early-Tertiary fractures trending northeast exist in the Morenci and Safford mining areas (Moolick and Durek, 1966, Robinson and others, 1966) on the northeast and southwest sides of the study area respectively. This suggests the possibility of occurrence of similar structures beneath the exposed rocks of the study area. Observed anisotropy in the AMT data also provides evidence for such structures at stations 12, 13 and 14 where the east-west apparent resistivity is lower than the north-south apparent resistivity. These data contrast to all other AMT data in the area except possibly at station 50. There is however, no geologic evidence that directly supports the existence of northeast-trending faults or fractures in the vicinity of the Gila River (Richter and Lawrence, 1982).

More moderate resistivities ranging from 20 to 100 ohm-m are believed to be the normal characteristic of the low-resistivity zone beneath the majority of stations. Four possibilities considered causative for this layer are: 1) increased pore-water content associated with a water-table in an otherwise geophysically uniform sequence of volcanic rock, 2) a relatively thin layer (10's of meters) of weathered volcaniclastic rock such as mapped at several localities on the south and southwest edges of the study area (Richter and Lawrence, 1982), 3) a physically distinct unit of older volcanic rock that because of porosity, weathering, alteration or pyritization is less resistive than the exposed Tertiary andesite or basaltic-andesites, 4) a contrast between the older Tertiary andesites, mapped at the lower elevations of the study area and the overlying Tertiary basaltic-andesite rocks that predominate on Turtle Mountain (Richter and Lawrence, 1981). Assuming that the rocks under consideration are not water saturated, the resistivity contrasts associated with explanations 2, 3, and 4 would presumeably result from more clay minerals in the less resistive rocks. Explanation 2 assumes that the volcaniclastic rocks are relatively young and that weathering would be the prime cause of the clay minerals, hence the less resistive part of the volcanoclastic rocks would be thin. Clay minerals could be more pervasive with depth in explanations 3 and 4 because for older rocks the probability increases that they have been subjected to the circulation of hydrothermal fluids from various sources.

The variable elevations of low resistivity zone (fig. 8 and 9) present a problem from the hydrological standpoint for explanation 1 (above), and the depths to the layer present a problem for explanation 4 when the elevations of the known outcrops of the andesite are considered.

A weathered volcaniclastic layer (explanation 3) cannot be ruled out. Such a layer is assumed to be thinner than the modelled thickness of the low resistivity layer but satisfactory models with lower resistivity for a thinner layer might be generated. Resistivities of less than about 3 ohm-m would probably be needed for such thin layer. However, the presence of a volcaniclastic layer with greater thickness but more realistic resistivities of 10 to 50 ohm-m could contribute to the resistivity contrast for any of the explanations considered.

Explanation 3 is preferred because the resistivities, inferred rock sequences, and depths are somewhat similar to the situation in the Safford area a few kilometers to the southwest (Strangway and others, 1973). This interpretation requires that Turtle Mountain be differentially uplifted compared to the rocks on the southwest, northeast and southeast in order to satisfy the depth-elevation relationships. Some of the vertical movement would be required to have occurred prior to the deposition the exposed volcanic rocks inasmuch as at least one of the fault systems along which movement would be necessary is not exposed, namely, that one postulated on the southeast (oriented northeast). Faulting is presumed to have occurred also along the northwest-trending faults mapped along Eagle Creek and those mapped west of Turtle Mountain (Richter and Lawrence, 1981) and may have included movement on the speculated fracture believed to be responsible for the resistivity low along stations 5, 3, 7.

Conclusions

Data from 18 audio-magnetotelluric stations in the San-Francisco Wilderness study area indicate that below a thin layer of variable resistivity there are two basic resistivity horizons, a resistive (300 ohm-m range) layer of about 200- to 400-m thickness that is thought to reflect the younger Tertiary volcanic rocks, and a deeper zone of lower resistivity (30 ohm-m range) starting at 150- to 400-m depth that is thought to reflect an older volcanic rock sequence. Two, possibly 3 stations, all near the eastern boundary of the survey area suggest a deeper and more resistive layer at a depth of about 900 m. This suggestion is tempered by the possibility that the data at these three stations detected lateral resistivity variations rather than a variation with depth.

Resistivities are in the 3-10 ohm-m range in the Gillard Geothermal area, and along a zone on the east flank of Turtle Mountain. The low resistivities in the Gillard area are at relatively shallow depths of 50 to 250 m and presumably are related to fractured rocks containing thermal waters. The geothermal system is not thought to be of major economic value because of its limited extent and moderate resistivities compared to those required for water in the 200^{o}C range. The low resistivities along the east flank of Turtle Mountain at depths of 250 to 500 m are thought to be related to an unmapped fault zone that may contain thermal waters or mineralized rocks. This zone is of about the same size as the Gillard area. There is no surface manifestations of thermal waters along this anomaly.

Acknowledgements

Francis M. Boler assisted in the acquisition of the present data. Donald H. Hoover and Carl Long (USGS) provided valuable assistance in providing the equipment and assisting in survey preparation. The construction of the USGS AMT system was accomplished by Charlie Tippens and others under the direction of D. H. Hoover; Jim Cooke designed and tested the newer modification. Dale Duncan assisted in the data processing and preparation of illustrations.

References

Bostick, F. X., Jr., 1977, A simple almost exact method of MT analysis. "Workshop on evaluation of electrical methods in the geothermal environment (WEEMGE)", Snowbird, Utah, November 1976: University Utah Report - Geothermal Workshop, January, 1977, p. 175-177.

Bostick, F. X., Jr., Smith, H. W., and Boehl, J. E., 1977, A simplified one-dimensional magnetotelluric inversion method, Appendix I in Magnetotelluric and DC dipole-dipole soundings on northern Wisconsin. Austin, University Texas, Final Technical Report May 15, 1977, prepared under contract N00014-76-C, 0484, Office Naval Research, and Grant GA-38827, National Science Foundation 52p.

Brant, R. A., 1966, Geophysics in the exploration for Arizona porphyry coppers, in Titley, S. R., and Hicks, C. L. (eds.), Geology of the porphyry copper deposits, southwestern North America. Tucson, University Arizona Press, p. 87-110.

Cagniard, L., 1953, Basic theory of the magnetotelluric method. Geophysics, v. 18 no. 3, p. 605-635.

Dakhnov, V. N., 1962, Geophysical well logging. Quarterly, Colorado School Mines, v. 57, 445 p.

Goldberg, S., and Rotstein, Y., 1982, A simple form of presentation of magnetotelluric data using the Bostick transform. Geophysical Prospecting, v. 30, p. 211-216.

Hoover, D. B., Frischknecht, F. C., and Tippens, C. L., 1976, Audio-magnetotelluric sounding as a reconnaissance exploration technique in Long Valley, California. J. Geophysical Research, v. 81, no. 5, p. 801-809.

Hoover, D. B., and C. L. Long, 1976, Audio-magnetotelluric methods in Reconnaissance geothermal exploration. Proceedings 2nd United Nations Symposium Development and Utilization Geothermal Resources, v. 2, p. 1059-1064.

Hoover, D. B., Long, C. L., and Senterfit, R. M., 1978, Some results from audiomagnetotelluric investigations in geothermal areas. Geophysics, v. 43, no. 7, p. 1501-1514.

Keller, G. V., 1970, Induction methods in prospecting for hot water. Geothermics, special issue 2, U.N. Symposium on the Development and Utilization of geothermal resources, Pisa vol. 2, part 1, p. 318-332.

Keller, G. V., and Frischknecht, F. C., 1966, Electrical methods in geophysical prospecting, Oxford, Pergamon Press, 517 p.

Klein, D. P., 1983, Gravity and aeromagnetic anomalies of the Gila-San Francisco Wilderness Study Area, Graham and Greenlee Counties, Arizona. U.S. Geological Survey Miscellaneous Field Studies Map MF-1315, in press.

Klein, D. P., Long, Carl, Christopherson, Karen, and Boler, F. M., 1980, Reconnaissance geophysics in the Clifton and Gillard geothermal areas, SE Arizona. U.S. Geological Survey Open-File Report 80-325, 19 p.

Larsen, J. C., 1975, Low frequency (0.1-6.0 cpd) electromagnetic study of deep mantle electrical conductivity beneath the Hawaiian Islands. Geophysical Journal Royal Astronomical Society, v. 45, p. 17-46.

Meidav, T., 1970, Application of electrical resistivity and gravimetry in deep geothermal exploration. Geothermics, special issue 2 (U.N. Symposium on the development and utilization of geothermal resources, Pisa), vol. 2., part 1, p. 303-310.

Moolick, R. T., and Durek, J. J., 1966, The Morenci District, in Titley, S.R. and Hicks, C. L. (eds.), Geology of the porphyry copper deposits, southwestern North America. Tucson, University Arizona Press, p. 221-231.

Oldenburg, D. W., 1979, One-dimensional inversion of natural source magnetotelluric observations. Geophysics, v. 44, no. 7, p. 1218-1244.

Richter, D. H., and Lawrence, V. A., 1981, Geological map of the Gila-San Francisco Wilderness Study Area, Graham and Greenlee Counties, Arizona. U.S. Geological Survey Miscellaneous Field Studies Map MF-1351-A.

Richter, D. H., Klein, D. P., Lawrence, V. A., and Lane, M. E., 1982, Mineral resource potential of the Gila-San Francisco wilderness study area, Graham and Greenlee Counties, Arizona. U.S. Geological Survey Map MF-1315-B.

Robinson, R. F., and Cook, Annan, 1966, The Safford Copper Deposit, Lone Star Mining District, Graham County, Arizona, in Titley, S. R., and Hicks, C. L. (eds.), Geology of the porphyry copper deposits, southwestern North America Tucson, University Arizona Press, p. 251-266.

Schmucker, Ulrich, 1971, Interpretation of induction anomalies above non-uniform surface layers. Geophysics, v. 36, no. 1, p. 156-165.

Strangway, D. W., 1970, Geophysical exploration through geologic cover. Geothermics, special issue 2, U.N. Symposium on the Development and Utilization of geothermal resources, Pisa. vol. 2, part 2, p. 1231-1243.

Strangway, D. W., and Kozier, A., 1979, Audio-frequency magnetotelluric sounding - a case history at the Cavendish geophysical test range. Geophysics, v. 44, no. 8, p. 1429-1446.

Strangway, D. W., Swift, C. M., and Holmer, R. C., 1973, The application of audio-frequency magnetotellurics (AMT) to mineral exploration. Geophysics, v. 38, no. 6, p. 1159-1175.

Vozoff, K., 1972, The magnetotelluric method in the exploration of sedimentary basins. Geophysics, v. 37, no. 1, p. 98-141.

Vozoff, K., Hasegawa, H., and Ellis, R. M., 1963, Results and limitations of magnetotelluric surveys in simple geologic situations. Geophysics, v. 28, no. 5, Part I, p. 778-792.

Weidelt, Peter, 1972, The inverse problem of gemagnetic induction. Journal Geophysics (Zeitschrift fur Geophysik), v. 38, p. 257-289.

Word, D. R., Smith, H. W., and Bostick, F. X., Jr., 1971, Crustal investigations by the magnetotelluric tensor impedance method, in Heacock, J. G. (ed.), The structure and physical properties of the Earth's Crust. Washington, D.C., American Geophysical Union, Geophysical Monograph 14, p. 145-167.

Wynn, J. C., and Zonge, K. L., 1975, EM coupling, its intrinsic value, its removal, and the cultural coupling problem, Geophysics, v. 40, no. 5, p. 831-850.

Appendix A

Tabulation of basic apparent resistivity data

Each table presents the following data for the stations described in this report:

STATION: Survey station number designation. Stations 1-16 were observed with a newer version of the AMT system than stations 50-54.

LAT-LONG: Location of each survey station given in degrees and minutes for the latitude and longitude of each station. Minutes are provided with decimal fractions.

E-LINE DIRECTION: Direction of the electric dipole lines, oriented in the geographic north-south direction (NS) and east-west direction (EW) for each station. The E-direction is orthogonal to the measured magnetic field for each data set.

HZ: Frequency of observation in Hertz.

N: Number of simultaneous sample peaks picked from each electric and magnetic field analog record for the purpose of computing apparent resistivity.

RESIS: Apparent resistivity: $p_a$ns for E-line direction NS and $p_a$ew for E-line direction EW. Appendix D presents the computational procedure.

ERR: 95-percent confidence internal in units of percent logarithmic cycle for each calculated apparent resistivity. See Appendix D.

AMT DATA

PROJECT: GILA

STATION: 1
LAT.,LONG.: 32 57.77, 109 31.00

E-LINE DIRECTION: NS

HZ	N	RESIS	ERR
4.5	8	166.0	12.0
7.5	8	42.0	11.0
13.6	8	92.0	8.0
27.0	8	21.0	11.0
45.0	10	22.0	11.0
75.0	13	80.0	10.0
136.0	11	29.0	15.0
270.0	11	140.0	10.0
450.0	9	153.0	8.0
750.0	6	85.0	10.0
1360.0	8	20.0	5.0
2700.0	7	8.0	7.0
4500.0	9	5.0	5.0
7500.0	11	97.0	9.0
13600.0	11	93.0	8.0
27000.0	4	57.0	1.4

E-LINE DIRECTION: EW

HZ	N	RESIS	ERR
4.5	11	6.0	17.0
7.5	13	38.0	12.0
13.6	14	175.0	16.0
27.0	14	190.0	15.0
45.0	7	94.0	7.0
75.0	9	115.0	4.0
136.0	11	103.0	11.0
270.0	9	223.0	8.0
450.0	10	266.0	5.0
750.0	6	296.0	5.0
1360.0	6	58.0	4.0
2700.0	9	23.0	13.0
4500.0	11	11.0	7.0
7500.0	9	95.0	7.0
13600.0	9	561.0	2.0
27000.0	6	260.0	2.0

AMT DATA

PROJECT: GILA

STATION: 2
LAT.,LONG.: 32 58.36, 109 29.28

E-LINE DIRECTION: NS

HZ	N	RESIS	ERR
4.5	8	14.0	27.0
7.5	10	24.0	17.0
13.6	11	24.0	11.0
27.0	8	93.0	51.0
45.0	12	62.0	12.0
75.0	8	52.0	19.0
136.0	17	98.0	19.0
270.0	11	101.0	9.0
450.0	9	186.0	11.0
750.0	10	84.0	18.0
1360.0	8	15.0	15.0
2700.0	2	6.0	2.0
4500.0	8	3.0	14.0
7500.0	9	173.0	11.0
13600.0	8	170.0	12.0
27000.0	6	39.0	39.0

E-LINE DIRECTION: EW

HZ	N	RESIS	ERR
4.5	8	302.0	21.0
7.5	8	191.0	14.0
13.6	6	48.0	9.0
27.0	10	58.0	13.0
45.0	5	86.0	9.0
75.0	6	118.0	12.0
136.0	10	120.0	8.0
270.0	7	147.0	7.0
450.0	6	120.0	7.0
750.0	5	24.0	11.0
1360.0	5	20.0	5.0
2700.0	6	14.0	8.0
4500.0	8	6.0	13.0
7500.0	7	44.0	6.0
13600.0	7	239.0	5.0
27000.0	4	225.0	1.0

AMT DATA

PROJECT: GILA

STATION: 3
LAT.,LONG.: 32 59.37, 109 27.77

E-LINE DIRECTION: NS

HZ	N	RESIS	ERR
4.5	9	5.0	12.0
7.5	7	6.0	11.0
13.6	7	38.0	16.0
27.0	9	3.0	23.0
45.0	11	11.0	18.0
75.0	13	15.0	14.0
136.0	14	28.0	11.0
270.0	12	57.0	14.0
450.0	7	93.0	6.0
750.0	9	40.0	12.0
1360.0	6	15.0	8.0
2700.0	2	6.0	15.0
4500.0	10	11.0	13.0
7500.0	8	42.0	13.0
13600.0	5	256.0	1.0
27000.0	6	19.0	0.8

E-LINE DIRECTION: EW

HZ	N	RESIS	ERR
4.5	7	12.0	14.0
7.5	8	3.0	17.0
13.6	10	5.0	9.0
27.0	6	2.0	23.0
45.0	9	11.0	12.0
75.0	4	160.0	8.0
136.0	6	74.0	6.0
270.0	7	170.0	19.0
450.0	7	240.0	5.0
750.0	5	198.0	16.0
1360.0	8	29.0	9.0
2700.0	5	19.0	28.0
4500.0	7	6.0	6.0
7500.0	8	32.0	7.0
13600.0	9	361.0	13.0
27000.0	5	237.0	3.0

AMT DATA

PROJECT: GILA

STATION: 4
LAT.,LONG.: 33 0.45, 109 26.37

E-LINE DIRECTION: NS

HZ	N	RESIS	ERR
4.5	5	25.0	12.0
7.5	15	100.0	23.0
13.6	7	78.0	13.0
27.0	12	251.0	8.0
45.0	10	168.0	13.0
75.0	15	178.0	14.0
136.0	7	158.0	15.0
270.0	9	64.0	21.0
450.0	9	47.0	15.0
750.0	9	28.0	15.0
1360.0	12	9.0	14.0
2700.0	2	2.0	31.0
4500.0	10	27.0	10.0
7500.0	11	299.0	13.0
13600.0	5	2260.0	3.0
27000.0	9	337.0	12.0

E-LINE DIRECTION: EW

HZ	N	RESIS	ERR
4.5	7	21.0	19.0
7.5	9	65.0	9.0
13.6	7	59.0	22.0
27.0	8	151.0	4.0
45.0	8	275.0	11.0
75.0	8	366.0	12.0
136.0	7	363.0	3.0
270.0	6	1148.0	4.0
450.0	11	229.0	6.0
750.0	8	133.0	12.0
1360.0	6	26.0	18.0
2700.0	5	41.0	21.0
4500.0	8	44.0	5.0
7500.0	8	181.0	6.0
13600.0	6	792.0	9.0
27000.0	6	695.0	2.0

AMT DATA

PROJECT: GILA

STATION: 5
LAT.,LONG.: 33 1.05, 109 27.65

E-LINE DIRECTION: NS

HZ	N	RESIS	ERR
4.5	6	16.0	27.0
7.5	8	16.0	14.0
13.6	6	20.0	5.0
27.0	6	30.0	7.0
45.0	6	43.0	4.0
75.0	7	79.0	12.0
136.0	8	89.0	9.0
270.0	7	73.0	18.0
450.0	10	155.0	5.0
750.0	8	82.0	7.0
1360.0	6	29.0	5.0
2700.0	6	18.0	16.0
4500.0	8	25.0	14.0
7500.0	6	48.0	6.0
13600.0	8	111.0	13.0

E-LINE DIRECTION: EW

HZ	N	RESIS	ERR
4.5	6	8.0	11.0
7.5	8	41.0	15.0
13.6	6	11.0	63.0
27.0	10	79.0	5.0
45.0	5	146.0	7.0
75.0	6	121.0	13.0
136.0	6	54.0	5.0
270.0	6	181.0	7.0
450.0	7	240.0	4.0
750.0	6	41.0	8.0
1360.0	5	21.0	6.0
2700.0	4	37.0	17.0
4500.0	6	54.0	14.0
7500.0	7	56.0	5.0
13600.0	7	138.0	6.0

AMT DATA

PROJECT: GILA

STATION: 6
LAT.,LONG.: 32 55.69, 109 25.05

E-LINE DIRECTION: NS

HZ	N	RESIS	ERR
4.5	6	74.0	16.0
7.5	10	109.0	20.0
13.6	8	39.0	11.0
27.0	7	35.0	13.0
45.0	6	47.0	8.0
75.0	8	55.0	12.0
136.0	9	78.0	17.0
270.0	7	7.0	17.0
450.0	7	100.0	7.0
750.0	6	121.0	10.0
1360.0	5	68.0	5.0
2700.0	7	112.0	8.0
4500.0	5	213.0	5.0
7500.0	8	246.0	4.0
13600.0	6	199.0	15.0
27000.0	4	46.0	4.0

E-LINE DIRECTION: EW

HZ	N	RESIS	ERR
4.5	8	74.0	13.0
7.5	10	62.0	12.0
13.6	6	66.0	7.0
27.0	10	93.0	5.0
45.0	6	108.0	14.0
75.0	6	127.0	8.0
136.0	7	148.0	3.0
270.0	5	49.0	9.0
450.0	11	186.0	8.0
750.0	5	211.0	2.0
1360.0	6	249.0	6.0
2700.0	8	83.0	5.0
4500.0	5	293.0	6.0
7500.0	5	245.0	2.0
13600.0	6	219.0	2.0
27000.0	5	353.0	4.0

AMT DATA

PROJECT: GILA

STATION: 7
LAT.,LONG.: 32 56.91, 109 27.45

E-LINE DIRECTION: NS

HZ	N	RESIS	ERR
4.5	6	4.0	18.0
7.5	9	2.0	9.0
13.6	8	2.0	10.0
27.0	6	2.0	5.0
45.0	6	65.0	3.0
75.0	7	94.0	7.0
136.0	7	79.0	2.0
270.0	7	67.0	9.0
450.0	6	129.0	5.0
750.0	6	111.0	4.0
1360.0	5	35.0	4.0
2700.0	9	79.0	9.0
4500.0	7	80.0	7.0
7500.0	7	117.0	3.0
13600.0	8	79.0	11.0
27000.0	5	16.0	3.0

E-LINE DIRECTION: EW

HZ	N	RESIS	ERR
4.5	7	20.0	7.0
7.5	7	21.0	11.0
13.6	7	20.0	22.0
27.0	7	31.0	6.0
45.0	8	44.0	9.0
75.0	8	56.0	8.0
136.0	8	89.0	3.0
270.0	5	89.0	5.0
450.0	9	98.0	2.0
750.0	12	93.0	15.0
1360.0	7	85.0	7.0
2700.0	6	22.0	5.0
4500.0	6	65.0	7.0
7500.0	5	132.0	3.0
13600.0	6	122.0	6.0
27000.0	5	176.0	2.0

AMT DATA

PROJECT: GILA

STATION: 8
LAT.,LONG.: 33 2.10, 109 25.62

E-LINE DIRECTION: NS

HZ	N	RESIS	ERR
4.5	5	39.0	17.0
7.5	9	5.0	14.0
13.6	8	17.0	9.0
27.0	7	25.0	9.0
45.0	5	27.0	8.0
75.0	7	29.0	14.0
136.0	7	23.0	7.0
270.0	10	35.0	58.0
450.0	8	43.0	9.0
750.0	11	42.0	12.0
1360.0	5	31.0	4.0
2700.0	6	38.0	4.0
4500.0	5	83.0	10.0
7500.0	11	54.0	9.0
13600.0	10	26.0	11.0
27000.0	6	91.0	7.0

E-LINE DIRECTION: EW

HZ	N	RESIS	ERR
4.5	12	23.0	23.0
7.5	7	43.0	7.0
13.6	10	64.0	9.0
27.0	7	50.0	4.0
45.0	11	70.0	11.0
75.0	8	62.0	8.0
136.0	6	59.0	5.0
270.0	4	73.0	10.0
450.0	6	62.0	3.0
750.0	6	49.0	3.0
1360.0	5	70.0	4.0
2700.0	6	58.0	7.0
4500.0	6	74.0	5.0
7500.0	6	37.0	2.0
13600.0	4	59.0	4.0
27000.0	4	304.0	2.0

AMT DATA

PROJECT: GILA

STATION: 9
LAT.,LONG.: 32 59.18, 109 25.40

E-LINE DIRECTION: NS

HZ	N	RESIS	ERR
4.5	12	63.0	24.0
7.5	6	36.0	9.0
13.6	5	23.0	4.0
27.0	7	30.0	9.0
45.0	7	41.0	5.0
75.0	6	62.0	5.0
136.0	9	72.0	8.0
270.0	6	94.0	2.0
450.0	10	219.0	10.0
750.0	8	8.0	12.0
1360.0	7	27.0	11.0
2700.0	6	105.0	22.0
4500.0	8	139.0	11.0
7500.0	6	216.0	5.0
13600.0	7	242.0	13.0
27000.0	5	50.0	1.0

E-LINE DIRECTION: EW

HZ	N	RESIS	ERR
4.5	5	224.0	32.0
7.5	5	53.0	5.0
13.6	5	55.0	5.0
27.0	6	91.0	12.0
45.0	6	91.0	9.0
75.0	7	90.0	9.0
136.0	5	135.0	4.0
270.0	11	191.0	10.0
450.0	6	166.0	8.0
750.0	7	190.0	5.0
1360.0	4	172.0	10.0
2700.0	8	54.0	13.0
4500.0	4	189.0	6.0
7500.0	7	268.0	7.0
13600.0	5	465.0	6.0
27000.0	4	424.0	2.0

AMT DATA

PROJECT: GILA

STATION: 10
LAT.,LONG.: 33 2.63, 109 28.95

E-LINE DIRECTION: NS

HZ	N	RESIS	ERR
4.5	10	21.0	18.0
7.5	7	19.0	14.0
13.6	8	19.0	8.0
27.0	8	35.0	21.0
45.0	5	23.0	4.0
75.0	6	28.0	12.0
136.0	5	54.0	12.0
270.0	7	58.0	9.0
450.0	5	52.0	5.0
750.0	4	32.0	3.0
1360.0	6	14.0	7.0
2700.0	9	20.0	15.0
4500.0	5	30.0	5.0
7500.0	6	28.0	3.0
13600.0	5	10.0	4.0
27000.0	5	2.0	3.0

E-LINE DIRECTION: EW

HZ	N	RESIS	ERR
4.5	8	76.0	23.0
7.5	9	93.0	11.0
13.6	9	77.0	11.0
27.0	7	22.0	6.0
45.0	7	99.0	7.0
75.0	7	111.0	8.0
136.0	7	186.0	4.0
270.0	6	172.0	7.0
450.0	6	275.0	5.0
750.0	6	85.0	5.0
1360.0	10	29.0	18.0
2700.0	7	13.0	13.0
4500.0	5	22.0	8.0
7500.0	4	28.0	5.0
13600.0	5	41.0	2.0
27000.0	5	18.0	2.0

AMT DATA

PROJECT: GILA

STATION: 11
LAT.,LONG.: 33 1.03, 109 33.18

E-LINE DIRECTION: NS

HZ	N	RESIS	ERR
4.5	8	32.0	10.0
7.5	8	28.0	8.0
13.6	17	35.0	6.0
27.0	29	29.0	7.0
45.0	11	42.0	8.0
75.0	22	55.0	7.0
136.0	12	47.0	5.0
270.0	10	50.0	5.0
450.0	16	71.0	6.0
750.0	9	53.0	4.0
1360.0	7	24.0	9.0
2700.0	7	39.0	6.0
4500.0	9	95.0	6.0
7500.0	11	132.0	3.0
13600.0	7	114.0	3.0
27000.0	6	17.0	2.0

E-LINE DIRECTION: EW

HZ	N	RESIS	ERR
4.5	4	59.0	15.0
7.5	4	58.0	5.0
13.6	13	32.0	6.0
27.0	8	68.0	5.0
45.0	8	71.0	5.0
75.0	21	66.0	3.0
136.0	4	77.0	3.0
270.0	7	69.0	4.0
450.0	6	87.0	4.0
750.0	7	103.0	4.0
1360.0	8	82.0	4.0
2700.0	13	76.0	18.0
4500.0	11	75.0	5.0
7500.0	8	84.0	4.0
13600.0	13	73.0	7.0
27000.0	5	103.0	3.0

AMT DATA

PROJECT: GILA

STATION: 12
LAT.,LONG.: 32 54.70, 109 27.82

E-LINE DIRECTION: NS

HZ	N	RESIS	ERR
4.5	6	35.0	22.0
7.5	7	21.0	11.0
13.6	5	25.0	7.0
27.0	5	26.0	5.0
45.0	7	1.2	4.0
75.0	6	1.3	2.0
136.0	5	1.4	2.0
270.0	6	1.3	5.0
450.0	6	52.0	3.0
750.0	7	44.0	12.0
1360.0	5	56.0	8.0
2700.0	7	42.0	8.0
4500.0	7	175.0	7.0
7500.0	4	116.0	6.0
13600.0	4	17.0	2.0
27000.0	5	10.0	6.0

E-LINE DIRECTION: EW

HZ	N	RESIS	ERR
4.5	15	14.0	20.0
7.5	10	35.0	14.0
13.6	11	15.0	11.0
27.0	7	32.0	11.0
45.0	8	31.0	9.0
75.0	8	36.0	14.0
136.0	7	14.0	7.0
270.0	8	21.0	18.0
450.0	12	17.0	7.0
750.0	6	15.0	4.0
1360.0	6	18.0	4.0
2700.0	6	19.0	11.0
4500.0	7	25.0	6.0
7500.0	8	51.0	16.0
13600.0	6	208.0	7.0
27000.0	5	102.0	2.0

AMT DATA

PROJECT: GILA

STATION: 13
LAT.,LONG.: 32 57.71, 109 24.60

E-LINE DIRECTION: NS

HZ	N	RESIS	ERR
4.5	6	37.0	15.0
7.5	10	42.0	11.0
13.6	5	32.0	7.0
27.0	5	110.0	9.0
45.0	7	105.0	19.0
75.0	7	160.0	8.0
136.0	4	347.0	5.0
270.0	5	414.0	2.0
450.0	7	437.0	6.0
750.0	4	295.0	6.0
1360.0	6	67.0	3.0
2700.0	7	27.0	7.0
4500.0	6	67.0	6.0
7500.0	5	178.0	4.0
13600.0	5	36.0	3.0
27000.0	4	11.0	1.0

E-LINE DIRECTION: EW

HZ	N	RESIS	ERR
4.5	9	50.0	10.0
7.5	6	62.0	6.0
13.6	7	74.0	7.0
27.0	6	69.0	3.0
45.0	6	64.0	2.0
75.0	5	77.0	1.0
136.0	8	95.0	3.0
270.0	7	67.0	6.0
450.0	9	69.0	1.0
750.0	5	56.0	2.0
1360.0	7	70.0	8.0
2700.0	8	55.0	11.0
4500.0	4	75.0	2.0
7500.0	6	64.0	4.0
13600.0	6	65.0	0.3
27000.0	5	48.0	0.9

AMT DATA

PROJECT: GILA

STATION: 14
LAT.,LONG.: 32 58.67, 109 21.86

E-LINE DIRECTION: NS

HZ	N	RESIS	ERR
4.5	9	31.0	20.0
7.5	8	18.0	12.0
13.6	5	17.0	12.0
27.0	9	22.0	10.0
45.0	9	46.0	10.0
75.0	6	56.0	7.0
136.0	7	62.0	8.0
270.0	7	78.0	9.0
450.0	7	141.0	12.0
750.0	8	162.0	7.0
1360.0	9	260.0	19.0
2700.0	12	43.0	13.0
4500.0	7	133.0	8.0
7500.0	8	218.0	9.0
13600.0	7	21.0	7.0
27000.0	5	5.0	3.0

E-LINE DIRECTION: EW

HZ	N	RESIS	ERR
4.5	6	19.0	6.0
7.5	7	21.0	9.0
13.6	7	24.0	9.0
27.0	6	32.0	3.0
45.0	5	32.0	7.0
75.0	6	31.0	7.0
136.0	7	45.0	9.0
270.0	5	42.0	1.0
450.0	9	58.0	5.0
750.0	6	55.0	9.0
1360.0	6	68.0	9.0
2700.0	5	71.0	10.0
4500.0	6	100.0	2.0
7500.0	5	96.0	4.0
13600.0	6	62.0	2.0
27000.0	4	42.0	3.0

AMT DATA

PROJECT: GILA

STATION: 15
LAT.,LONG.: 32 55.80, 109 23.42

E-LINE DIRECTION: NS

HZ	N	RESIS	ERR
4.5	4	55.0	23.0
7.5	7	56.0	7.0
13.6	7	52.0	7.0
27.0	8	68.0	4.0
45.0	7	68.0	4.0
75.0	5	118.0	2.0
136.0	9	191.0	8.0
270.0	5	478.0	9.0
450.0	6	246.0	7.0
750.0	5	335.0	15.0
1360.0	11	299.0	9.0
2700.0	6	275.0	5.0
4500.0	6	408.0	5.0
7500.0	7	393.0	6.0
13600.0	8	157.0	9.0
27000.0	6	29.0	2.0

E-LINE DIRECTION: EW

HZ	N	RESIS	ERR
4.5	4	5.0	43.0
7.5	7	1.0	11.0
13.6	6	0.7	6.0
27.0	2	50.3	5.0
45.0	7	20.0	29.0
75.0	6	90.0	14.0
136.0	6	60.0	10.0
270.0	7	40.0	17.0
450.0	9	20.0	20.0
750.0	7	40.1	18.0
1360.0	8	80.1	13.0
2700.0	6	60.2	5.0
4500.0	5	80.1	4.0
7500.0	7	10.0	7.0
13600.0	8	10.0	8.0
27000.0	6	10.0	4.0

AMT DATA

PROJECT: GILA

STATION: 16
LAT.,LONG.: 32 57.80, 109 22.55

E-LINE DIRECTION: NS

HZ	N	RESIS	ERR
4.5	4	32.0	14.0
7.5	5	11.0	9.0
13.6	7	18.0	13.0
27.0	7	24.0	5.0
45.0	10	18.0	12.0
75.0	7	16.0	13.0
136.0	5	19.0	7.0
270.0	6	23.0	9.0
450.0	5	30.0	9.0
750.0	8	34.0	11.0
1360.0	7	24.0	16.0
2700.0	6	129.0	3.0
4500.0	6	102.0	9.0
7500.0	7	88.0	5.0
13600.0	6	69.0	3.0
27000.0	5	15.0	4.0

E-LINE DIRECTION: EW

HZ	N	RESIS	ERR
4.5	7	36.0	21.0
7.5	7	26.0	5.0
13.6	6	30.0	8.0
27.0	5	48.0	6.0
45.0	6	62.0	3.0
75.0	6	86.0	11.0
136.0	8	102.0	3.0
270.0	6	97.0	2.0
450.0	9	102.0	8.0
750.0	6	86.0	6.0
1360.0	6	114.0	3.0
2700.0	6	85.0	3.0
4500.0	6	159.0	5.0
7500.0	5	110.0	1.0
13600.0	6	99.0	3.0
27000.0	4	87.0	2.0

AMT DATA

PROJECT: GILA

STATION: 50
LAT.,LONG.: 32 58.38, 109 20.92

E-LINE DIRECTION: NS

HZ	N	RESIS	ERR
7.5	9	9.1	5.0
10.0	12	11.1	8.0
14.0	7	10.1	5.0
27.0	9	6.1	3.0
76.0	11	11.0	3.0
285.0	11	8.1	5.0
685.0	7	13.6	5.0
3300.0	6	3.4	3.0
6700.0	7	6.6	2.4
18600.0	7	9.0	1.0

E-LINE DIRECTION: EW

HZ	N	RESIS	ERR
7.5	11	4.8	11.0
10.0	8	6.8	5.0
14.0	10	5.3	4.0
27.0	9	5.8	4.0
76.0	11	8.3	3.0
285.0	9	7.1	6.0
685.0	11	3.0	4.0
3300.0	6	0.9	14.0
6700.0	7	35.6	4.1
18600.0	7	27.0	3.0

AMT DATA

PROJECT: GILA

STATION: 51
LAT.,LONG.: 32 59.36, 109 19.90

E-LINE DIRECTION: NS

HZ	N	RESIS	ERR
7.5	5	48.0	10.5
10.0	7	1.4	17.1
14.0	7	11.0	24.1
27.0	9	39.0	18.8
76.0	13	7.6	13.2
285.0	13	8.6	18.0
685.0	10	5.9	8.9
6700.0	10	34.0	7.0
10200.0	3	41.0	25.0
18600.0	5	26.0	1.0

E-LINE DIRECTION: EW

HZ	N	RESIS	ERR
7.5	7	10.4	29.0
10.0	5	3.5	19.1
14.0	7	15.0	17.1
27.0	9	25.0	18.4
76.0	20	20.2	16.6
285.0	9	12.8	7.1
685.0	10	24.7	14.5
6700.0	7	51.0	3.8
10200.0	3	15.0	53.0
18600.0	5	105.0	2.0

AMT DATA

PROJECT: GILA

STATION: 52
LAT.,LONG.: 32 58.00, 109 19.87

E-LINE DIRECTION: NS

HZ	N	RESIS	ERR
7.5	7	11.0	16.5
10.0	9	5.0	26.7
14.0	5	0.0	49.0
27.0	9	66.0	16.0
76.0	10	12.0	20.0
285.0	6	16.0	8.0
685.0	6	29.0	17.0
3300.0	6	142.0	16.0
6700.0	7	65.0	8.0
10200.0	4	26.0	4.0

E-LINE DIRECTION: EW

HZ	N	RESIS	ERR
7.5	8	4.2	25.3
10.0	8	2.4	37.3
14.0	5	0.5	33.0
27.0	9	86.2	15.0
76.0	10	13.0	16.0
285.0	6	28.0	13.0
685.0	9	14.0	22.0
3300.0	6	23.0	11.0
6700.0	7	37.0	6.0
10200.0	4	30.0	4.0

AMT DATA

PROJECT: GILA

STATION: 53
LAT.,LONG.: 33 5.52, 109 18.20

E-LINE DIRECTION: NS

HZ	N	RESIS	ERR
7.5	13	180.0	16.0
10.0	9	170.0	32.0
14.0	12	105.0	19.0
27.0	12	190.0	12.0
76.0	10	405.0	16.0
285.0	15	640.0	11.0
6700.0	8	174.0	4.0
10200.0	7	71.0	4.0

E-LINE DIRECTION: EW

HZ	N	RESIS	ERR
7.5	13	391.0	20.0
10.0	9	399.0	33.0
14.0	12	186.0	15.0
27.0	12	283.0	18.0
76.0	11	648.0	15.0
285.0	15	422.0	9.0
6700.0	8	123.0	8.0
10200.0	7	74.0	11.0

AMT DATA

PROJECT: GILA

STATION: 54
LAT.,LONG.: 33 4.80, 109 18.05

E-LINE DIRECTION: NS

HZ	N	RESIS	ERR
7.5	8	5.2	22.0
10.0	10	2.9	19.0
14.0	8	3.2	6.0
27.0	9	3.2	10.0
76.0	10	3.7	5.0
285.0	14	6.8	10.0
6700.0	10	27.0	6.0
10200.0	6	41.0	23.0
18600.0	4	29.0	1.0

E-LINE DIRECTION: EW

HZ	N	RESIS	ERR
7.5	8	5.8	38.0
10.0	11	13.0	26.0
14.0	8	4.9	27.0
27.0	9	25.0	10.0
76.0	10	18.0	6.0
285.0	14	51.0	15.0
6700.0	10	12.0	8.0
10200.0	6	8.4	12.0
18600.0	4	28.0	2.0

Appendix B

Graphs of edited data and their cubic-polynomial approximation

The cubic-polynomial, shown as the smooth solid line was fitted to the logarithmic mean of the $p_a$ns (squares) and $p_a$ew (crosses) data. The plots are bilogarithmic apparent resistivity against frequency (Hz); some data has been rejected because it did not show consistency to the general trends of the $p_a$ns or $p_a$ew curves (compare to the data tables of Appendix A). Generally, those frequencies for which one of the apparent resistivities have been rejected are shown by overplots of the square and cross.

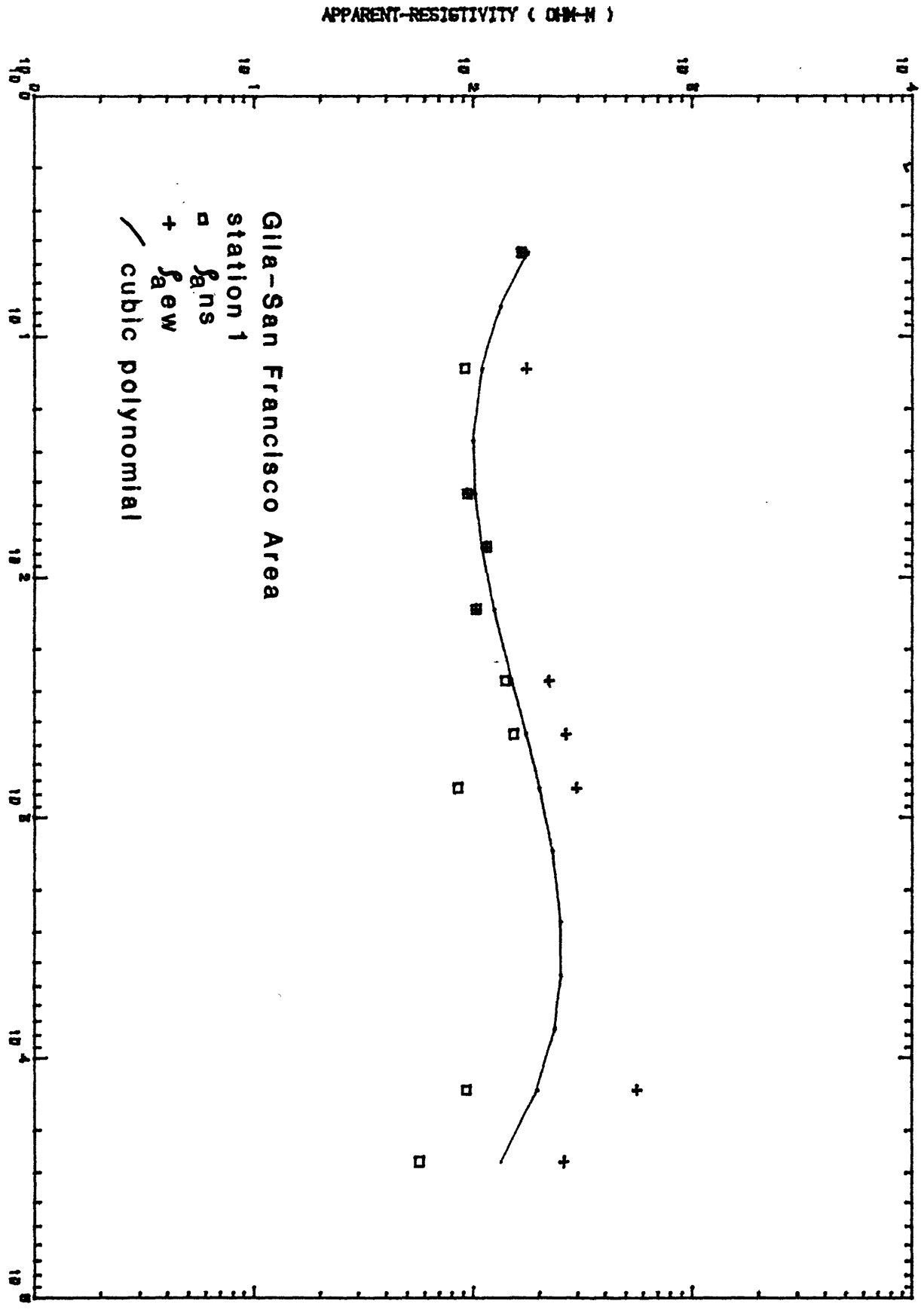
APPARENT-RESISTIVITY (OHM-M)
FREQUENCY (HERTZ)
Gila-San Francisco Area
station 1
□ ρ_{a} ns
+ ρ_{a} ew
/ cubic polynomial

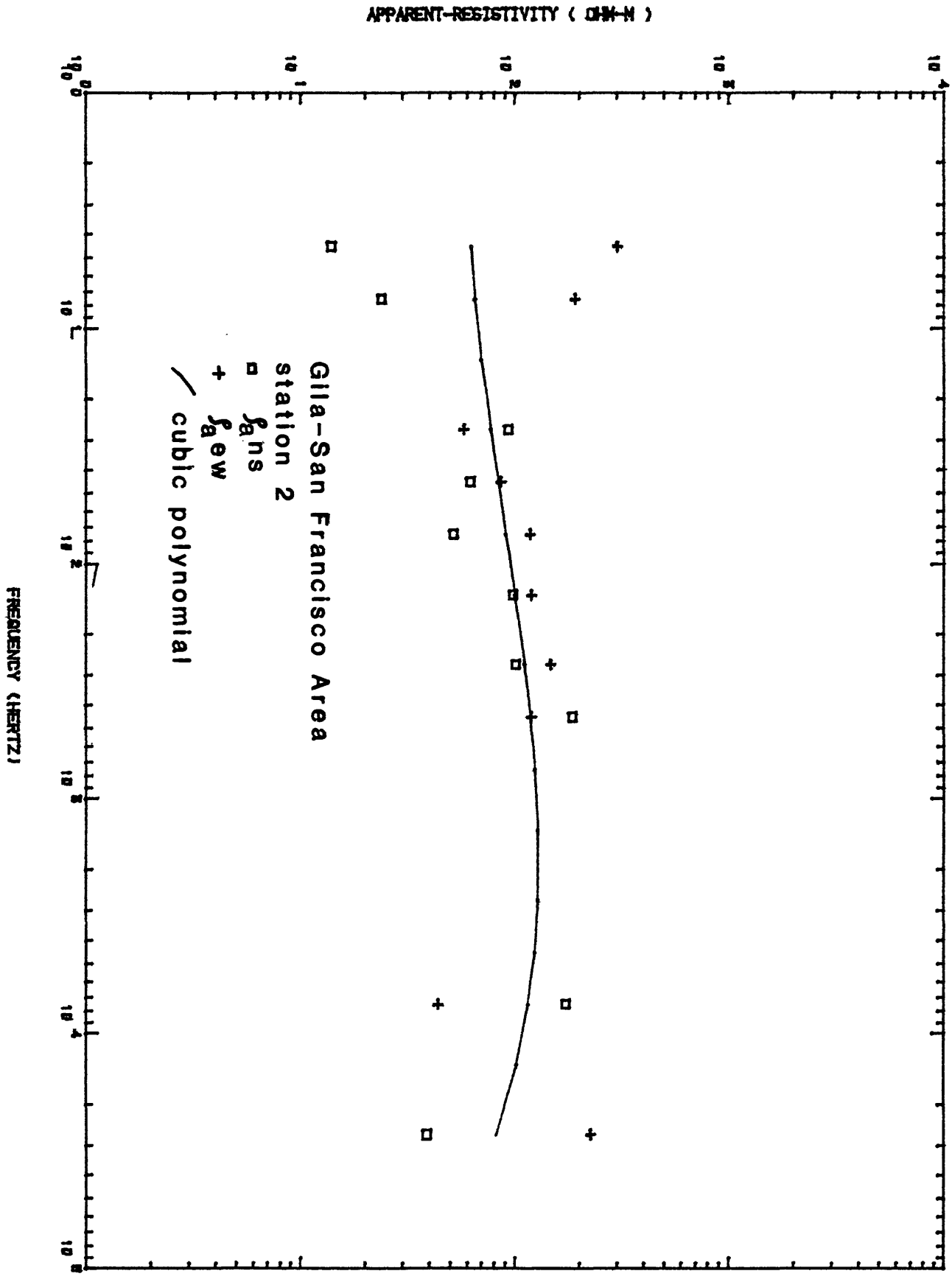
APPARENT-RESISTIVITY (OHM-M)
FREQUENCY (HERTZ)
Gila-San Francisco Area
station 2
□ ρ_a ns
+ ρ_a ew
/ cubic polynomial

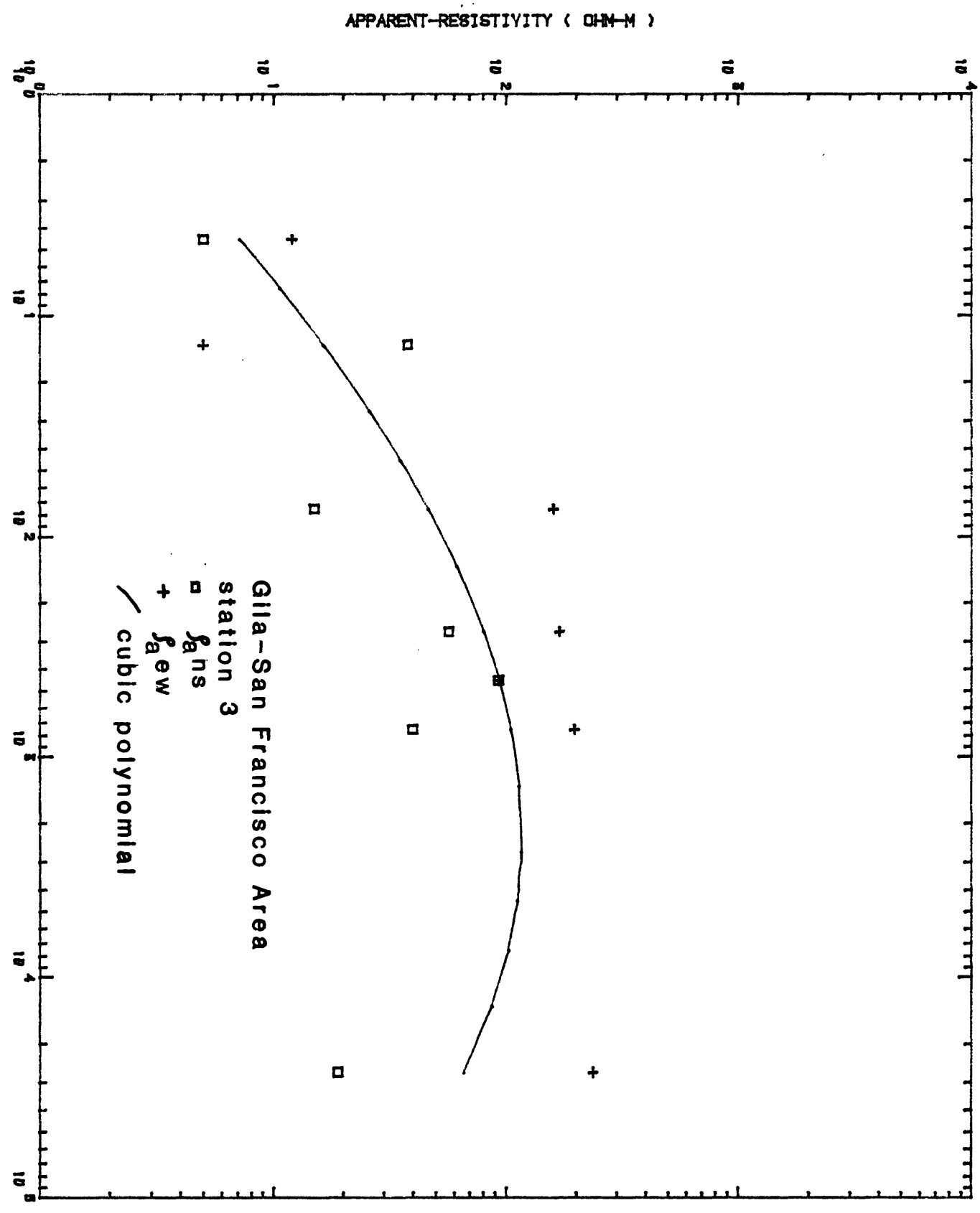
APPARENT-RESISTIVITY (OHM-M)
FREQUENCY (HERTZ)
Gila-San Francisco Area
station 3
□ ρ_a ns
+ ρ_a ew
cubic polynomial

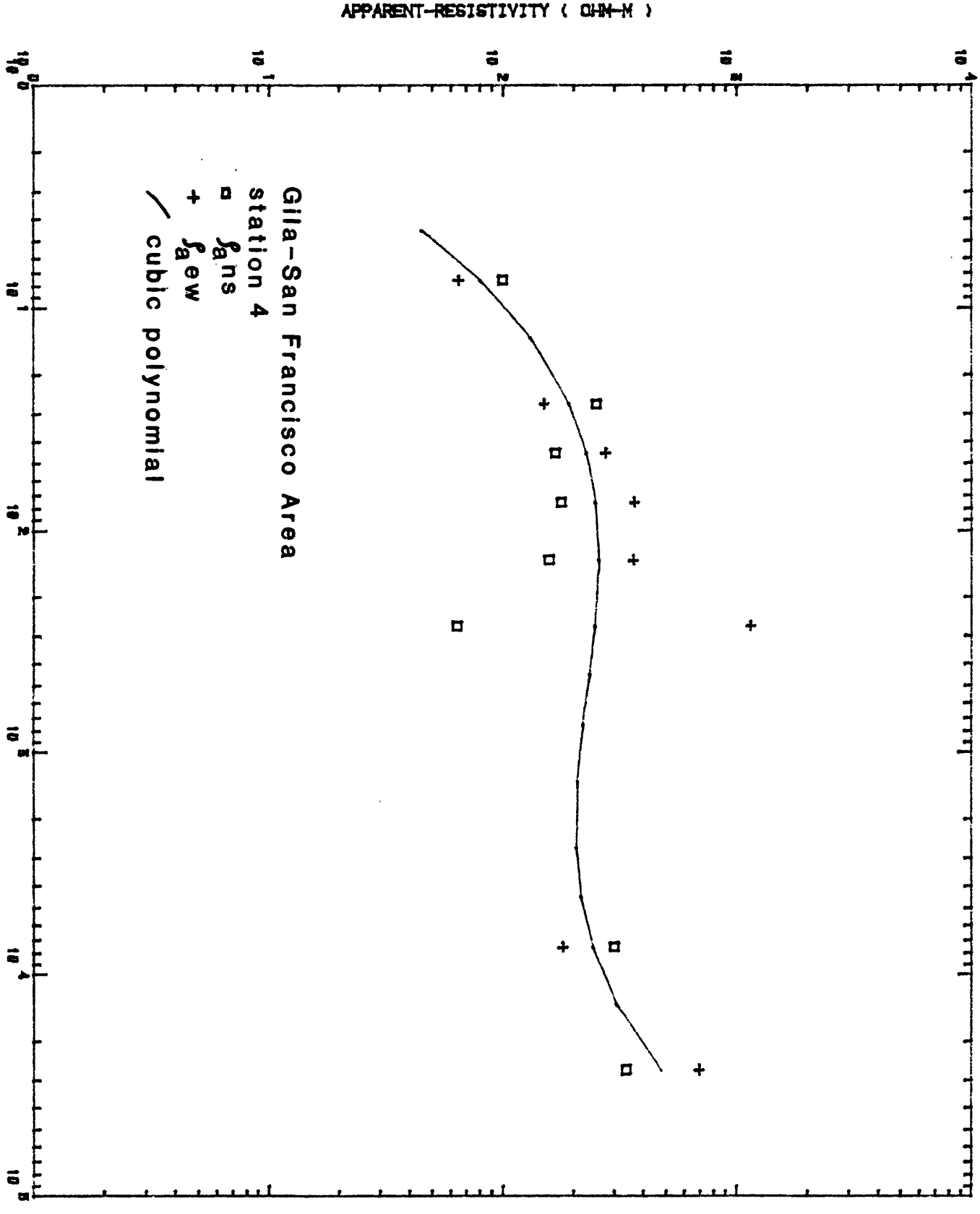
APPARENT-RESISTIVITY (OHM-M)
FREQUENCY (HERTZ)
Gila-San Francisco Area
station 4
□ ρ_{ans}
+ ρ_{aew}
cubic polynomial

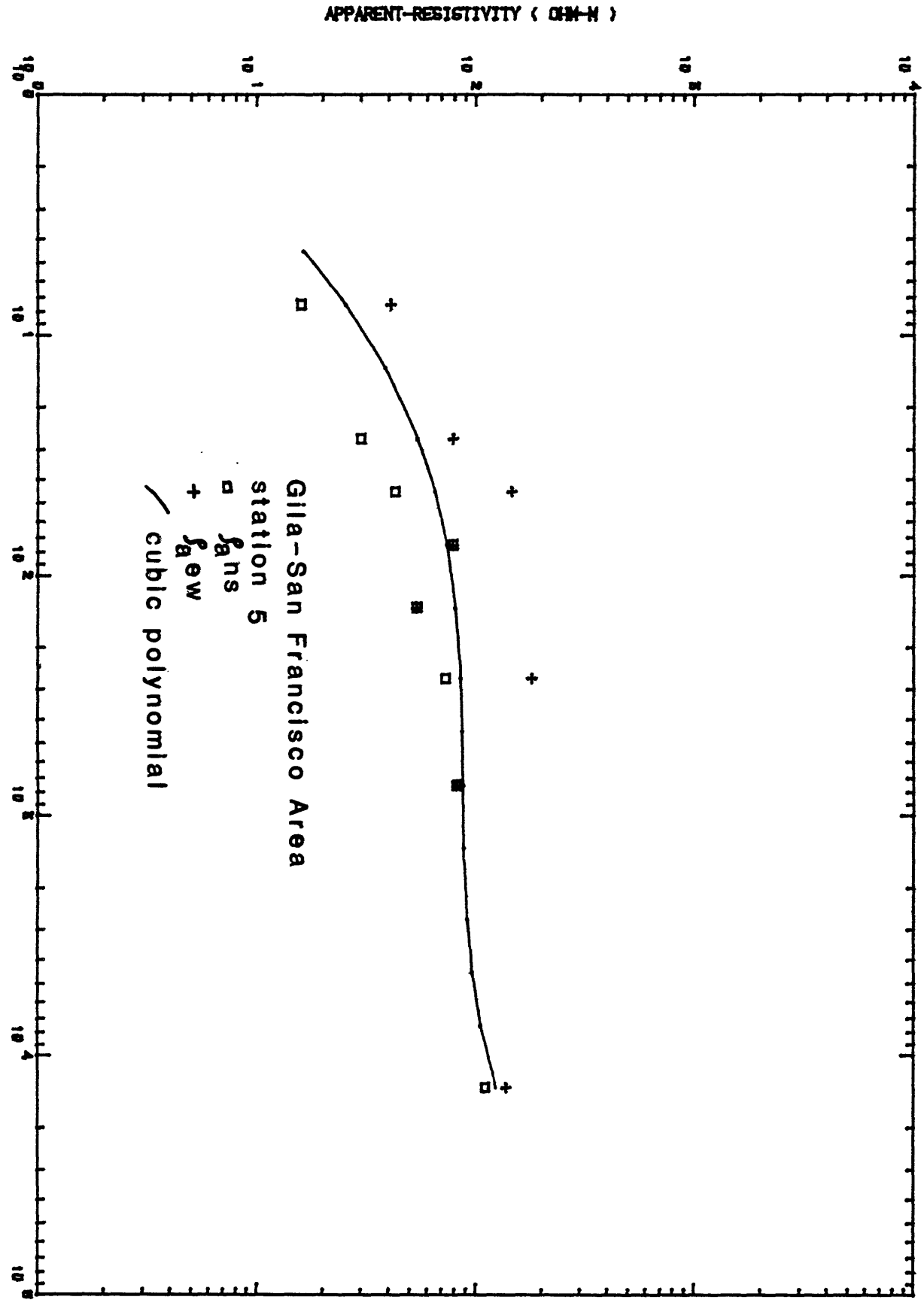
APPARENT-RESISTIVITY (OHM-M)
FREQUENCY (HERTZ)
Gila-San Francisco Area
station 5
□ ρ_{ans}
+ ρ_{aew}
/ cubic polynomial

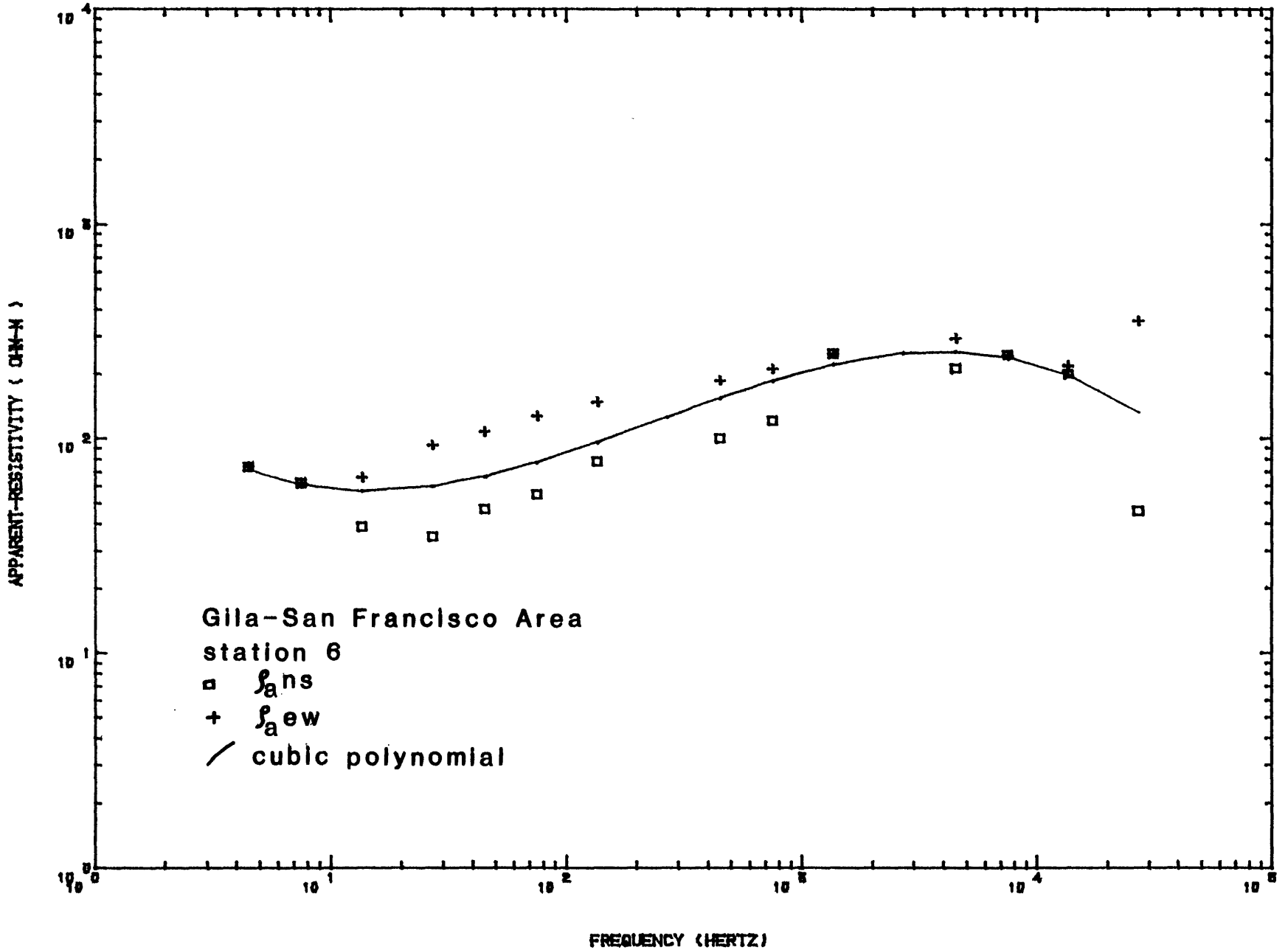
APPARENT-RESISTIVITY (OHM-M)
FREQUENCY (HERTZ)
Gila-San Francisco Area
station 6
ρ_a ns
ρ_a ew
cubic polynomial

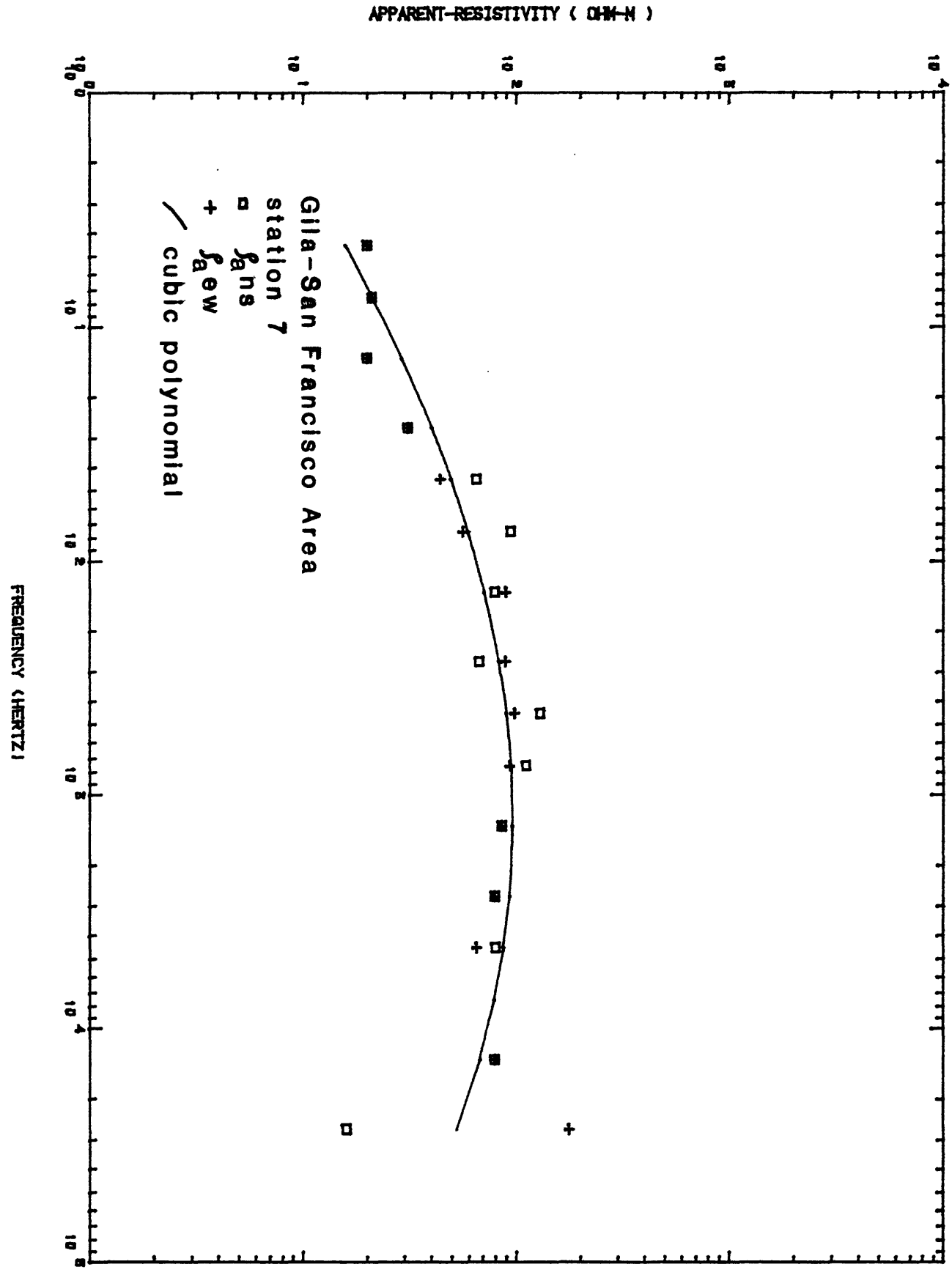
APPARENT-RESISTIVITY (OHM-M)
FREQUENCY (HERTZ)
Gila-San Francisco Area
station 7
□ ρ_a ns
+ ρ_a ew
/ cubic polynomial

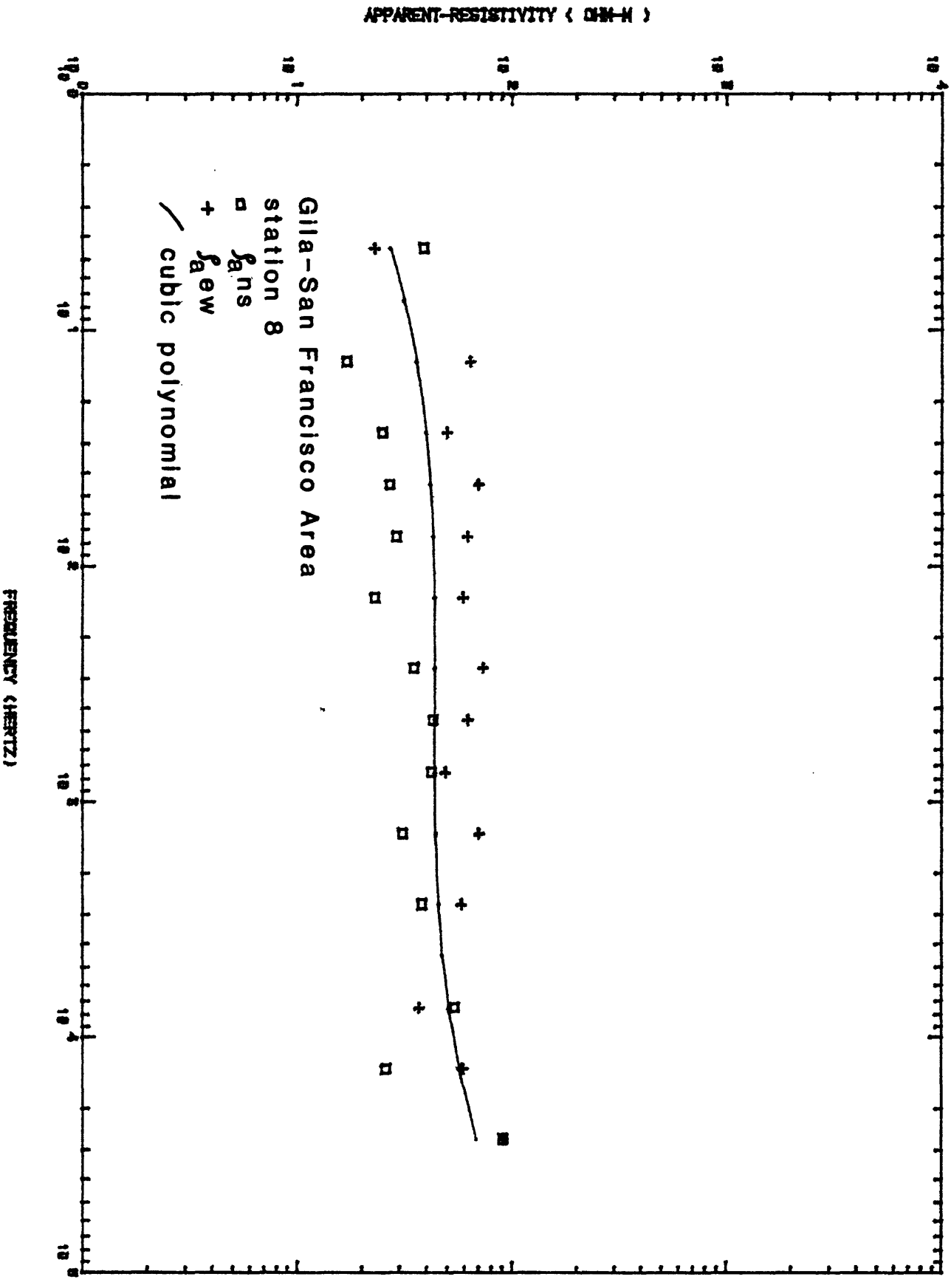
APPARENT-RESISTIVITY (OHM-M)
FREQUENCY (HERTZ)
Gila-San Francisco Area
station 8
□ ρ_{ans}
+ ρ_{aew}
/ cubic polynomial

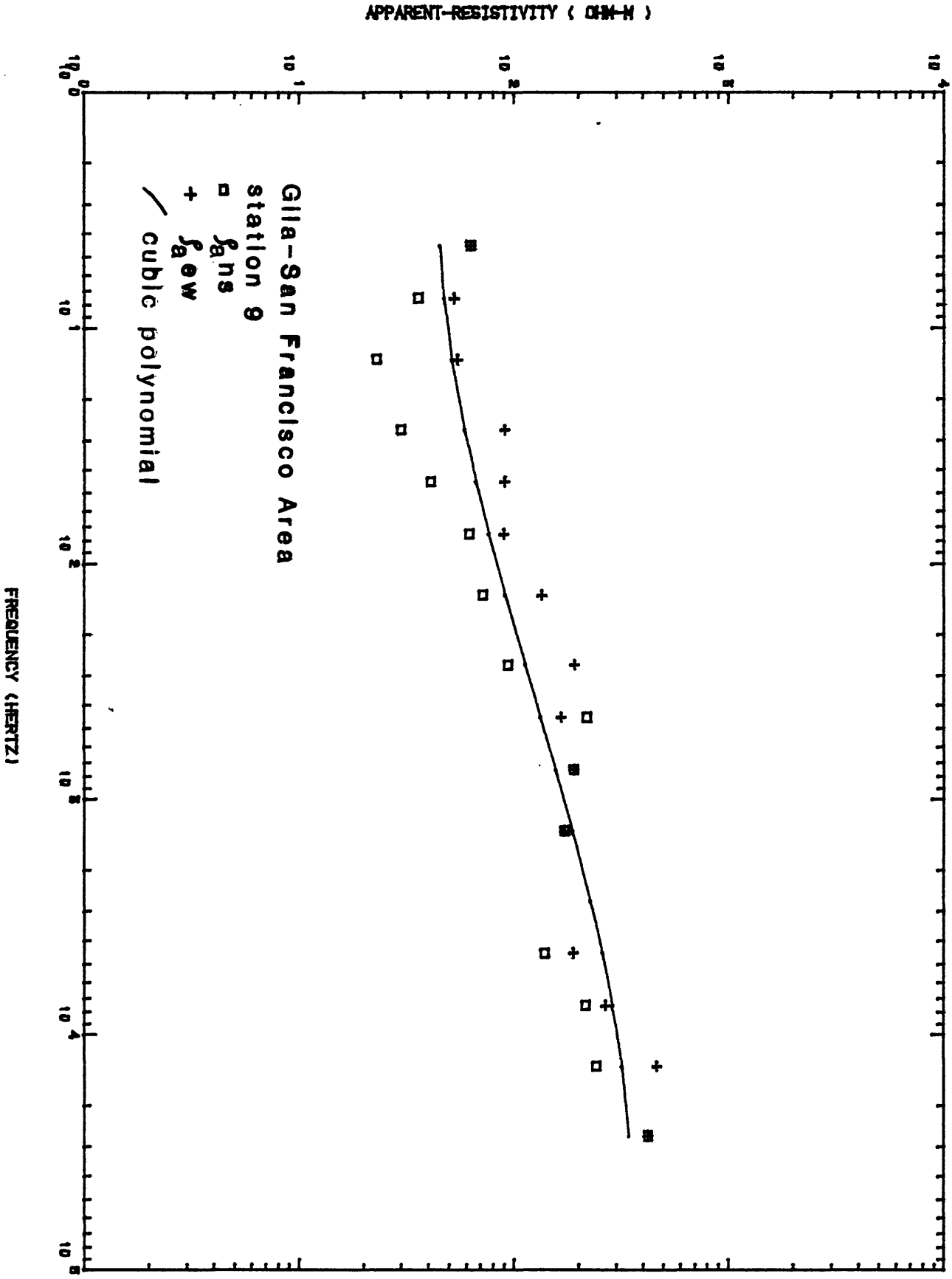
APPARENT-RESISTIVITY (OHM-M)
FREQUENCY (HERTZ)
Gila-San Francisco Area
station 9
□ ρ_{ans}
+ ρ_{aew}
/ cubic polynomial

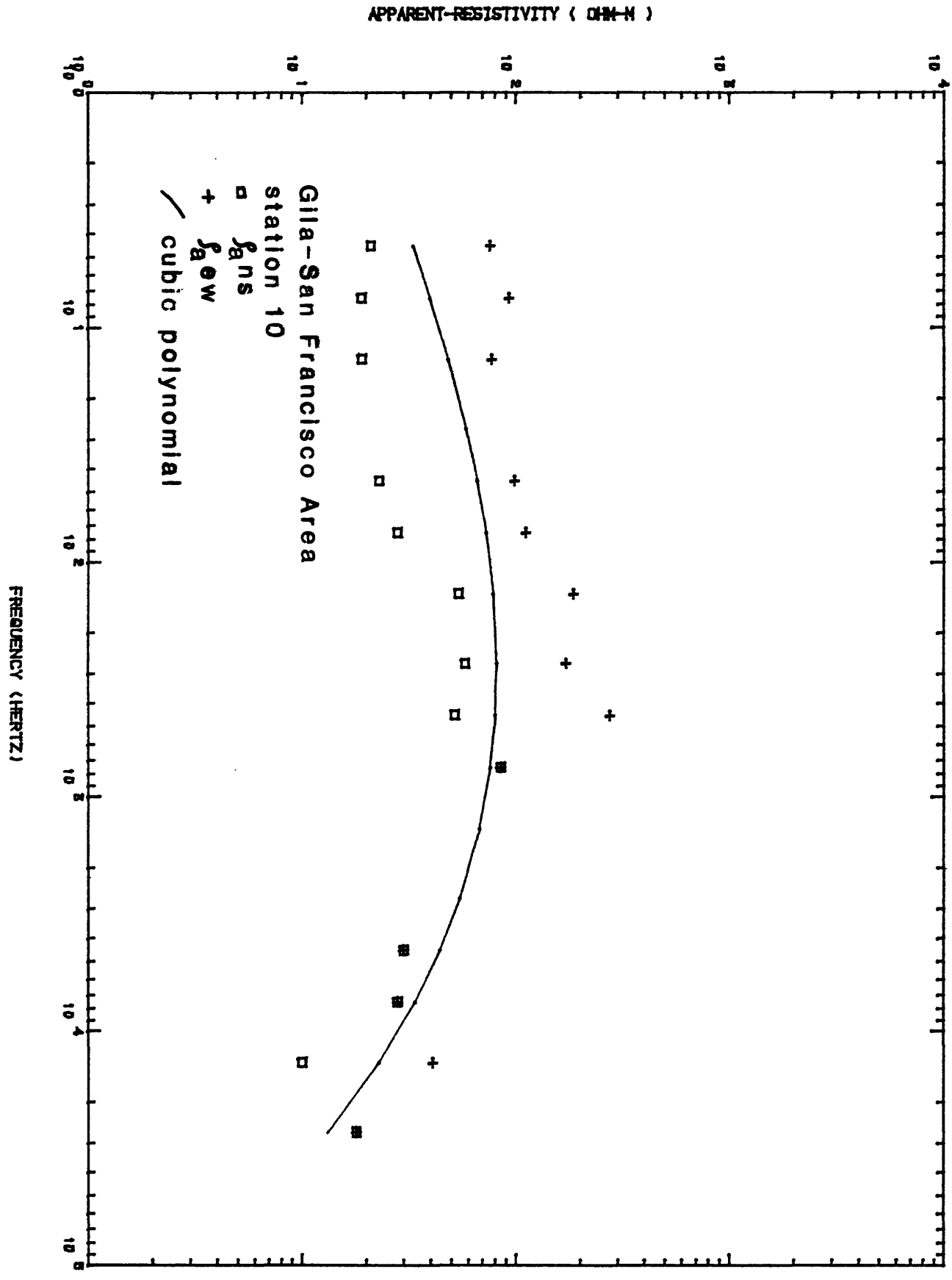
APPARENT-RESISTIVITY (OHM-M)
FREQUENCY (HERTZ)
Gila-San Francisco Area
station 10
□ ρ_{ans}
+ ρ_{aow}
cubic polynomial

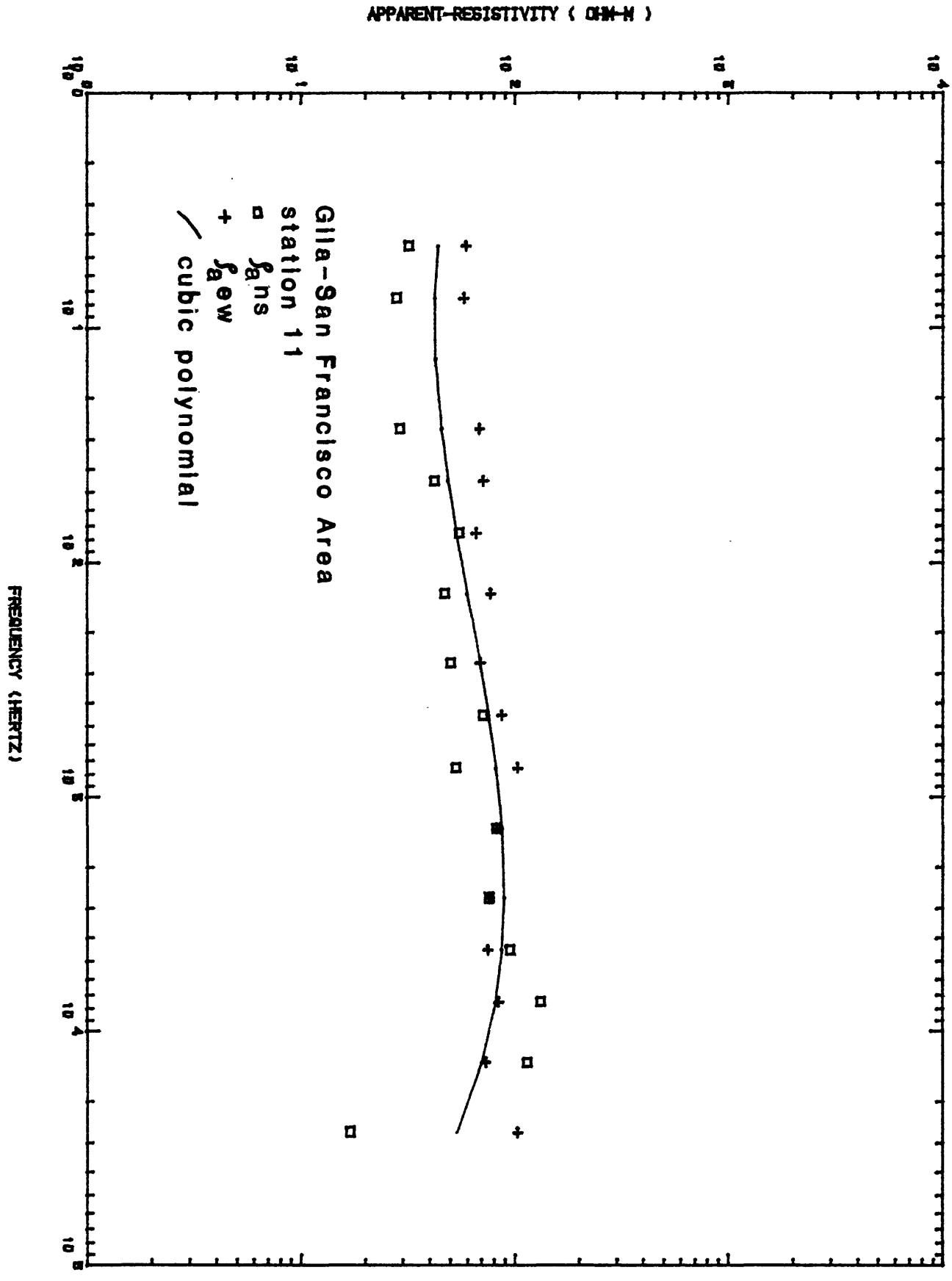
APPARENT-RESISTIVITY (OHM-M)
FREQUENCY (HERTZ)
Gila-San Francisco Area
station 11
□ ρ_{ans}
+ ρ_{aew}
cubic polynomial

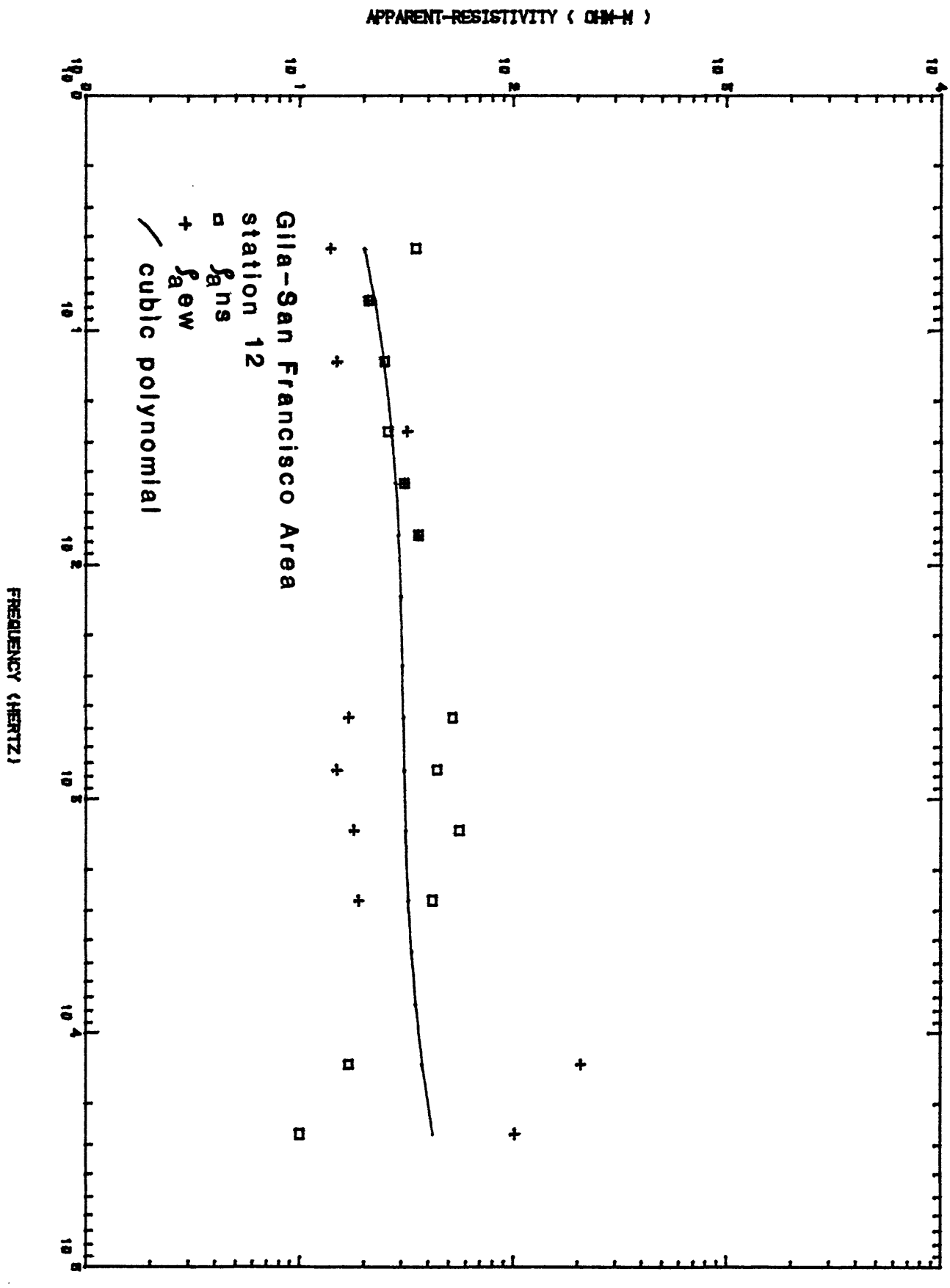
APPARENT-RESISTIVITY (OHM-M)
FREQUENCY (HERTZ)
Gila-San Francisco Area
station 12
□ ρ_{ans}
+ ρ_{aew}
cubic polynomial

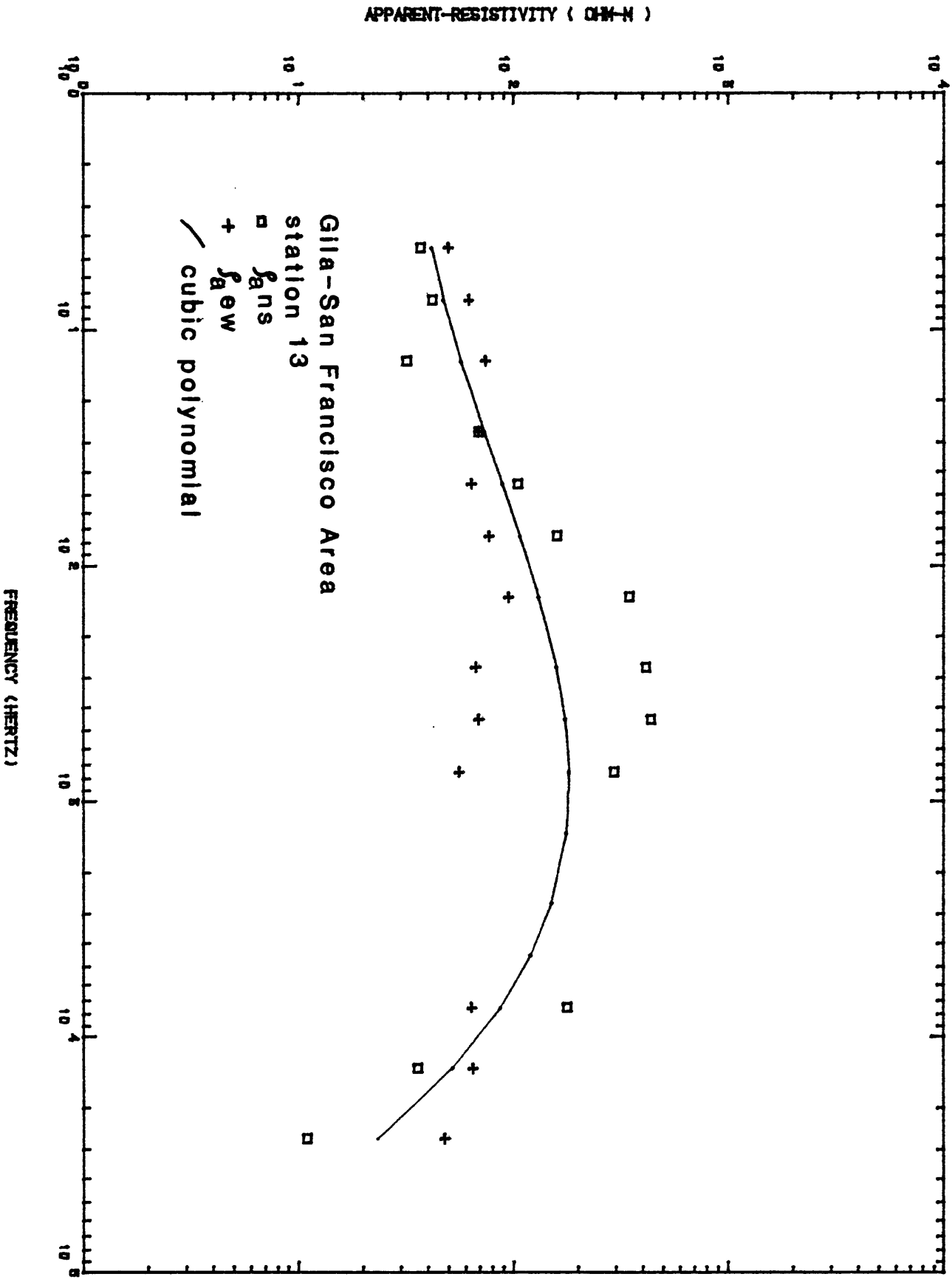
APPARENT-RESISTIVITY (OHM-M)
FREQUENCY (HERTZ)
Gila-San Francisco Area
station 13
□ ρans
+ ρaew
cubic polynomial

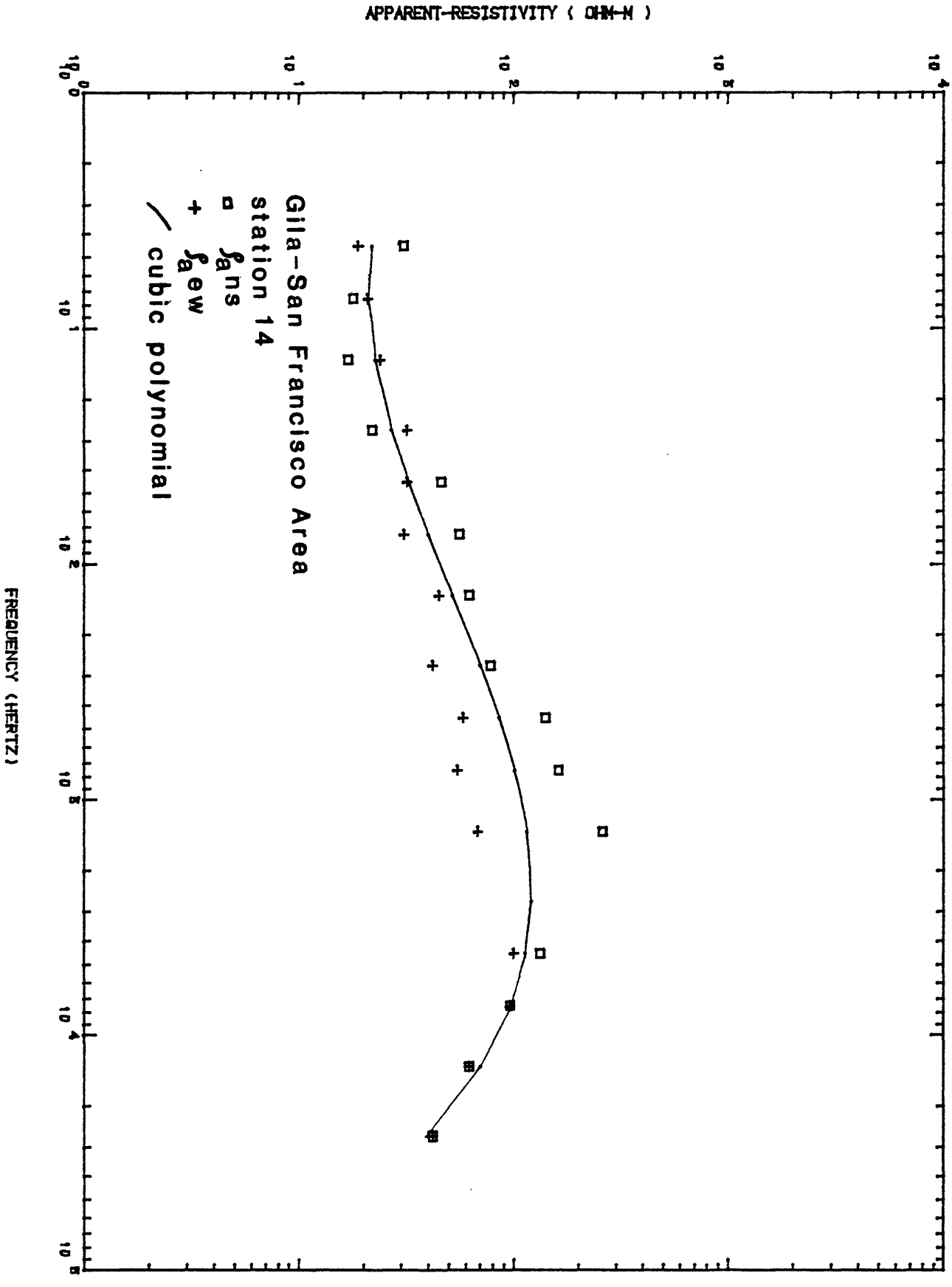
APPARENT-RESISTIVITY (OHM-M)
FREQUENCY (HERTZ)
Gila-San Francisco Area
station 14
□ ρa ns
+ ρa ew
/ cubic polynomial

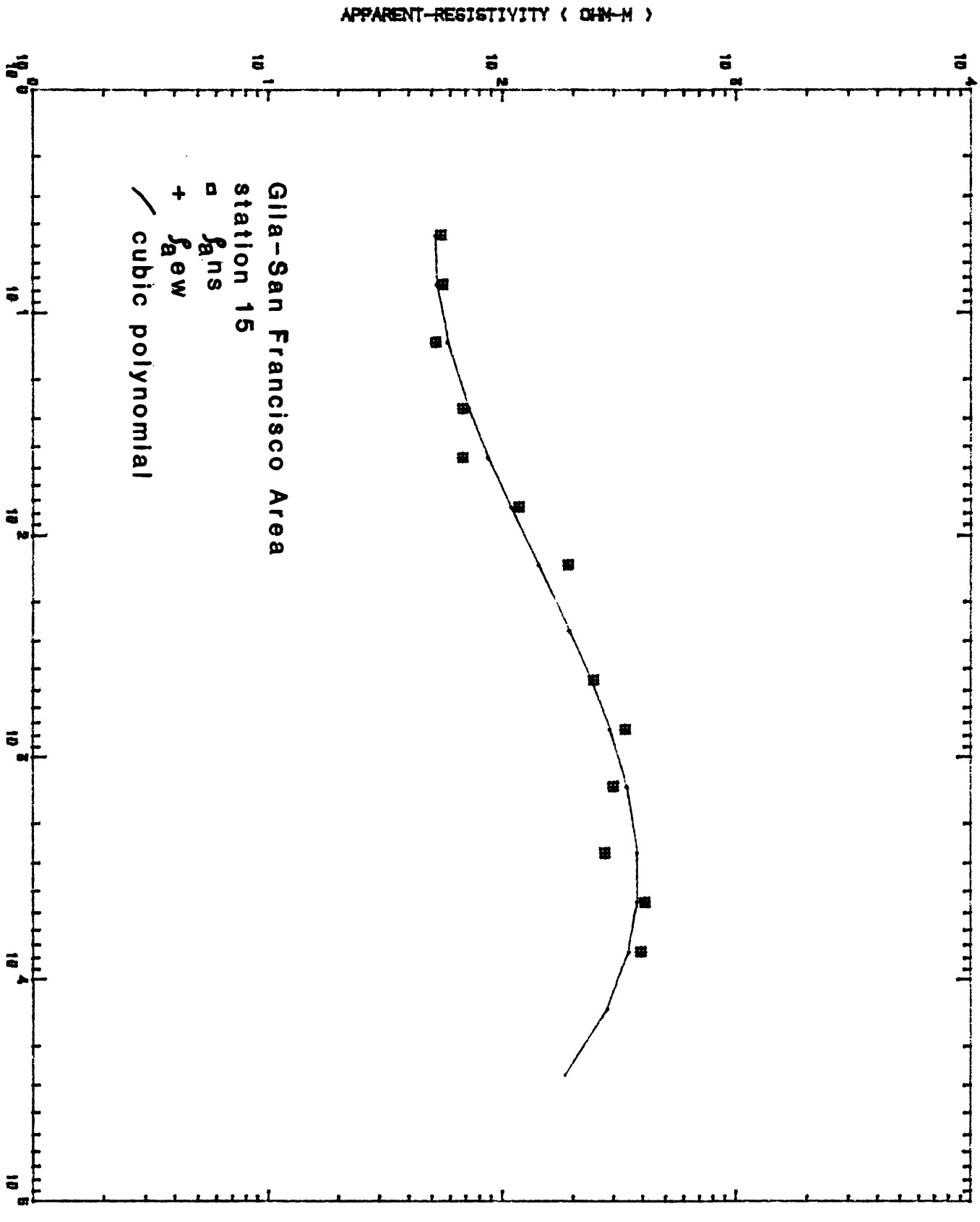
APPARENT-RESISTIVITY (OHM-M)
FREQUENCY (HERTZ)
Gila-San Francisco Area
station 15
□ ρ_{ans}
+ ρ_{aew}
/ cubic polynomial

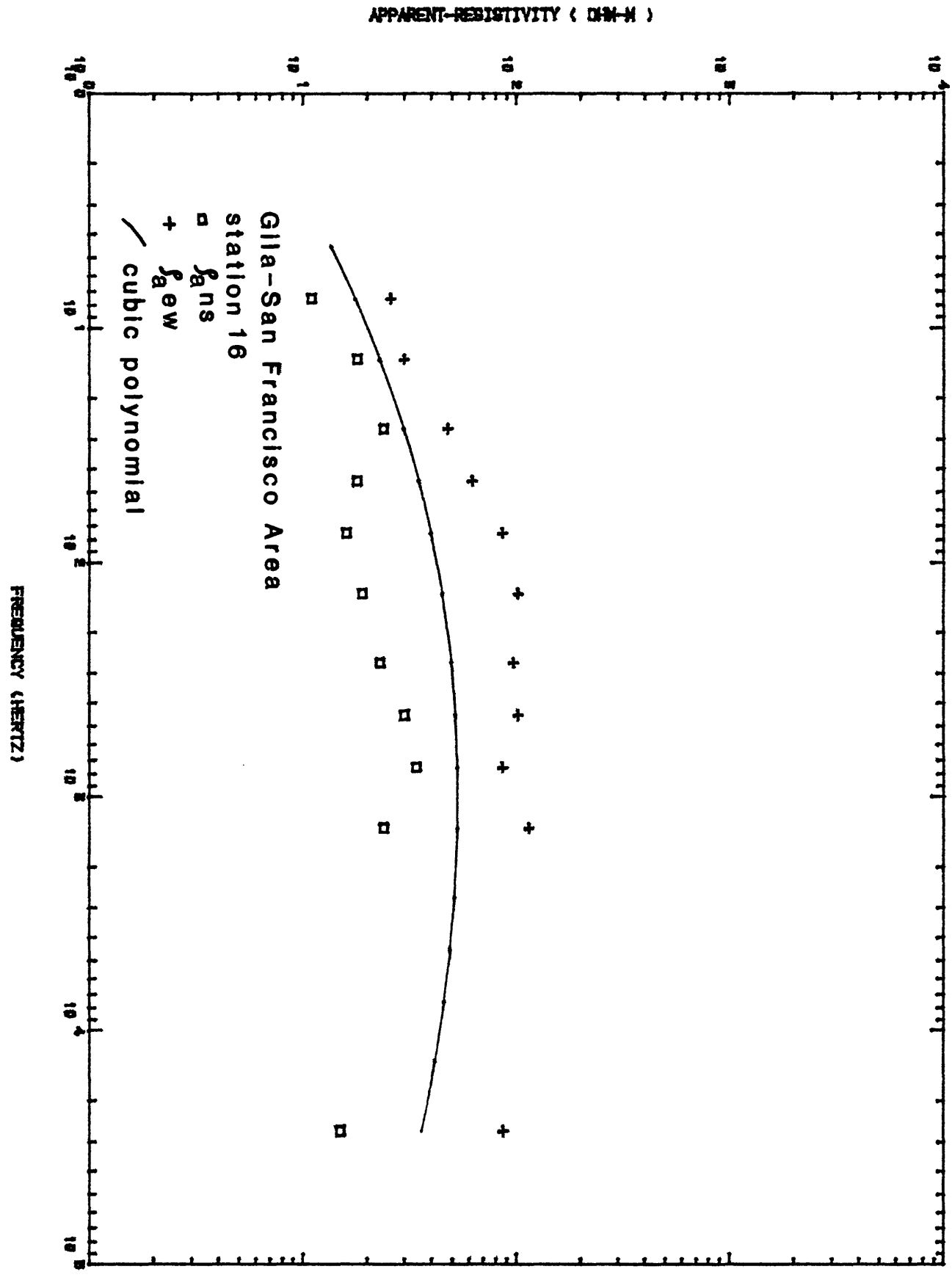
APPARENT-RESISTIVITY (OHM-M)
FREQUENCY (HERTZ)
Gila-San Francisco Area
station 16
□ ρ_{ans}
+ ρ_{aew}
cubic polynomial

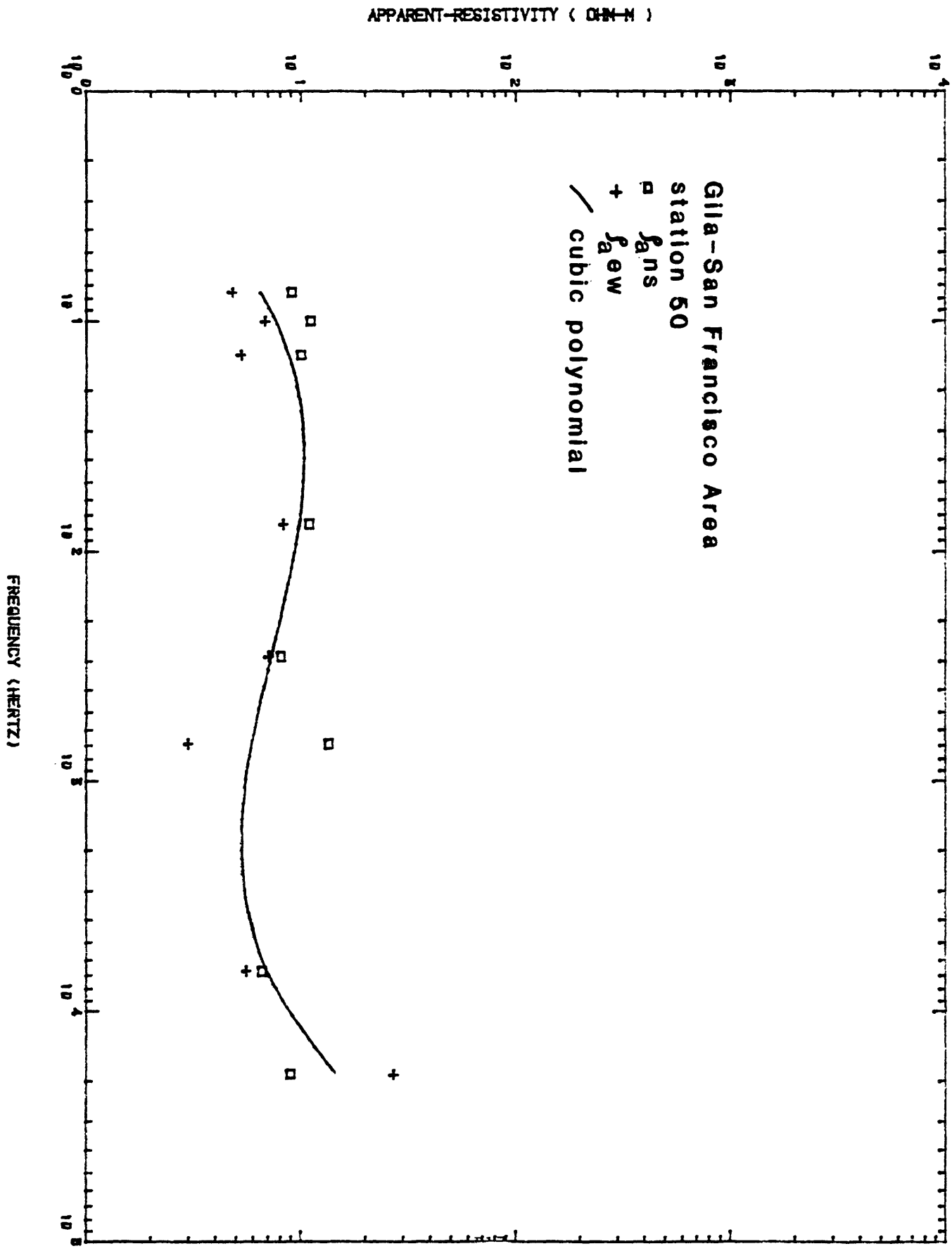
APPARENT-RESISTIVITY (OHM-M)
FREQUENCY (HERTZ)
Gila-San Francisco Area
station 50
□ ρ_a ns
+ ρ_a ew
/ cubic polynomial

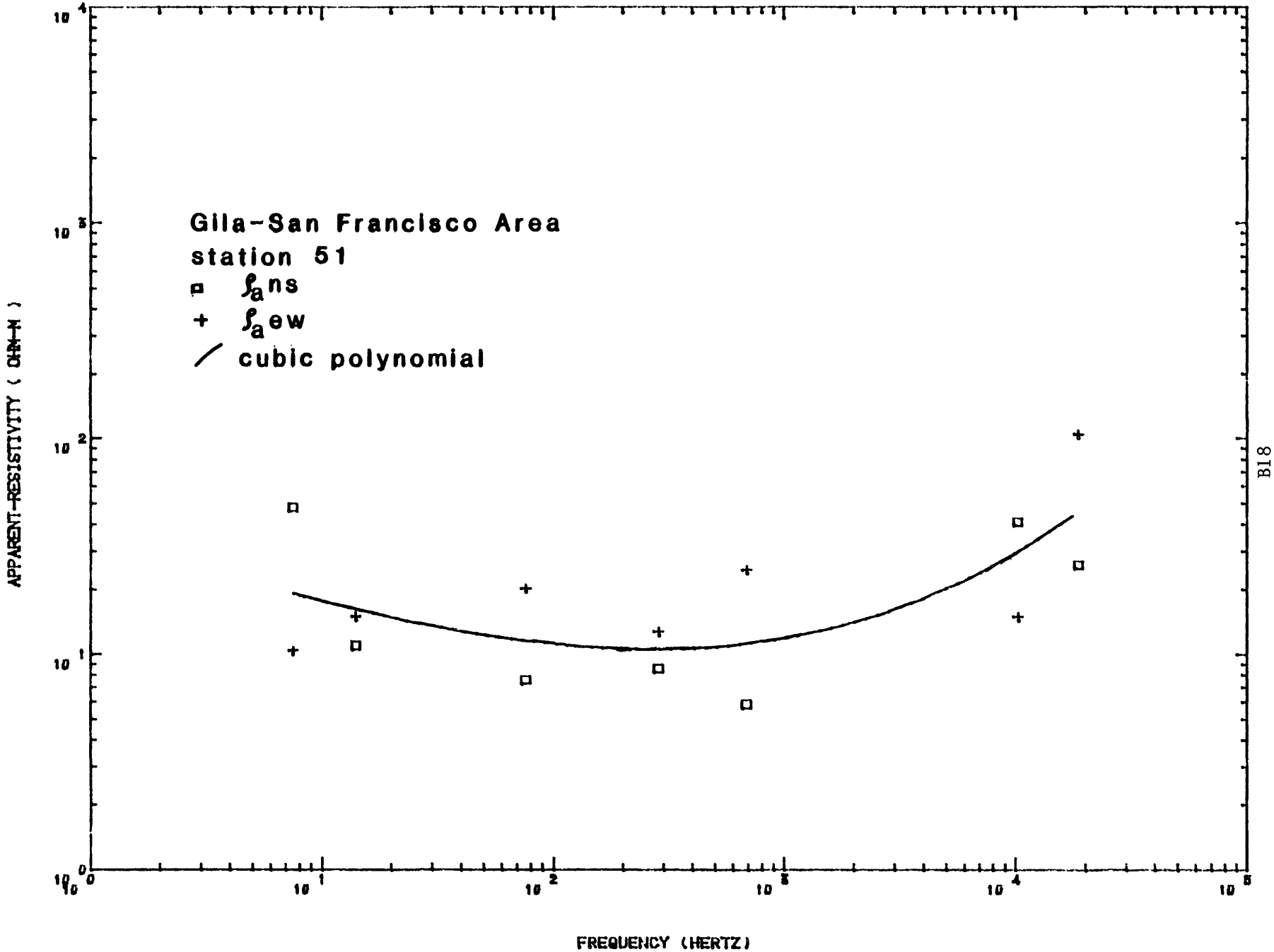
Gila-San Francisco Area
station 51
□ ρ_a ns
+ ρ_a ew
cubic polynomial
APPARENT RESISTIVITY (OHM-M)
FREQUENCY (HERTZ)
10^4
10^3
10^2
10^1
10^0
10^{-1}
10^0
10^1
10^2
10^3
10^4
10^5

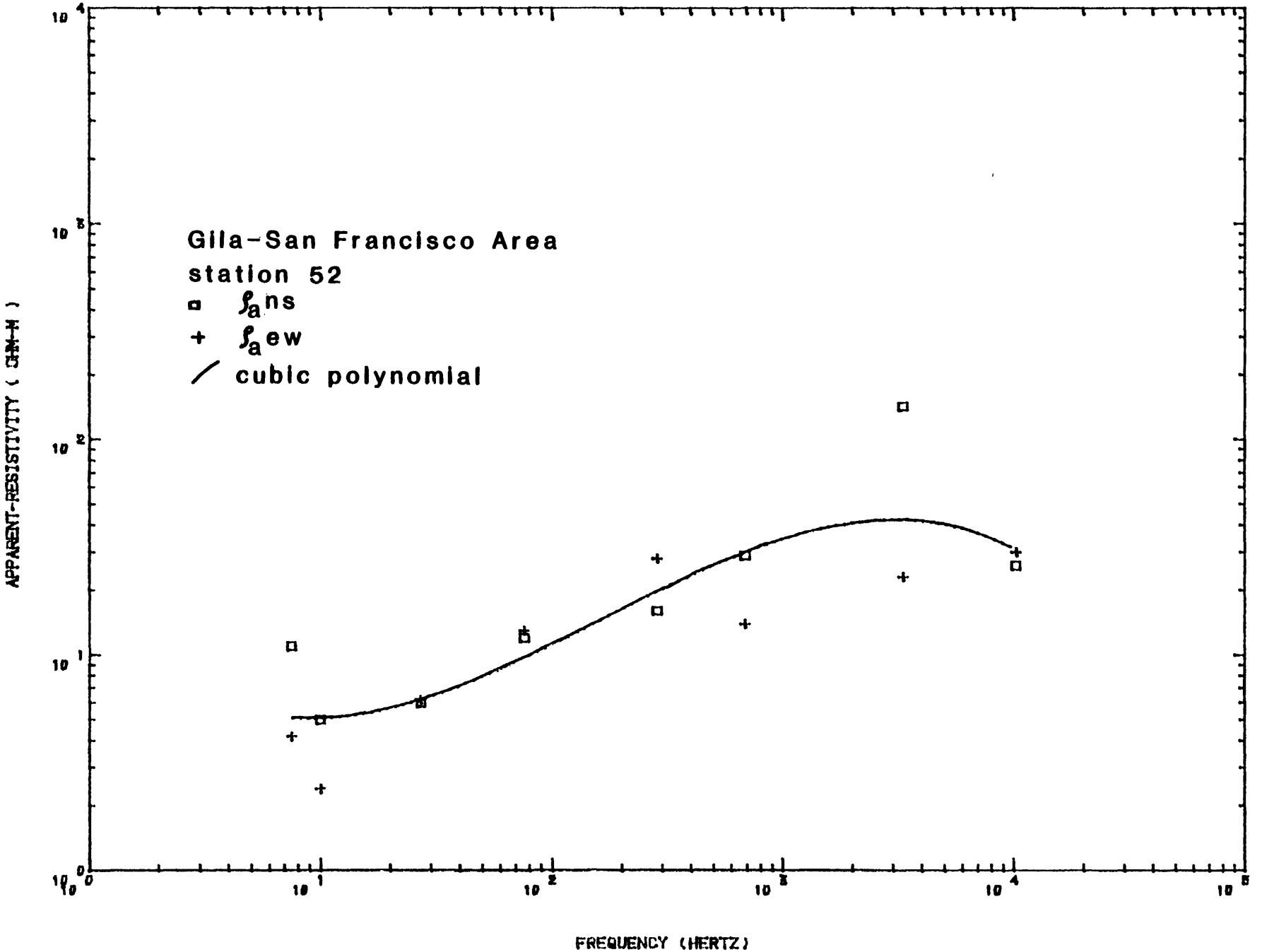
Gila-San Francisco Area
station 52
□ ρa ns
+ ρa ew
cubic polynomial
APPARENT-RESISTIVITY (OHM-M)
FREQUENCY (HERTZ)

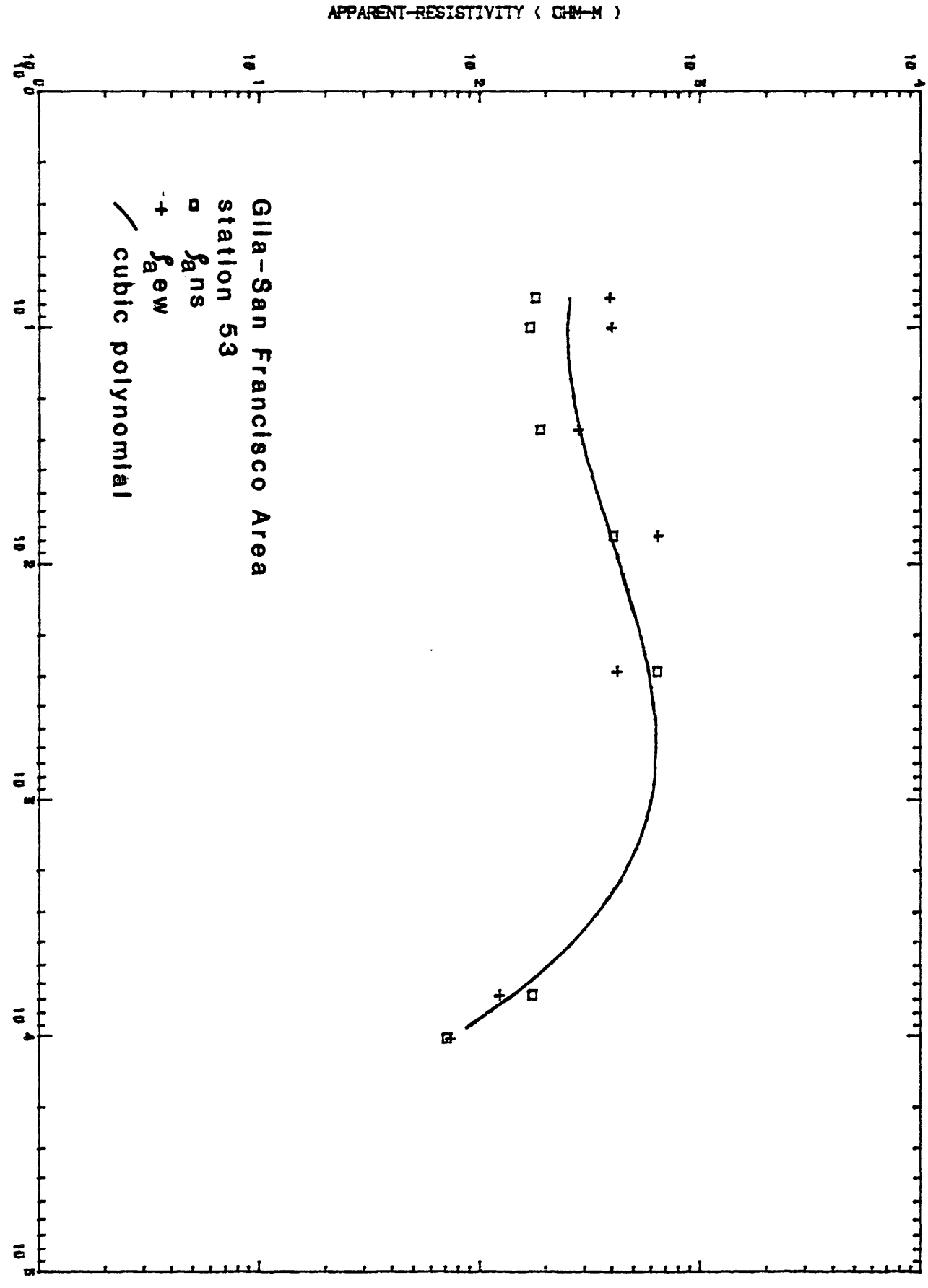
APPARENT-RESISTIVITY (OHM-M)
FREQUENCY (HERTZ)
Gila-San Francisco Area
station 53
□ ρ_a ns
+ ρ_a ew
cubic polynomial

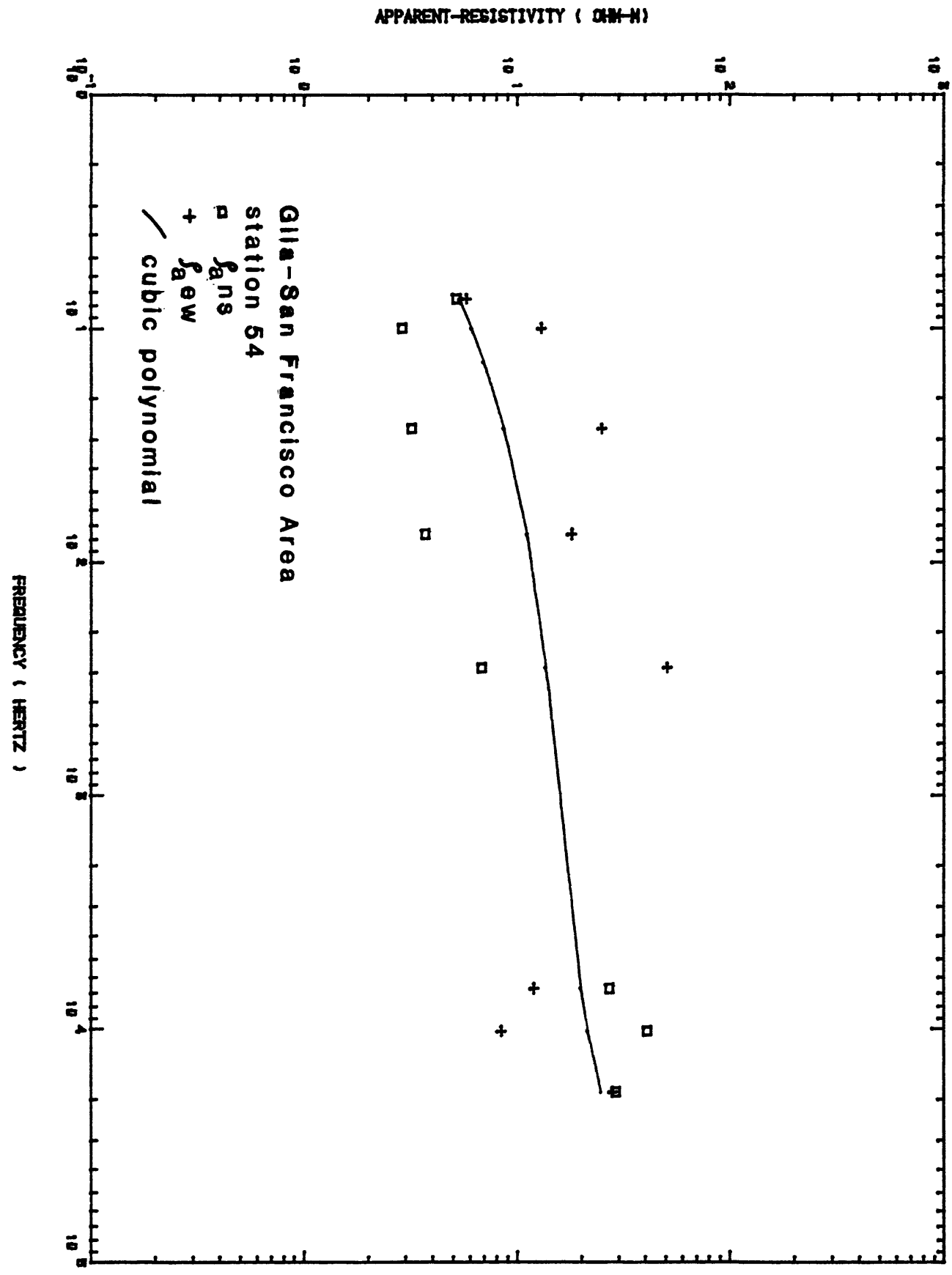
APPARENT-RESISTIVITY (OHM-M)
FREQUENCY (HERTZ)
Gila-San Francisco Area
station 54
□ $\rho_{a\,ns}$
+ $\rho_{a\,ew}$
cubic polynomial

Appendix C

Graphs of one-dimensional models of resistivity. Each bilogarithmic plot shows the resistivity-depth model (solid line) for each station along with the smoothed observed data (squares) and the forward solution (crosses) for the model presented. The observed data and the forward solution are plotted as apparent resistivity against apparent skin-depth. The starting model for each station was a layered equivalent to the Bostick transform of the bicubic polynomial approximation to the data (smoothed observed data) that is presented in Appendix B.

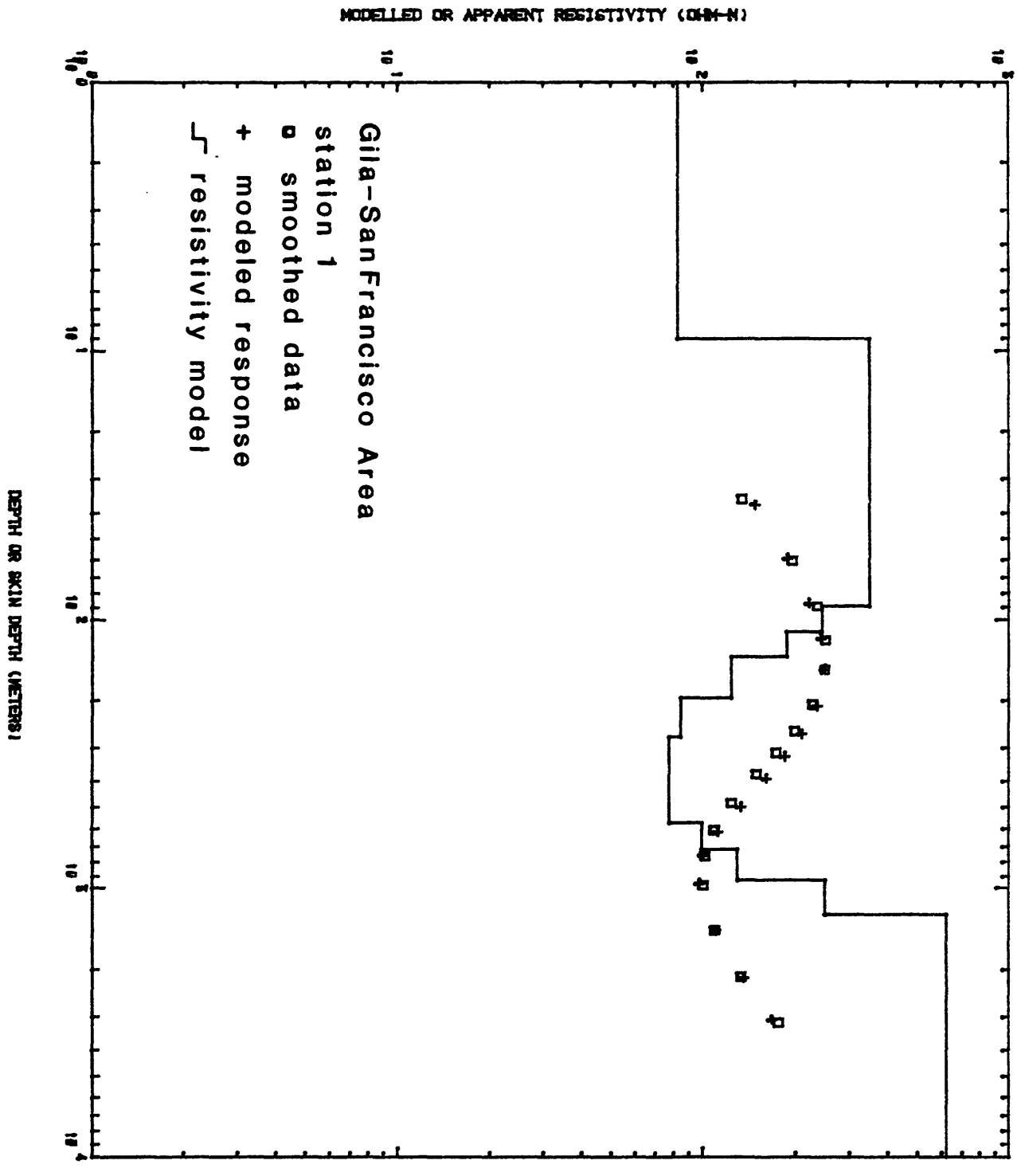
MODELLED OR APPARENT RESISTIVITY (OHM-M)
DEPTH OR SKIN DEPTH (METERS)
Gila-SanFrancisco Area
station 1
smoothed data
modeled response
resistivity model

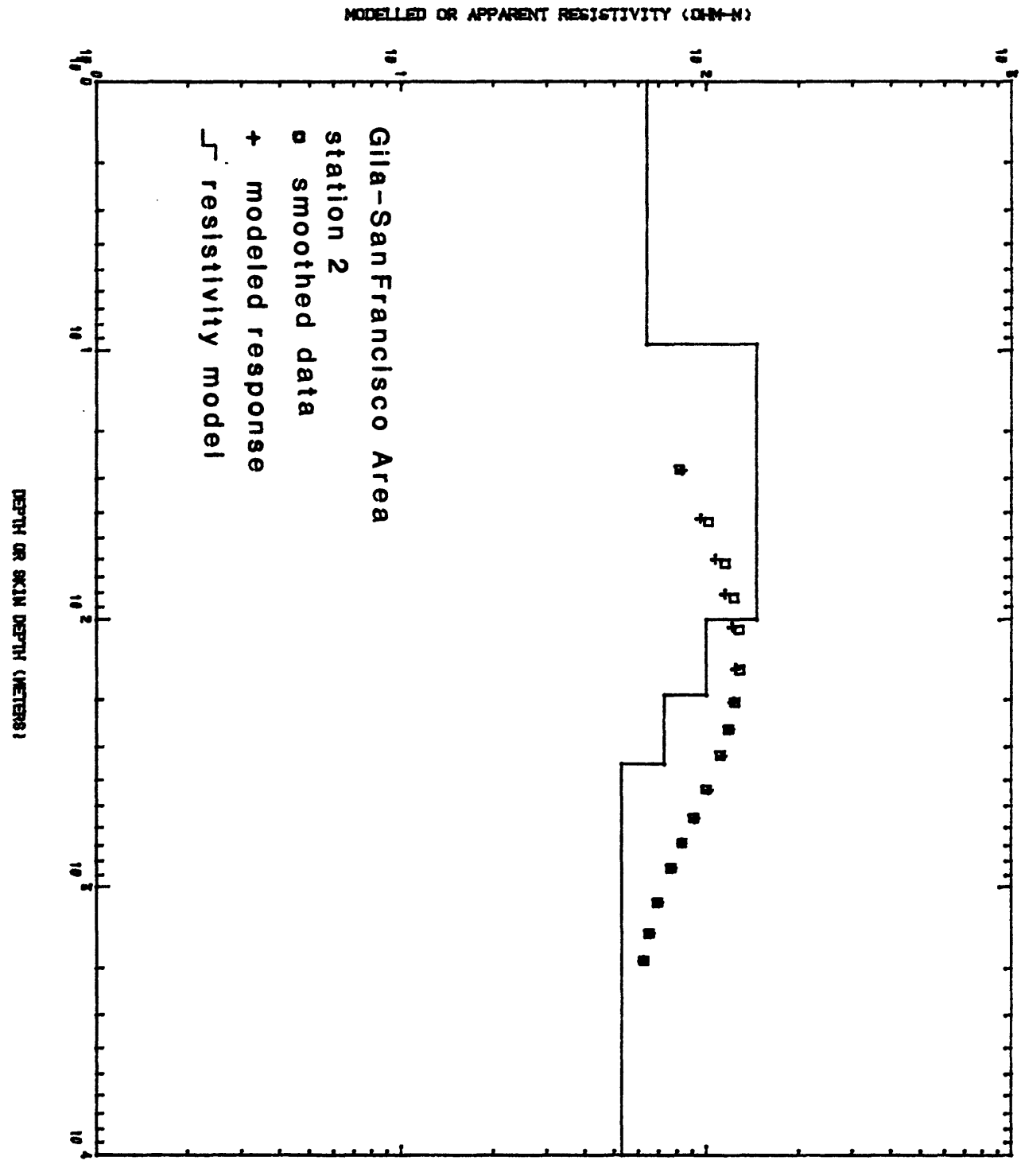
MODELLED OR APPARENT RESISTIVITY (OHM-M)
DEPTH OR SKIN DEPTH (METERS)
Gila-San Francisco Area
station 2
smoothed data
modeled response
resistivity model

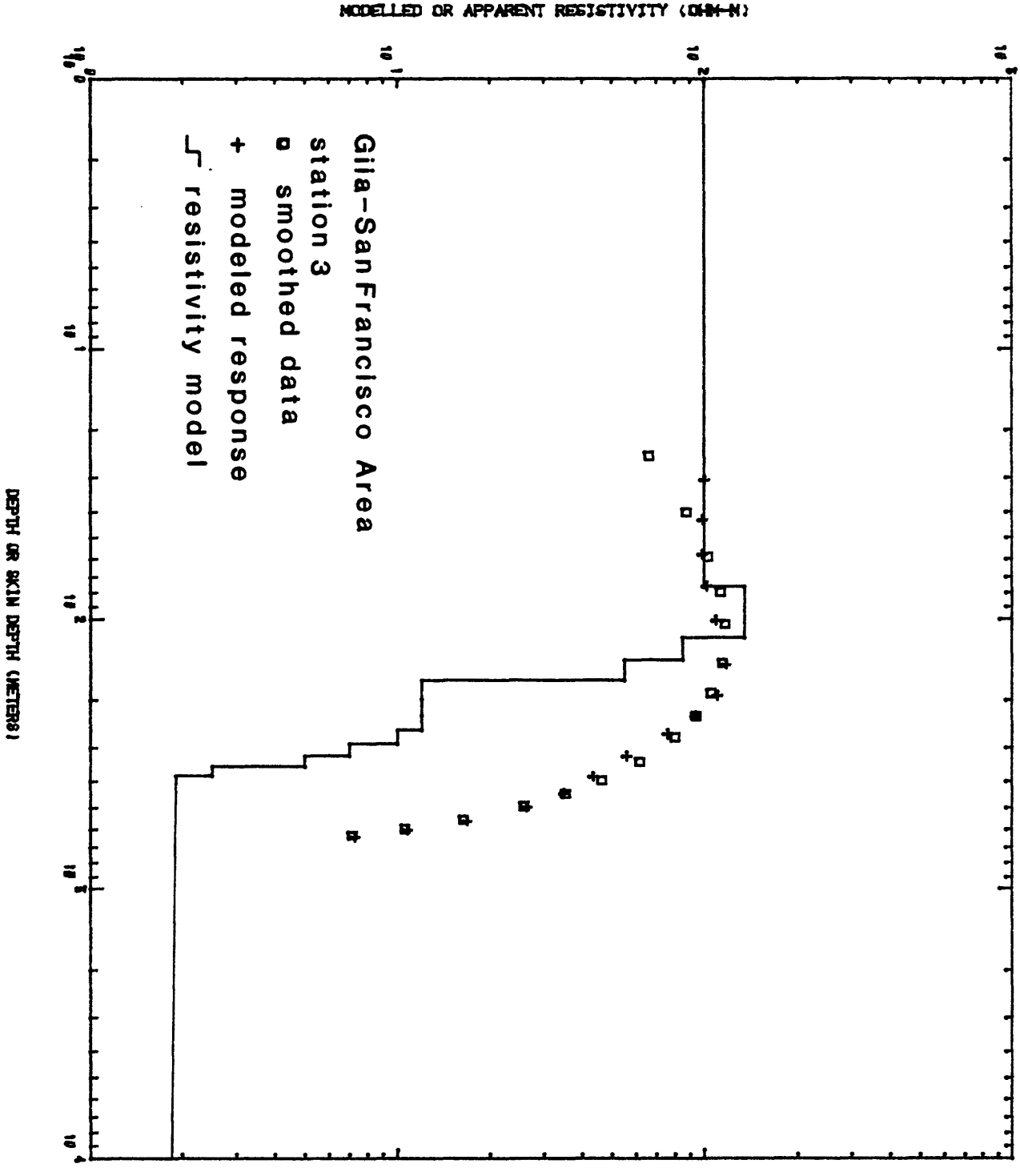
MODELLED OR APPARENT RESISTIVITY (OHM-M)
DEPTH OR SKIN DEPTH (METERS)
Gila-San Francisco Area
station 3
smoothed data
modeled response
resistivity model

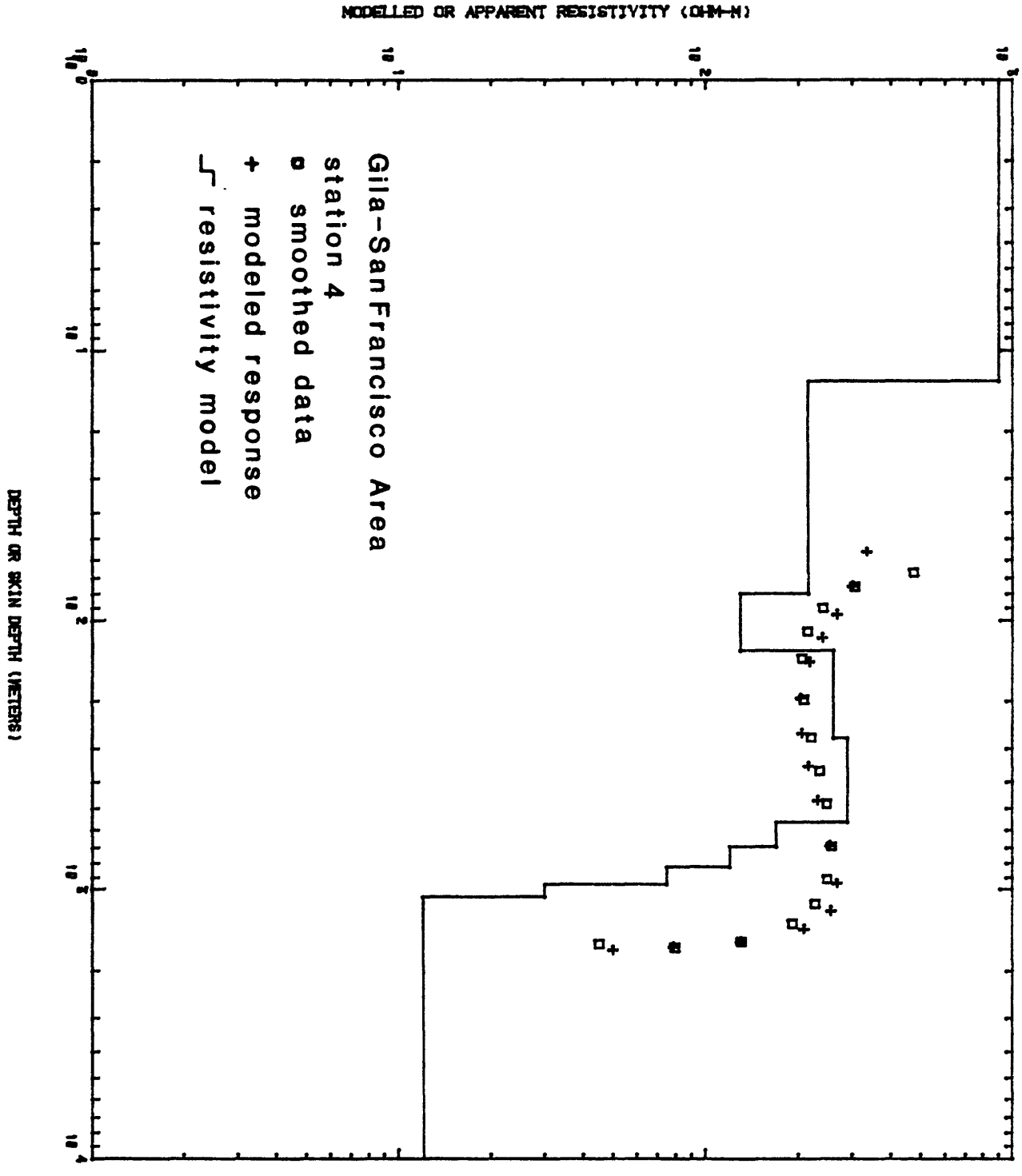
MODELLED OR APPARENT RESISTIVITY (OHM-M)
DEPTH OR SKIN DEPTH (METERS)
Gila-San Francisco Area
station 4
smoothed data
modeled response
resistivity model

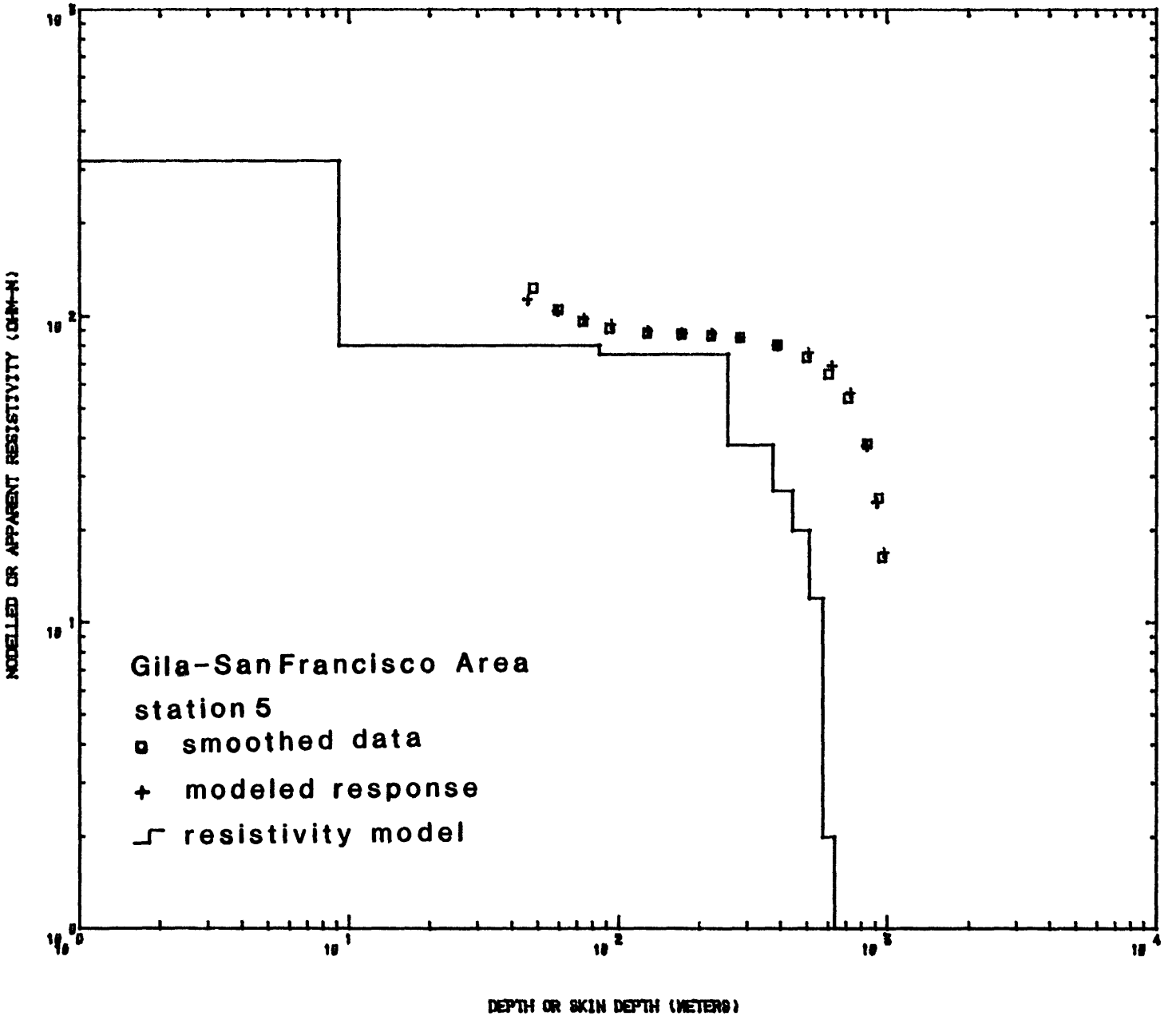
MODELLED OR APPARENT RESISTIVITY (OHM-M)
DEPTH OR SKIN DEPTH (METERS)
Gila-San Francisco Area
station 5
smoothed data
modeled response
resistivity model

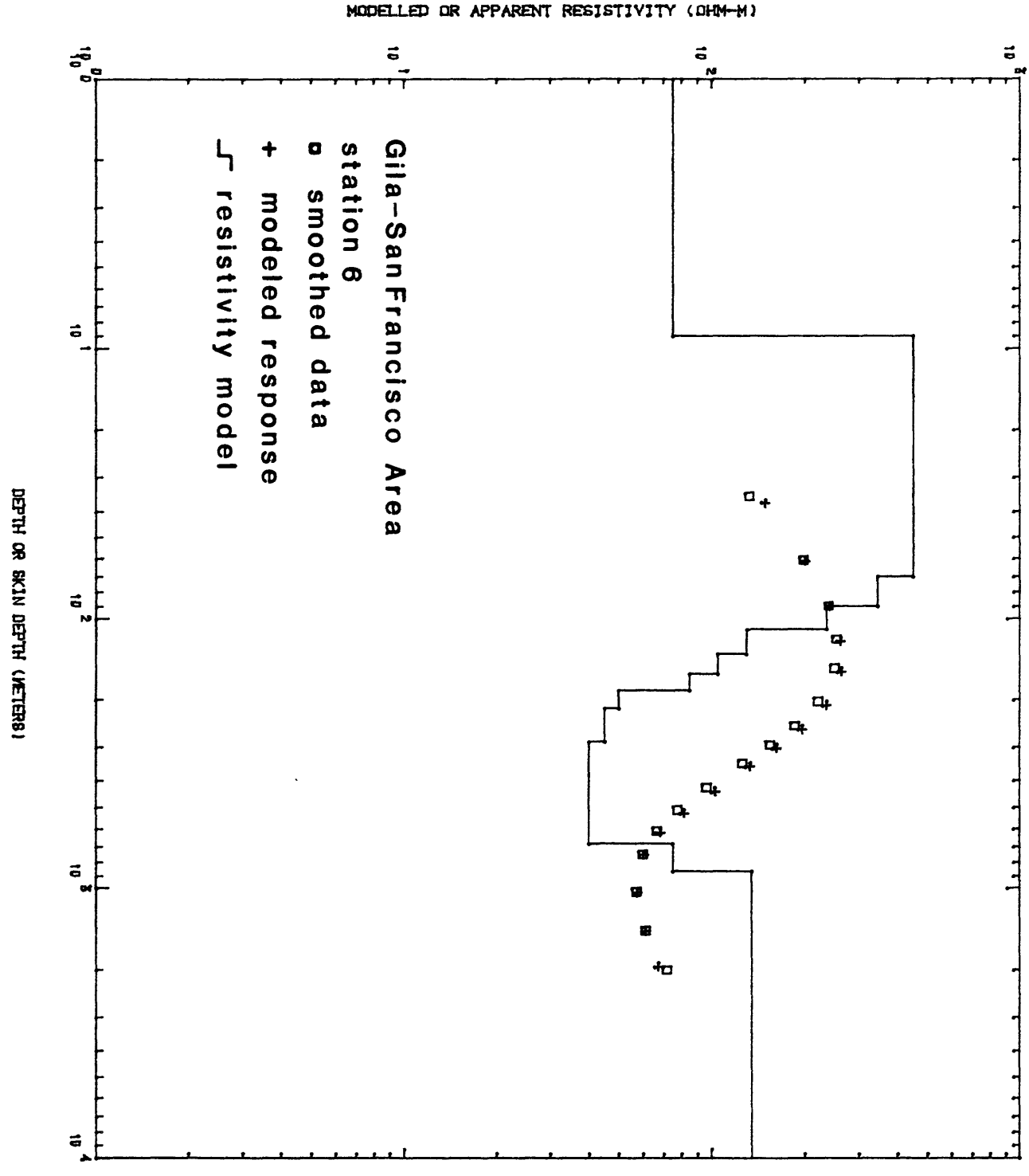
MODELLED OR APPARENT RESISTIVITY (OHM-M)
DEPTH OR SKIN DEPTH (METERS)
Gila-San Francisco Area
station 6
smoothed data
modeled response
resistivity model

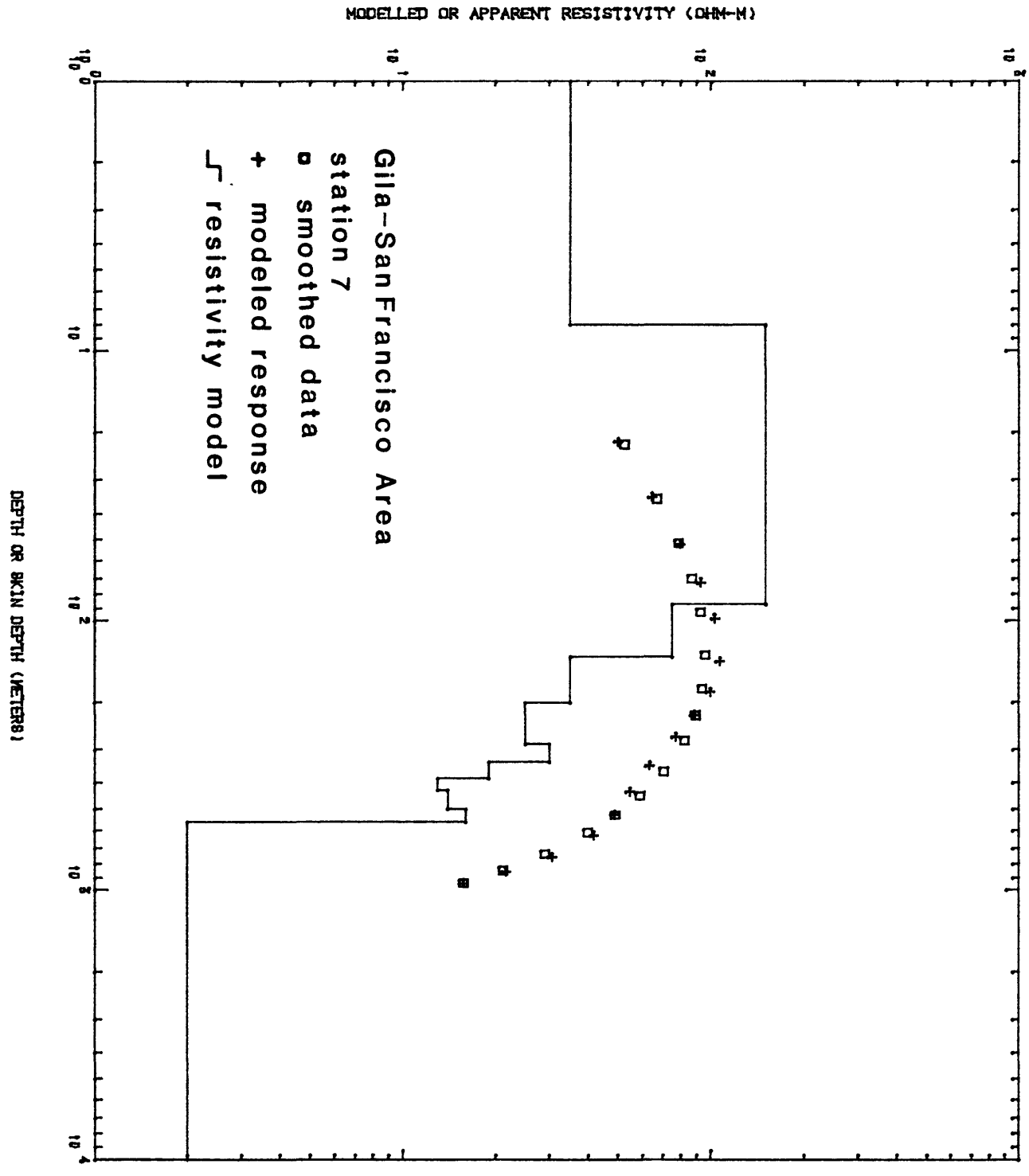
MODELLED OR APPARENT RESISTIVITY (OHM-M)
DEPTH OR SKIN DEPTH (METERS)
Gila-San Francisco Area
station 7
smoothed data
modeled response
resistivity model

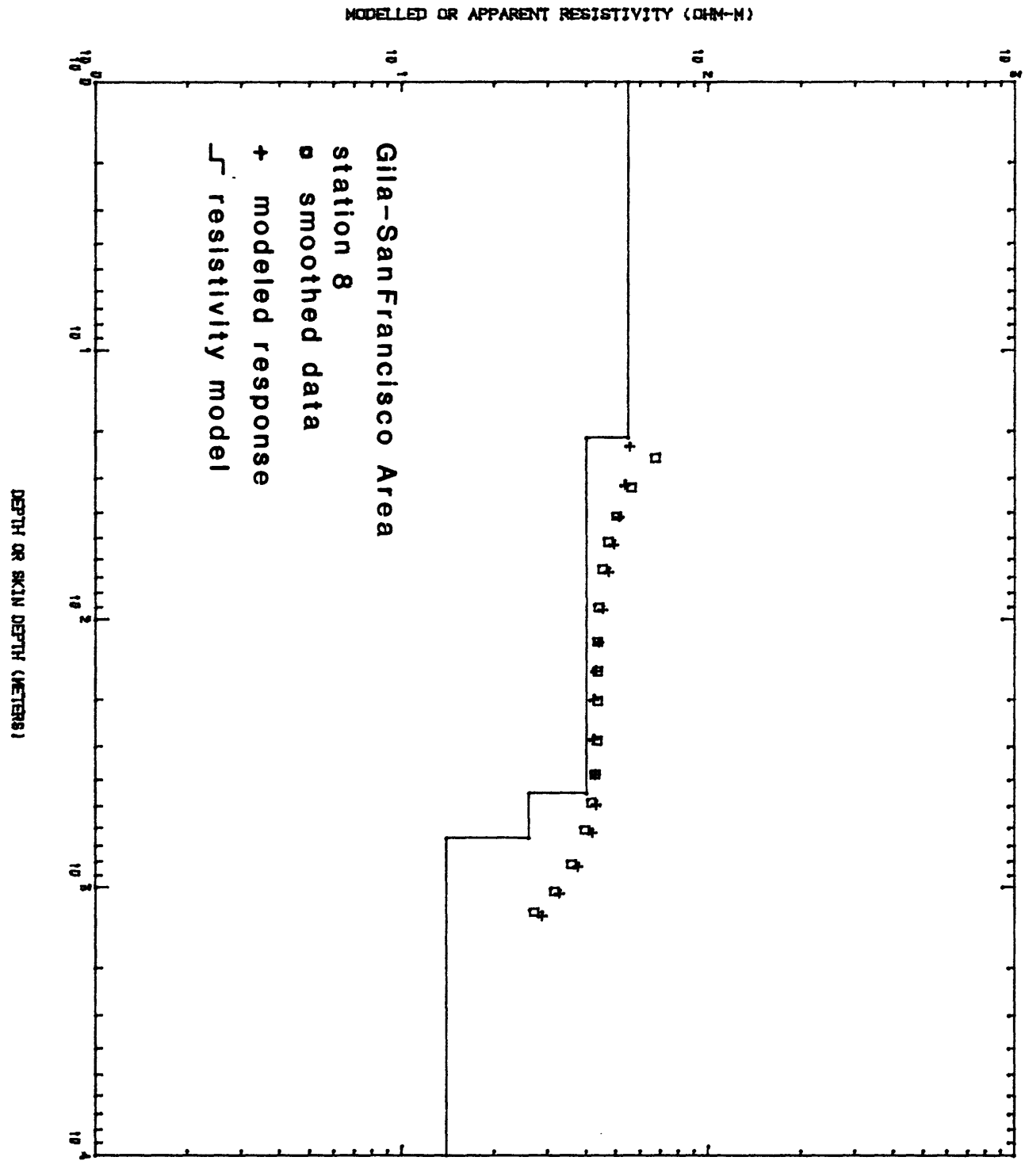
MODELLED OR APPARENT RESISTIVITY (OHM-M)
DEPTH OR SKIN DEPTH (METERS)
Gila-SanFrancisco Area
station 8
smoothed data
+ modeled response
resistivity model

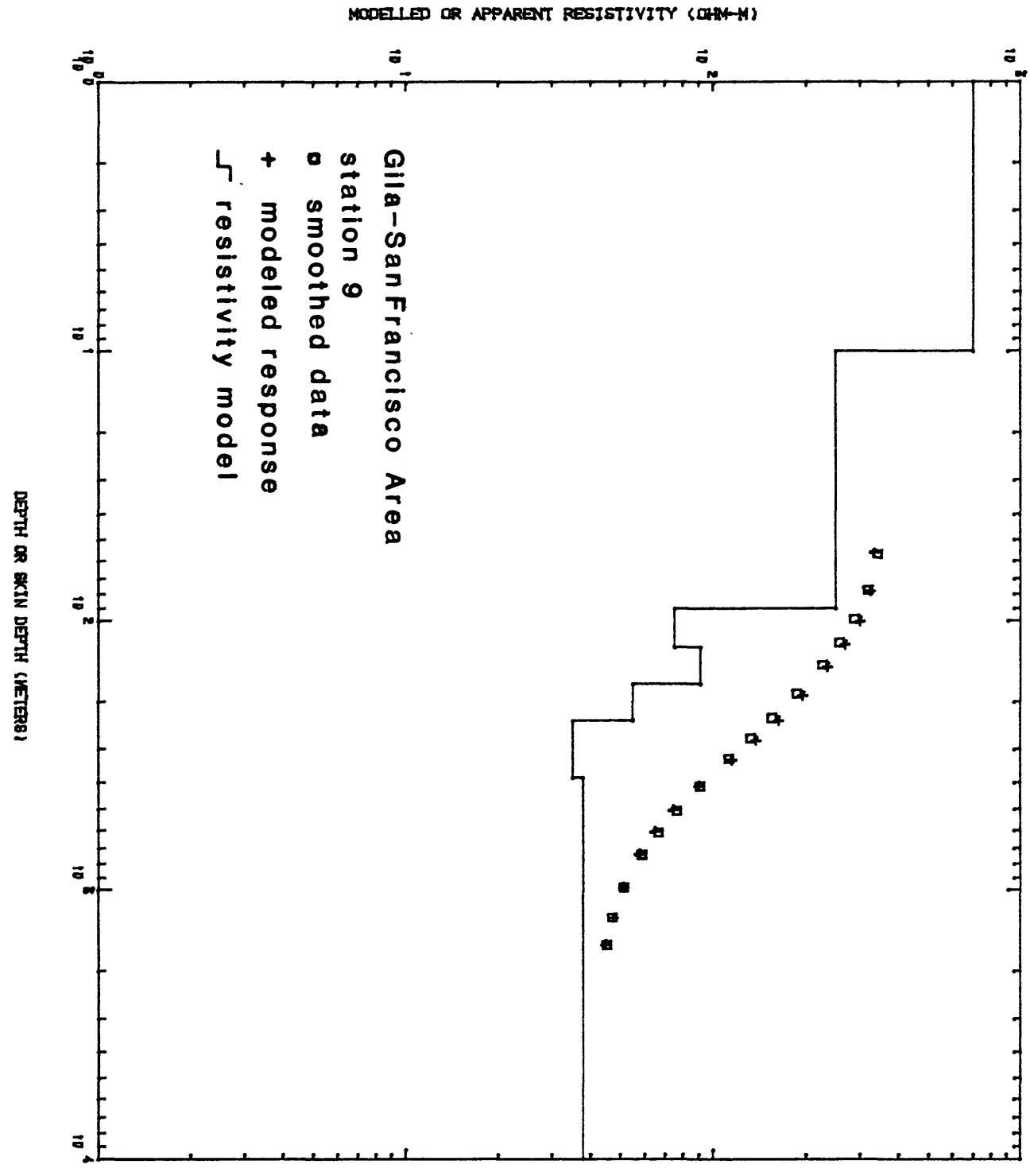
MODELLED OR APPARENT RESISTIVITY (OHM-M)
DEPTH OR SKIN DEPTH (METERS)
Gila-San Francisco Area
station 9
smoothed data
modeled response
resistivity model

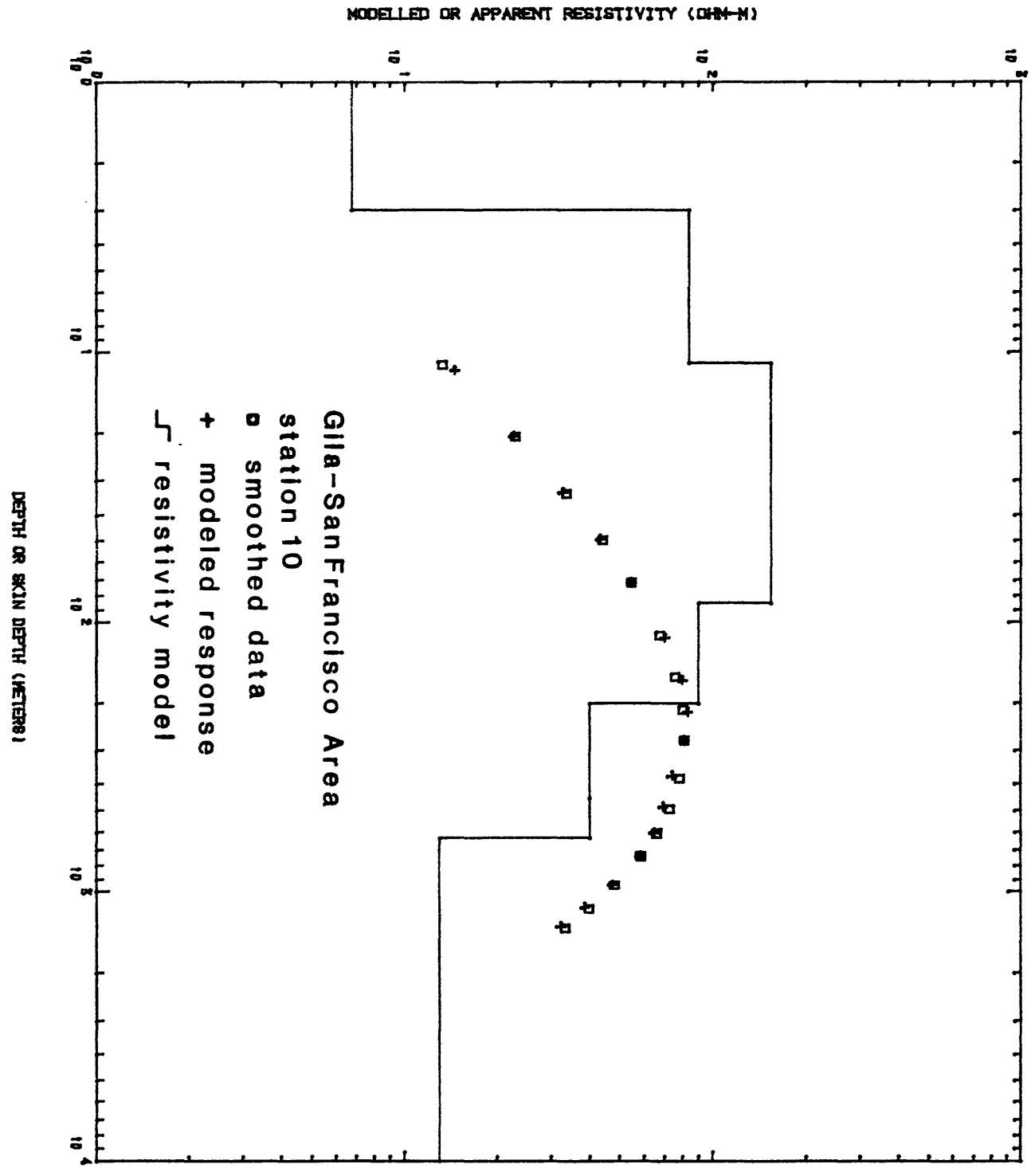
MODELLED OR APPARENT RESISTIVITY (OHM-M)
DEPTH OR SKIN DEPTH (METERS)
Gila-SanFrancisco Area
station 10
smoothed data
+ modeled response
resistivity model

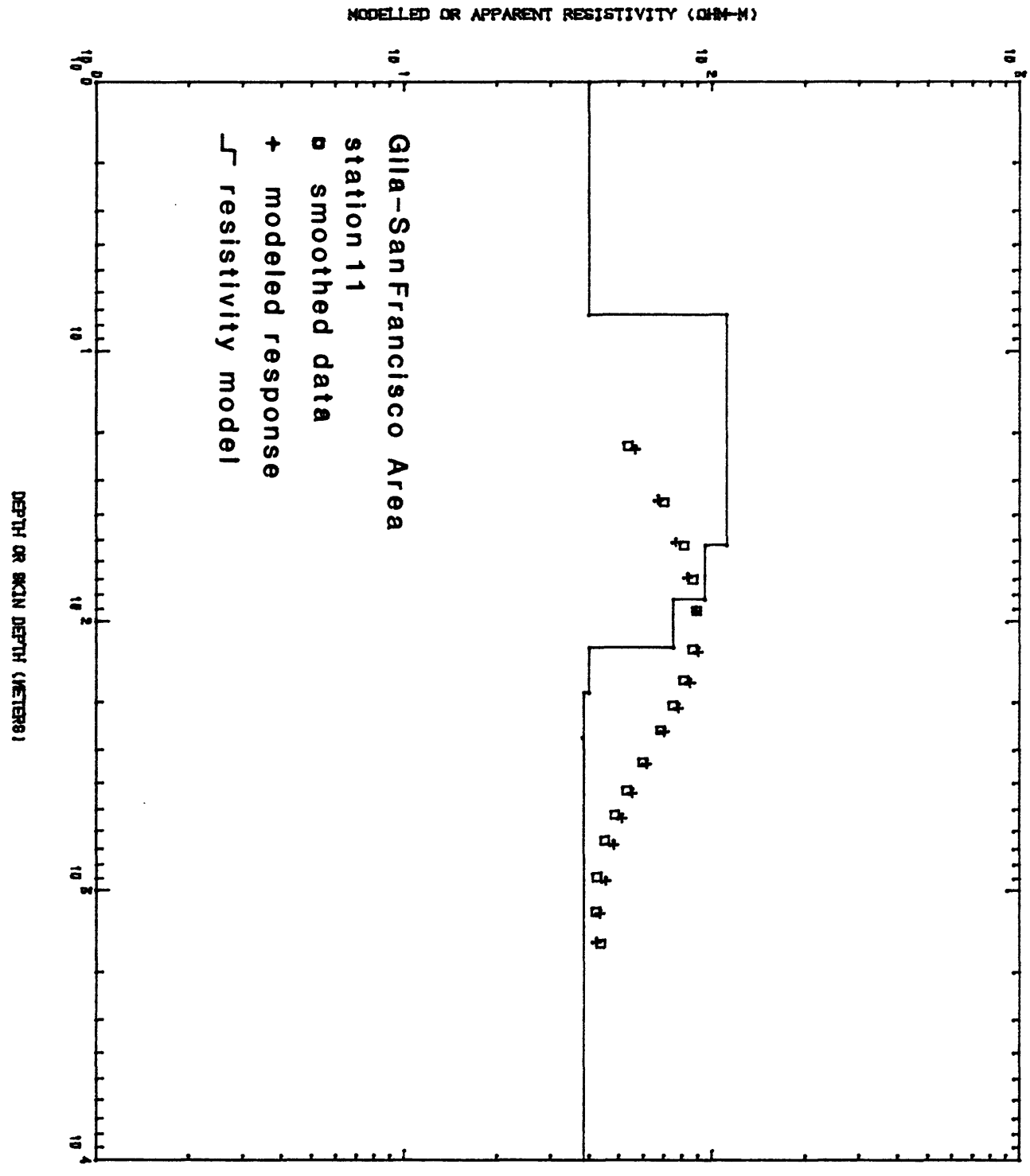
MODELLED OR APPARENT RESISTIVITY (OHM-M)
Gila-SanFrancisco Area
station 11
smoothed data
modeled response
resistivity model
DEPTH OR SKIN DEPTH (METERS)

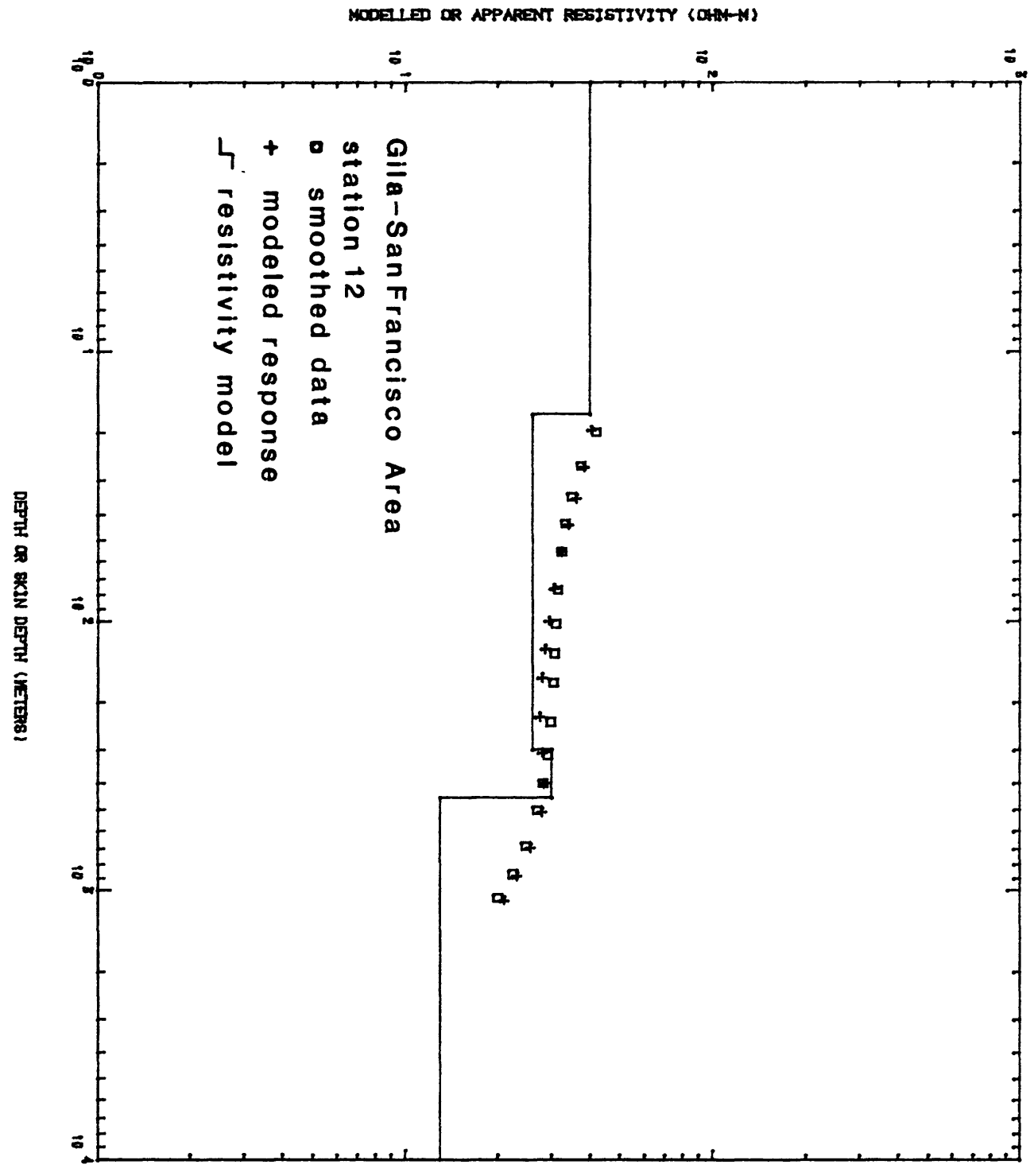
MODELLED OR APPARENT RESISTIVITY (OHM-M)
DEPTH OR SKIN DEPTH (METERS)
Gila-SanFrancisco Area
station 12
smoothed data
modeled response
resistivity model

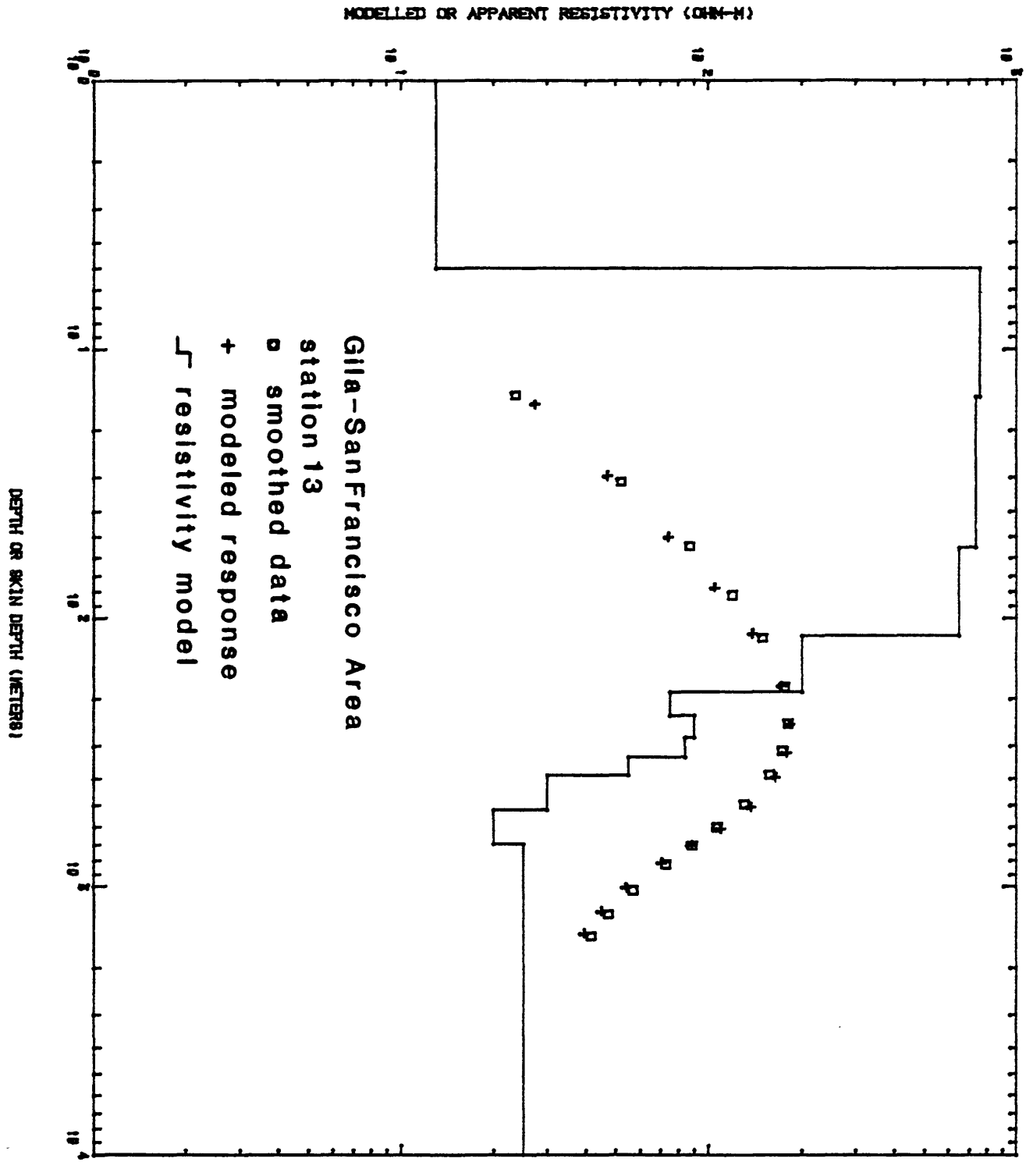
MODELLED OR APPARENT RESISTIVITY (OHM-M)
DEPTH OR SKIN DEPTH (METERS)
Gila-SanFrancisco Area
station 13
□ smoothed data
+ modeled response
⌐ resistivity model

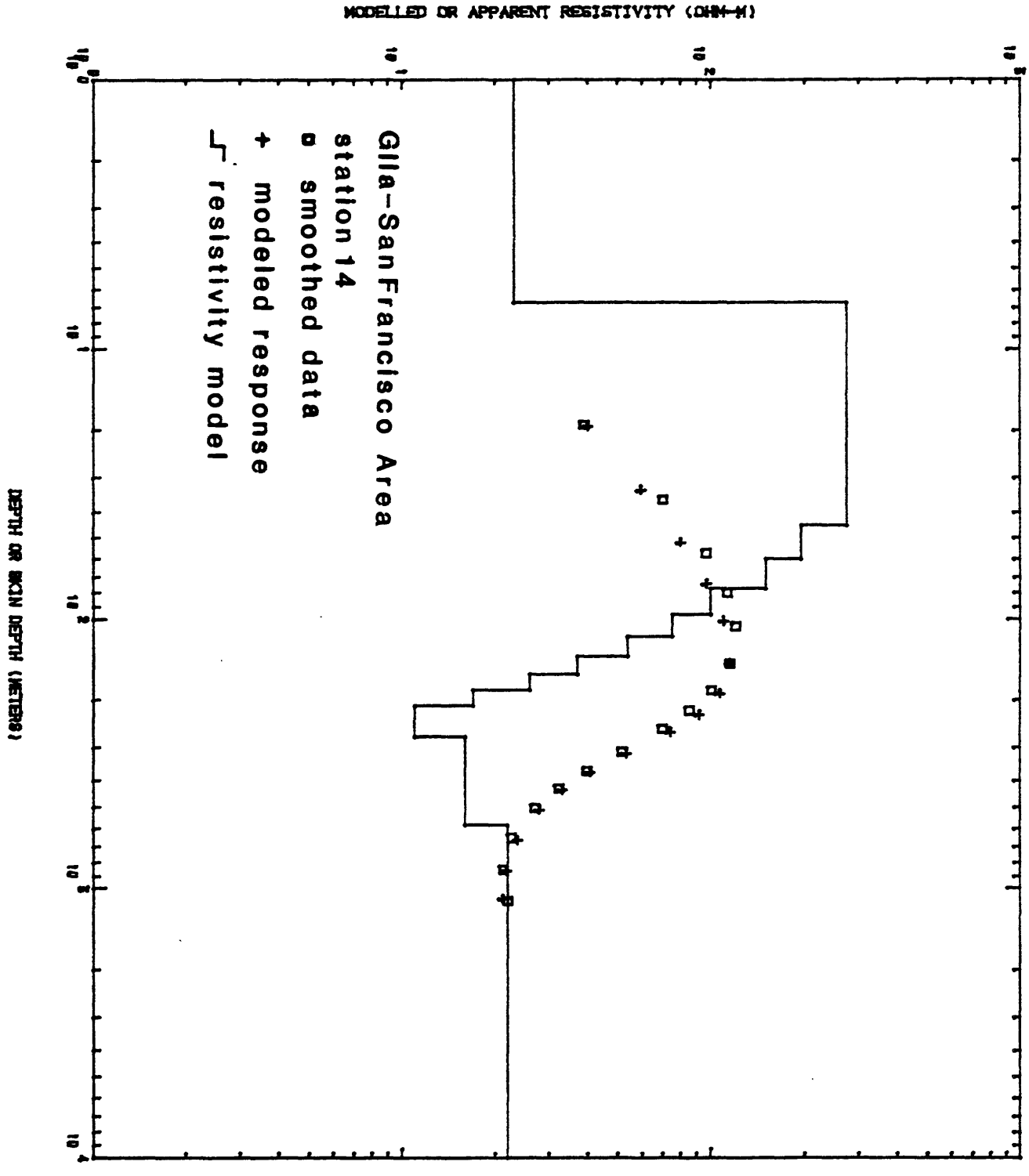
MODELLED OR APPARENT RESISTIVITY (OHM-M)
DEPTH OR BOTTOM DEPTH (METERS)
Gila-San Francisco Area
station 14
smoothed data
modeled response
resistivity model

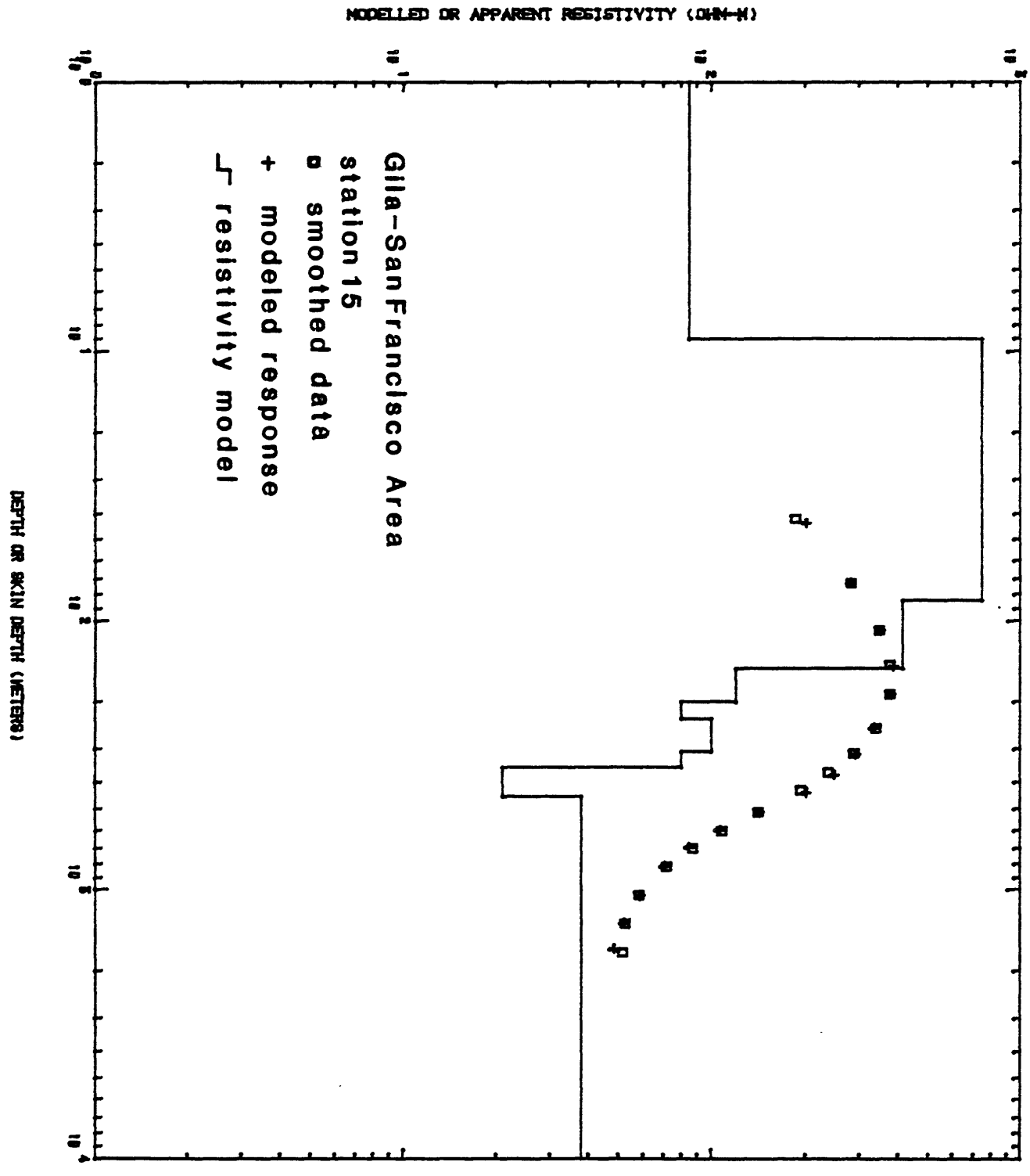
MODELLED OR APPARENT RESISTIVITY (OHM-M)
DEPTH OR SKIN DEPTH (METERS)
Gila-SanFrancisco Area
station 15
smoothed data
+ modeled response
resistivity model

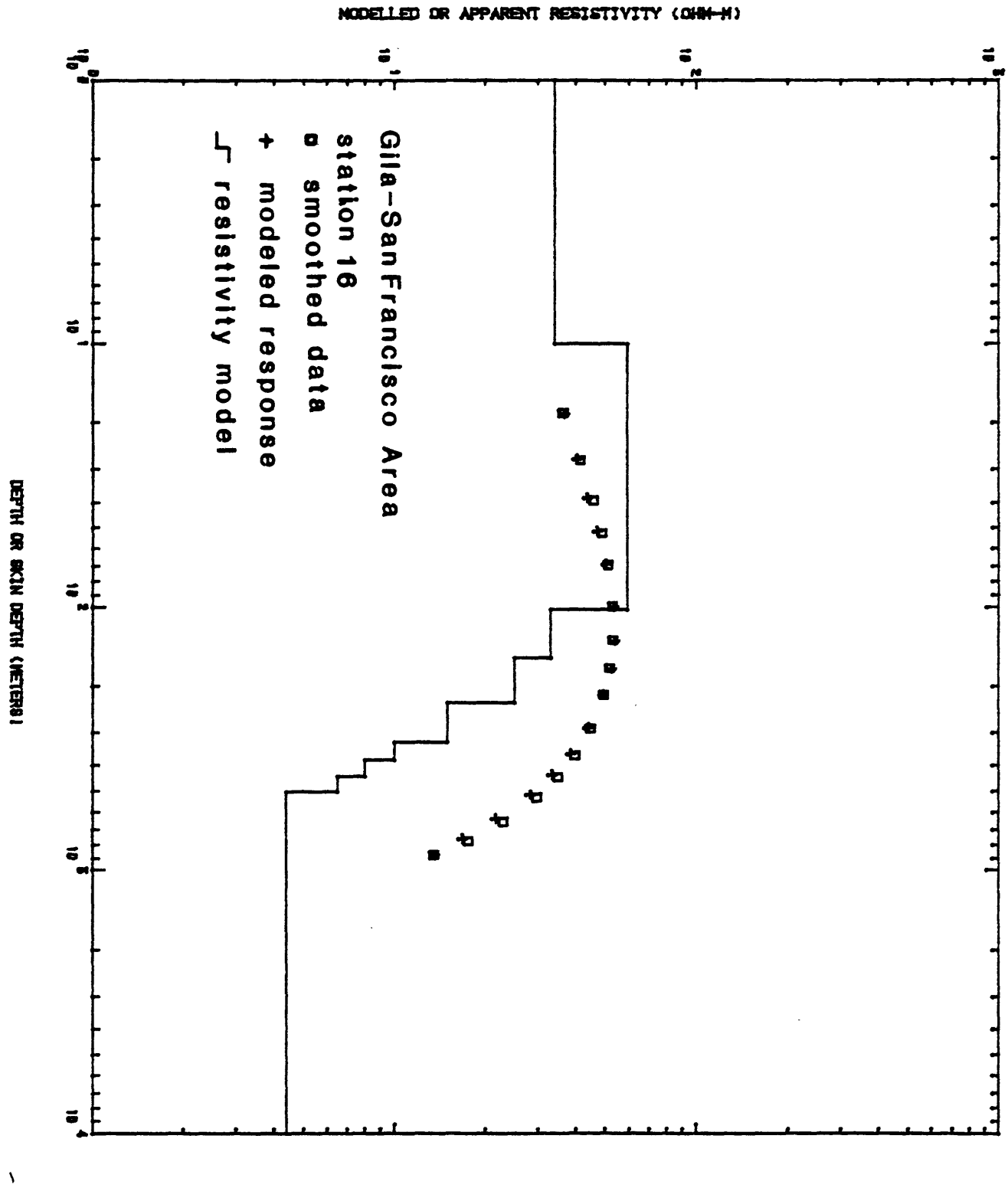
MODELLED OR APPARENT RESISTIVITY (OHM-M)
DEPTH OR SKIN DEPTH (METERS)
Gila-San Francisco Area
station 16
□ smoothed data
+ modeled response
⌐ resistivity model

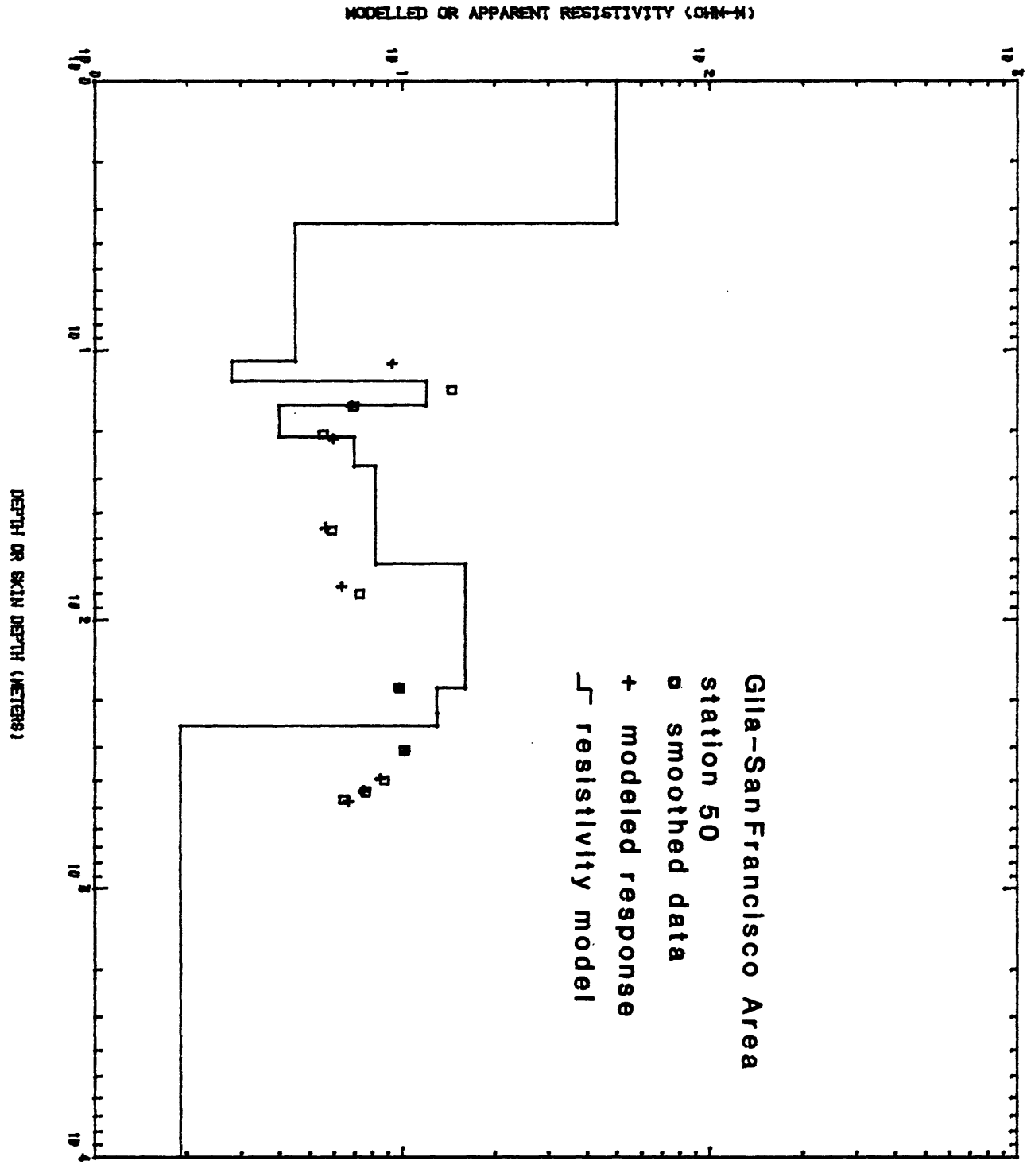
MODELLED OR APPARENT RESISTIVITY (OHM-M)
DEPTH OR SKIN DEPTH (METERS)
Gila-SanFrancisco Area
station 50
smoothed data
modeled response
resistivity model

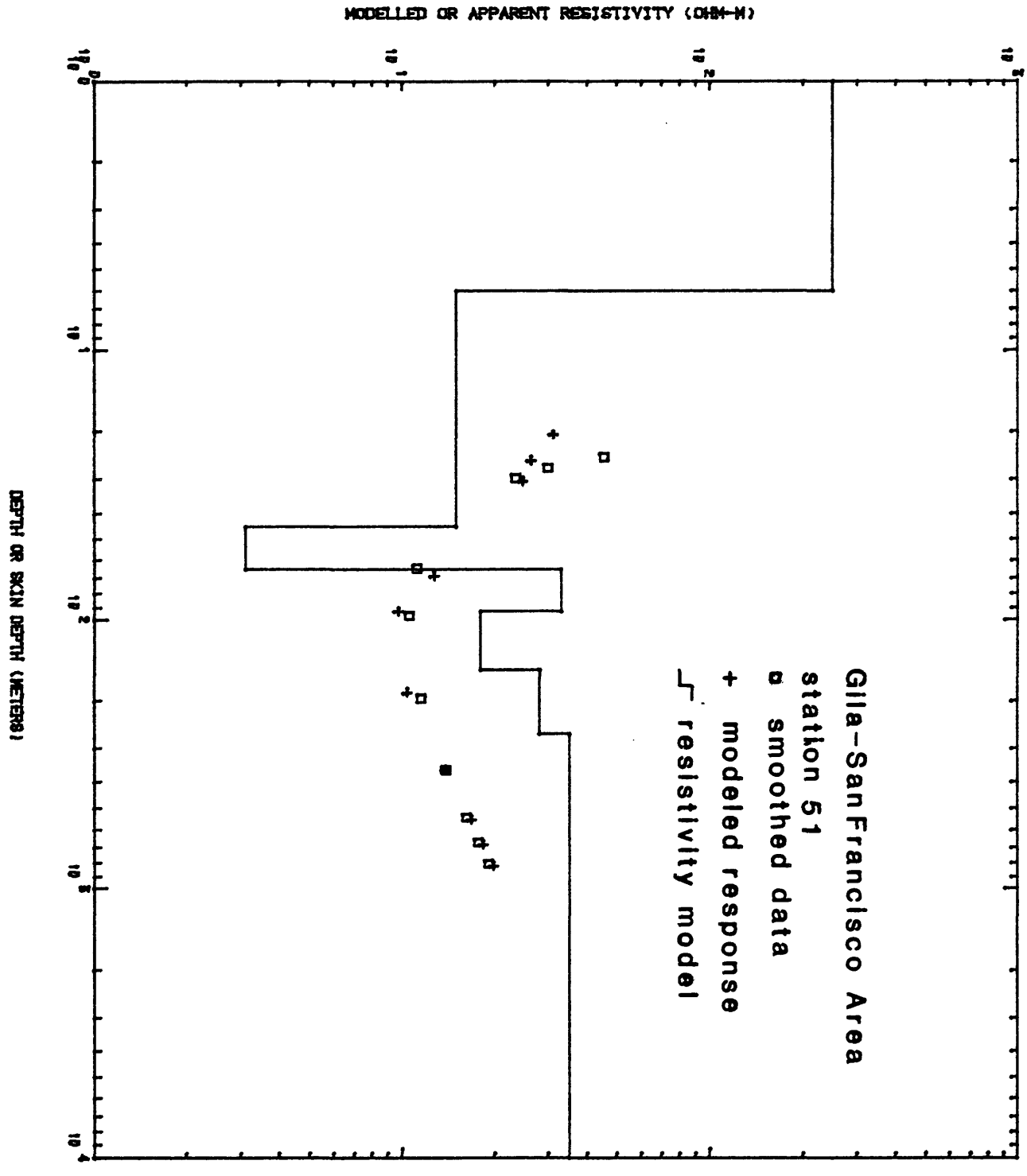
MODELLED OR APPARENT RESISTIVITY (OHM-M)
DEPTH OR SKIN DEPTH (METERS)
Gila-San Francisco Area
station 51
smoothed data
+ modeled response
resistivity model

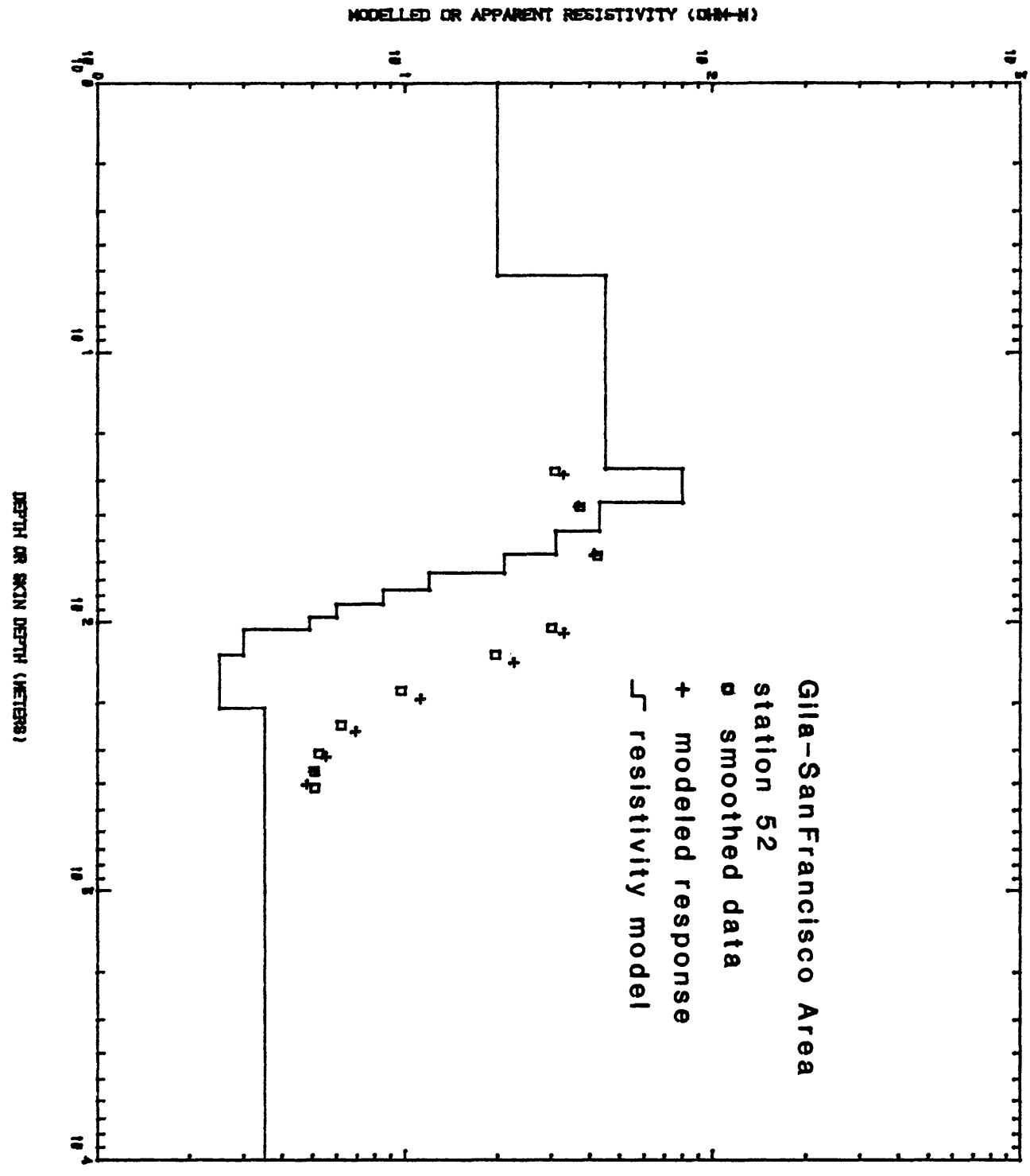
MODELLED OR APPARENT RESISTIVITY (OHM-M)
DEPTH OR SKIN DEPTH (METERS)
Gila-SanFrancisco Area
station 52
smoothed data
modeled response
resistivity model

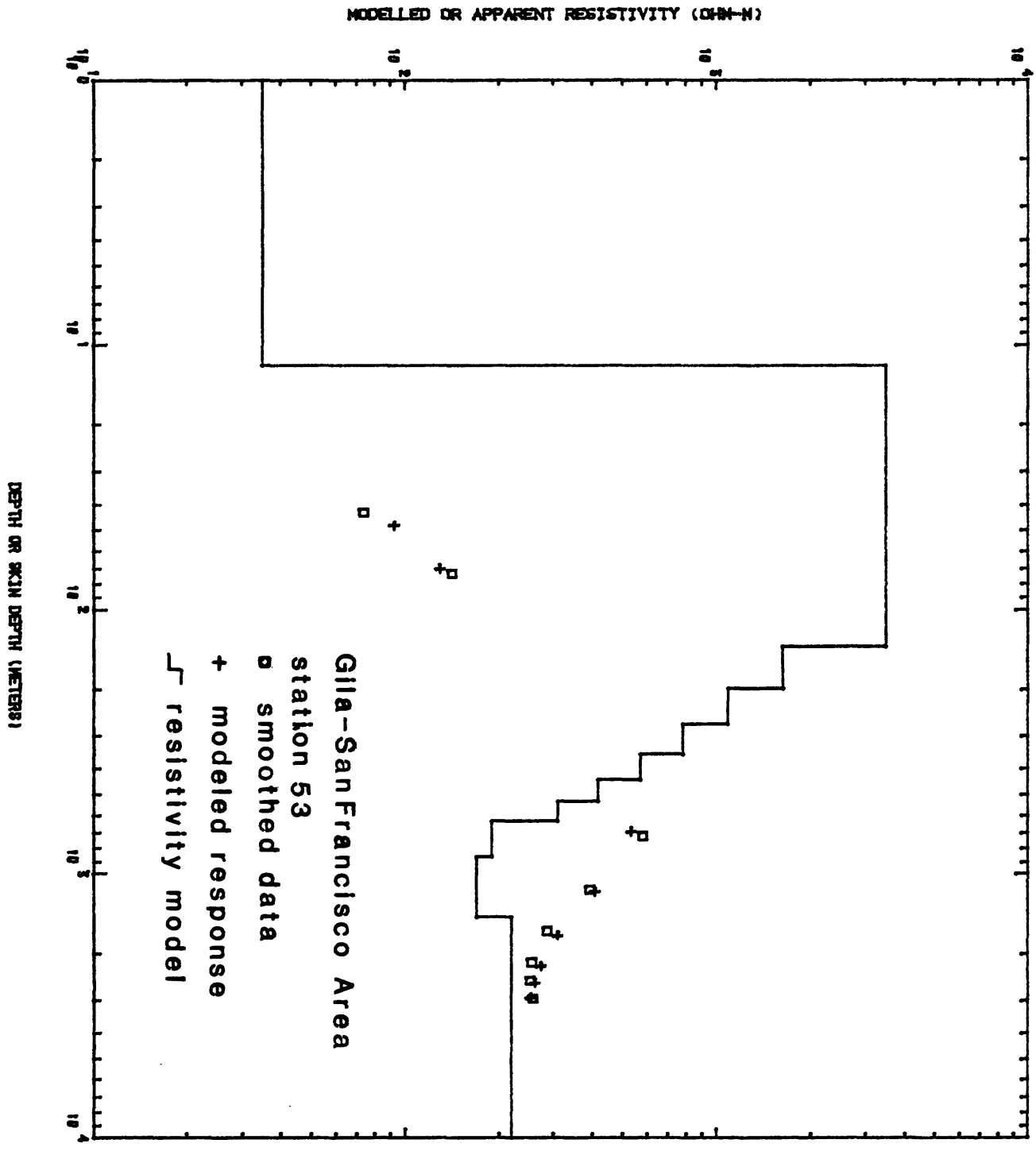
MODELLED OR APPARENT RESISTIVITY (OHM-M)
DEPTH OR SKIN DEPTH (METERS)
Gila-San Francisco Area
station 53
smoothed data
+ modeled response
resistivity model

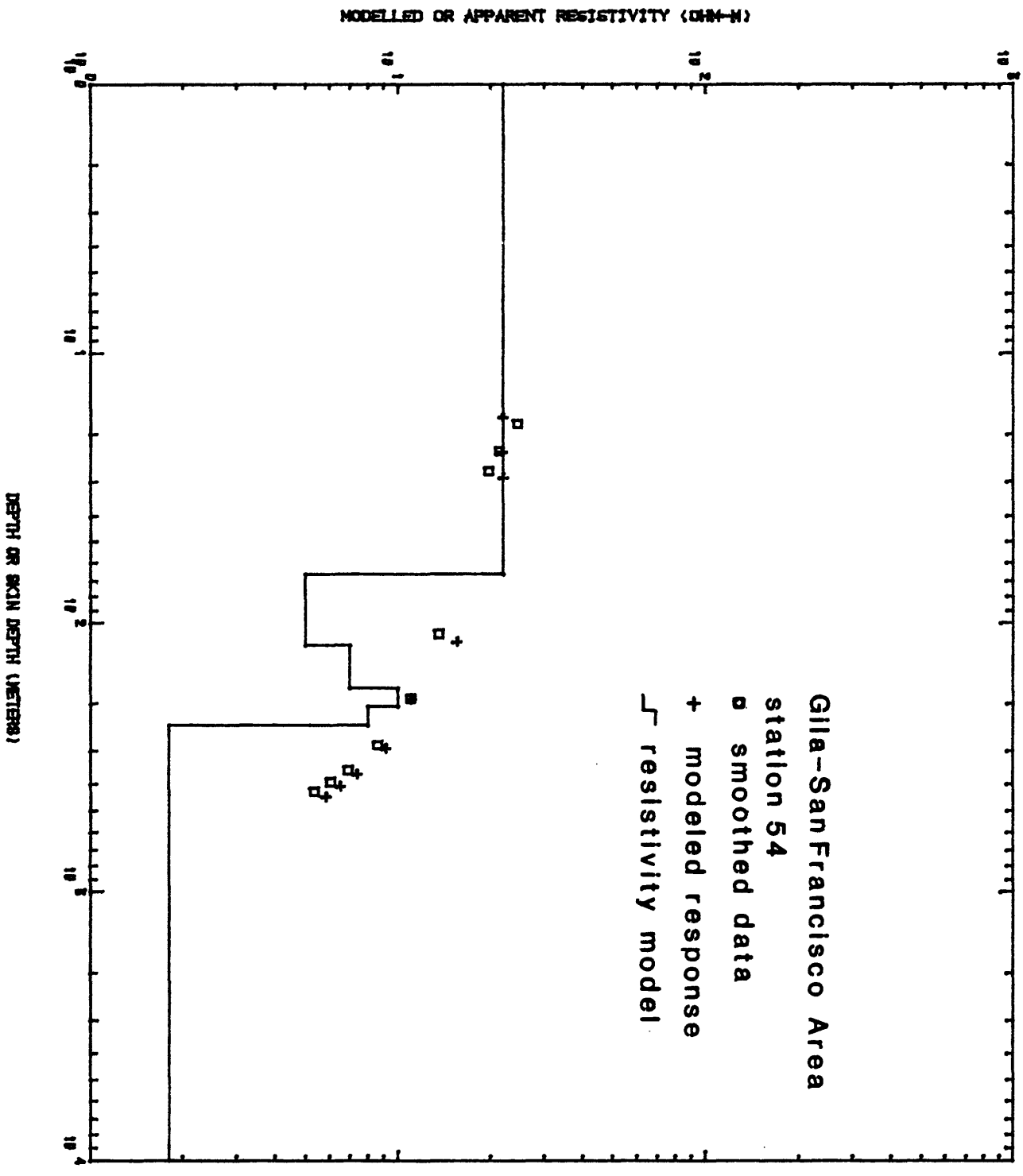
MODELLED OR APPARENT RESISTIVITY (OHM-M)
DEPTH OR SKIN DEPTH (METERS)
Gila-SanFrancisco Area
station 54
smoothed data
modeled response
resistivity model

Appendix D

A calculator program for basic reduction of AMT data. The formulae used are programmed for the Texas Instruments Calculator TI-59*

Contents

*The use of commercial trade names is for descriptive purpose and does not imply endorsement by the USGS.

TITLE AMT 1 PAGE 1 OF 9

PROGRAMMER D. Klein DATE 7-3-80

TI Programmable **Program Record**

Partitioning (Op 17) 4,7,9,5,9 Library Module Standard Printer Optional Cards 1

Sides 1 and 2

PROGRAM DESCRIPTION

Reduction of Scalar AMT Data:

This program computes the geometric (logarithmic) mean apparent resistivity, $\hat{\rho}_a$, and the 95% confidence interval S_{95} (as % of log-cycle) given the instrument system response, K; the receiver gains GE and GH (in db), and measured e and h_i.

USER INSTRUCTIONS

STEP	PROCEDURE	ENTER	PRESS			DISPLAY
1	Enter K (system response factor)	K			A	K
2	Enter G_E (E-gain, db)	G_E			R/S	G_E
3	Enter G_H (H-gain, db)	G_H			R/S	G_H
4	Enter ej (E-field measure)	ej			B	e_j
5	Enter hj (H -field measure)	hj			R/S	h_j
	repeat steps 4 and 5 for N data pairs until $\hat{S}_{95}$ is satisfactory					
6	Recall N (number of measurements)	-----		RCL	03	N
7	Recall $\log \hat{\rho}_a$	-----		RCL	13	$\log \hat{\rho}_a$

8	Recall $\hat{\rho}_a$				x⇄t	$\hat{\rho}_a$

USER DEFINED KEYS	DATA REGISTERS (INV Int)		LABELS (Op 08)
A Enter K	0^0	1^0 log E/H	001 11 A
B Enter e, h	0^1 Σ log (E/H)	1^1 log K	016 13 C
C Change gains	0^2 Σ log $(E/H)^2$	1^2 log $(G_E/G_N)^2$	036 12 B
D	0^3 N	1^3 log $\hat{\rho}_a$	060 10 E'
E	4	1^4 $\hat{S}_{95}$	083 98 ADV
A'	5	1^5 $\hat{\rho}_a$	099 78 Σ+
B'	6	1^6 dummy	112 58 FIX
C'	7	7	129 79 $\bar{x}$
D'	8	8	138 33 x^2
E' for j > 1	9	9	163 34 FX
			182 99 PRT

FLAGS 0 1 2 3 ✓ 4 5 6 7 8 9

1014966-1

User Instructions (Continued)

STEP	PROCEDURE	ENTER	PRESS	DISPLAY
4.1	Remove last (erroneous) data pair. This step is valid only if $j \geq 3$ and resets registers 01,02,03 re-enter ej, hj using steps 4 and 5.		SBR FIX	previous $\hat{S}_{95}$
5.1	Change gains. Re-enter G_E and G_H using step 2 and 3.		C	previous G_H
9.	Compute skin depth. Enter apparent resistivity from step 8.	$\hat{\rho}_a$	SBR $\sqrt{x}$	$(\hat{\rho}_a)^{1/2}$
9.1	Enter frequency (Hz)	f	R/S	δ (skin depth, m)
10.	List results (printer option). Enter frequency (Hz).	f	SBR PRT R/S	FREQ? --Hz --N --ER ($\hat{S}_{95}$) --LOGR (log $\hat{\rho}_a$) --R ($\hat{\rho}_a$)

EXAMPLE

THEORETICAL NOISY DATA TEST

f = 10 Hz (true ρ = 85)

STEP	PROCEDURE	ENTER	PRESS	DISPLAY	
1.	INPUT K	.02	A	K	(.02)
2.	G_E	20	A/S	G_E	(20.)
3.	G_H	40	R/S	G_H	(40.)
4.	E_1	758	B	E_1	(758.)
5.	H_1	104	R/S	$\hat{S}_{95}$	(100.)
4.	E_2	646	B	E_2	(646.)
5.	H_2	104	R/S	$\hat{S}_{95}$	(13.6--)
5.1	CHANGE GAINS	---	C	G_H	(40.)
2.	INPUT GE	20	R/S	GE	(20.)
3.	G'_H	50	R/S	G'_H	(50.)
4.	E_3	653	B	E_3	(653.)
5.	H_3	332	R/S	$\hat{S}_{95}$	(9.03--)
4.	E_4	645	B	E_4	(645.)
5.	H_4	383	R/S	$\hat{S}_{95}$	(10.9--)
4.	E_5	668	B	E_5	(668.)
5.	(ERROR) H'_5	2977	R/S	$\hat{S}_{95}$	(74.4--)
4.1	REMOVE ERROR	--	SBR 2nd FIX	$\hat{S}_{95}$	(10.9--)
4.	REPLACE E_5	668	B	E_5	(668.)
5.	H_5	297	R/S	$\hat{S}_{95}$	(9.59--)
4.	INPUT E_6	666	B	E_6	(666.)
5.	H_6	335	R/S	$\hat{S}_{95}$	(7.84--)
6.	RECALL J	--	RCL 03	J	(6.)
7.	LOG $\hat{\rho}_a$	--	RCL 13	LOG $\hat{\rho}_a$	(1.90--)
8.	$\hat{\rho}_a$	--	x-t	$\hat{\rho}_a$	(81.2--)
9.	FIND SKIN DEPTH	--	SBR $\sqrt{x}$	$(\hat{\rho}_a)^{1/2}$	(9.01--)
9.1	INPUT f	10	R/S	δ	(718.--)
10.	PRINTER LIST (OPTIONAL)	--	SBR PRT	FREQ?	
	INPUT f	10	R/S	$\hat{\rho}_a$	(81.2--)

PRINTER LIST
FREQ?
10. HZ
6. N
7.847565615 ER
1.909836835 LOGR
81.25251924 R

EXPLANATORY NOTES

EQUATIONS

The apparent resistivity equation is given by

$$\rho_a = K \left(\frac{G_H}{G_E} \frac{e}{h_\perp}\right)^2, \qquad (1)$$

where the parameters, all functions of frequency, are

e, $h_\perp$: electric, magnetic measurements in arbitrary but equivalent units.

G_H, G_E: system receiver gains expressed in db as

$$G = 20 \log g$$

where g is the actual gain

$$K: = \frac{0.2}{f} \left(\frac{R_E}{R_H}\right)^2, \text{ where}$$

f = frequency (Hz)

R_E, R_H = system response factors

The estimated apparent resistivity based on the geometric (or log) mean is

$$\hat{\rho}_a = \log^{-1} \left[\log K + 2\left\langle \log \frac{G_H}{G_E} + \log \frac{E}{H_\perp} \right\rangle\right], \qquad (2)$$

where $\frac{E}{H} = \frac{G_H}{G_E} \frac{e}{h}$ and $\langle f \rangle = \frac{1}{N} \sum_{j=1}^{N} f_j$ symbolizes the calculation of the mean value.

The 95% confidence interval (1/2 of the 95% confidence bar) expressed as percent of a log-cycle is given as:

$$\hat{S}_{95} = 100 \frac{1.96}{\sqrt{N}} 2 S_{\log E/H} \qquad (3)$$

$$= \frac{392}{\sqrt{N}} S_{\log E/H}$$

where N is the number of measurement pairs and $S_{\log E/H}$ is the standard deviation of $\log E/H_{\perp}$.

The standard deviation is given by

$$S_x = \left[\frac{1}{N-1} (N \langle x^2 \rangle - \langle x \rangle^2\right]^{1/2} \qquad (4)$$

Skin depth, in SI units is given by

$$\delta = 503.292 \ (\hat{\rho}/f)^{1/2}, \qquad (5)$$

where ρ = resistivity (ohm-m) and f = frequency (Hertz).

THEORETICAL DATA

The data of the example was generated for a homogeneous Earth model using the equation:

$$E = 5H(f\rho)^{1/2} \quad (SI)$$

$$f = 10 \text{ Hz}$$

$$\rho = 85 \text{ ohm-m}$$

Thus, for a theoretical H = .001 nT, we find E = 65.192 μv/km. The noisy data was generated using the random number subroutine in the standard TI59 module; Gaussian random values about E = 65.192 ± 7.1 using the seed value of 9432 and H = 1.0 ± .071 using the seed value of 5629 multiplied by appropriate gains (10 for E; 100 and 316 for H) form the data set.

PROGRAM FLOW (refer to listing, p. 8)

Register	Procedure	Operations
00-19	1. enter K	clear memory, set flag, initialize, store: k to 16 $\hat{S}_{95}$ to 14 log K to 11
20-21	2. enter G_E	
22-34	3. enter G_H	computer and store: $\log (\frac{G_H}{G_E})^2$ to 12 G_H to 16
35-38	4. enter ε_j	
39-50	5. enter h_j	computer log $(E/H_\perp)$, and sums needed for standard deviation using subroutine $\Sigma+$
51-58		compute $\hat{\rho}_a$ for j = 1 using subroutine ADV, remove flag, store: log $\hat{\rho}_a$ to 13 log $\hat{\rho}_a$ to 15 and t-register
59-81		compute $\hat{\rho}_a$ for j>1 using subroutine $\bar{X}$ and ADV, compute $\hat{S}_{95}$ using routine x^2, store $\hat{S}_{95}$ to 14.
89-97	SUBR, ADV (returns $\hat{\rho}_a$)	compute $\hat{\rho}_a$ and log $\hat{\rho}_a$.
98-110	SUBR. Σ + (returns log E/H)	compute and store: Σ log E/H to 01 Σ log $(E/H)^2$ to 02 N to 03
111-127	SUBR. FIX (returns $\hat{S}_{95}$)	removes the most recent log E/H and log $(E/H)^2$ from 01 and 02, decrements 03, and recomputes $\hat{S}^{95}$ and $\hat{\rho}^a$

Program Flow (Continued)

128-136	SUBR. X (returns <log E/H>)	computes <log E/H>
137-161	SUBR. X^2 (returns standard deviation)	computes the standard deviation of log E/H
162-179	SUBR. $\sqrt{X}$ returns skin depth	computes the skin depth
180-251	SUBR. PRT	optional printer list of N, $\hat{S}_{95}$, log $\hat{\rho}_a$, $\hat{\rho}_a$

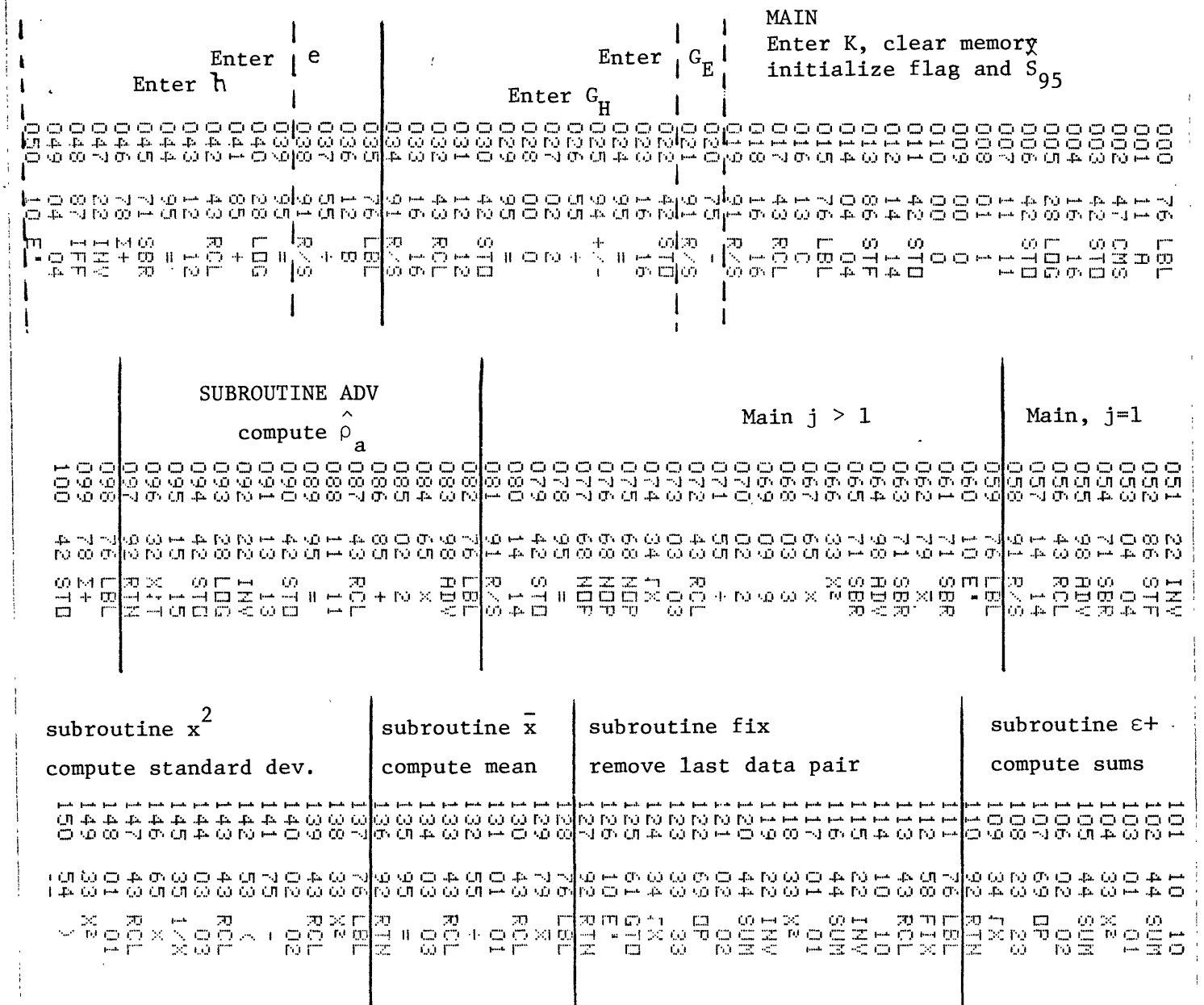
MAIN
Enter K, clear memory, initialize flag and S_{95}
Enter G_E
Enter G_H
Enter e
Enter h
Main, j=1
Main j > 1
SUBROUTINE ADV
compute $\hat{\rho}_a$
subroutine fix
remove last data pair
subroutine ε+
compute sums
subroutine $\bar{x}$
compute mean
subroutine x^2
compute standard dev.

PROGRAM LIST (continued)

```
                151  95  =
                152  55  ÷
                153  53  (
                154  43  RCL
                155  03  03
                156  75  -
                157  01  1
                158  54  )
                159  95  =
                160  34  √x
                161  92  RTN
subroutine √x   162  76  LBL
compute skin    163  34  √x
depth           164  34  √x
                165  55  ÷
                166  91  R/S
                167  34  √x
                168  65  ×
                169  05  5
                170  00  0
                171  03  3
                172  93  .
                173  09  9
                174  02  2
                175  09  9
                176  55  ÷
                177  02  2
                178  95  =
                179  92  RTN
subroutine PRT  180  68  NOP
                181  76  LBL
printer list    182  99  PRT
of results      183  69  DP
                184  00  00
                185  02  2
                186  01  1
                187  03  3
                188  05  5
                189  01  1
                190  07  7
                191  03  3
                192  04  4
                193  07  7
                194  01  1
                195  69  DP
                196  01  01
                197  69  DP
                198  05  05
                199  02  2
                200  03  3
                201  04  4
                202  06  6
                203  69  DP
                204  04  04
                205  91  R/S
                206  69  DP
                207  06  06
                208  03  3
                209  01  1
                210  69  DP
                211  04  04
                212  43  RCL
                213  03  03
                214  69  DP
                215  06  06
                216  01  1
                217  07  7
                218  03  3
                219  05  5
                220  69  DP
                221  04  04
                222  43  RCL
                223  14  14
                224  69  DP
                225  06  06
                226  02  2
                227  07  7
                228  03  3
                229  02  2
                230  02  2
                231  02  2
                232  03  3
                233  05  5
                234  69  DP
                235  04  04
                236  43  RCL
                237  13  13
                238  69  DP
                239  06  06
                240  03  3
                241  05  5
                242  69  DP
                243  04  04
                244  43  RCL
                245  15  15
                246  69  DP
                247  06  06
                248  98  ADV
                249  98  ADV
                250  98  ADV
                251  92  RTN
                252  00  0
                253  00  0
```